Integration of Parallel Processing Streams in the Inferior Colliculus of the Barn Owl

Thesis by

James Allan Mazer

In Partial Fulfillment of the Requirements

for the Degree of

Doctor of Philosophy

California Institute of Technology

Pasadena, California

1995

(Submitted May 29, 1995)

Acknowledgements

I would like to thank my advisor, Dr. Masakazu Konishi, without whom this work would never have been possible. Dr. Konishi's deep commitment to the neuroethological study of the nervous system provided the intellectual and physical foundations upon which this thesis was built. His perspectives on and insights into the function of the nervous system and animal behavior have shaped my own ideas and guided this work at every step. Over the years, Dr. Konishi's laboratory provided an exciting and ever fascinating environment in which to work. My thesis committee, Drs. John Allman, Gilles Laurent, Scott Fraser and Richard Andersen, provided support in the form of focus, direction, valuable advice and even an occasional push to keep things moving. I would especially like to thank Drs. Susan Volman and Ralph Adolphs for teaching me virtually everything I know today about electrophysiology, histology and basic neurobiology and for always having the patience to put up with my endless questions. I am indebted to Mike Lewicki, Drs. Allison Doupe, David Perkel and Jack Gallant for their help and support throughout this work and to Christiane Dräger who reminded me, time and time again, that a light really does shine at the end of the tunnel.

Finally, I would like to thank Margaret Schwartz, who long ago showed me the importance of both teaching and science and who demonstrated how a good teacher can influence the future of his or her students in a beneficial way. Her unique style and enthusiasm kindled my own interest and excitement with science and forever changed the direction of my life.

Abstract

The study of the neural mechanisms underlying sensation has demonstrated than an intimate relationship exists between behavioral function and neural structure. One common structural theme in sensory processing is the use of parallel processing streams. Parallel processing occurs in virtually every sensory modality and in almost every species studied to date. This work describes the integration of parallel auditory processing streams for time, intensity and frequency in the inferior colliculus of the barn owl, *Tyto alba*, which leads to the formation of a centrally synthesized map of auditory space.

Interaural time differences (ITDs) provide the primary cue for localization in the horizontal plane. ITDs are extracted from the firing patterns of auditory nerve fibers by a coincidence detection circuit located in the owl's brainstem. Interaural level differences, which are used by the owl for vertical plane localization, are computed by an anatomically distinct and parallel circuit. The brainstem and midbrain structures that process time and level differences are independent up to the level of the inferior colliculus. In the lateral shell division of the central nucleus of the inferior colliculus, these two processing streams are combined by single neurons that exhibit spatially restricted auditory receptive fields.

The first part of this thesis characterizes the detailed physiological properties of lateral shell neurons and describes a model of hierarchical integration within the shell that underlies the synthesis of space-specific neurons located in the topographic auditory space map in the external nucleus of the inferior colliculus (ICx). The second part examines the integration of the parallel, narrow band frequency channels arising at the level of the brain stem coincidence detector, nucleus laminaris. The output of single coincidence detector neurons, which encode interaural phase difference, does not unambiguously signal horizontal location. Multiple phase ambiguous narrow band frequency channels are integrated in the lateral shell to eliminate phase ambiguity. Experiments presented here describe the relationship between signal bandwidth and phase ambiguity in an attempt to elaborate the neural circuitry underlying the integration of parallel, narrow band, interaural phase difference channels.

Contents

Chapter 1 Introduction

> It seems, therefore, that the centres of each level of the hierarchical system control a type of appetitive behavior. This is more generalized in the higher levels and more restricted or more specialized in the lower levels ... The hypothesis ... of a hierarchical system of nerve centres each of which has integrative functions of the "collecting and redispatching" type, has been developed on a foundation of facts of an indirect nature. ... future work [analyzing this hierarchical organization] could only be done by workers who are fully acquainted with the instinctive behavior as a whole and with its analysis, and at the same time are in command of neurophysiological methods and techniques.
>
> – Nikolaas Tinbergen, *The Study of Instinct*

Neuroethology is the study of the relationship between the natural behavior of animals and the nervous system. Neuroethological studies of sensory processing are founded on the basic premise that an understanding of natural behavior is crucial to understanding the nervous system. This philosophy stems in part from observations that have demonstrated the design of the nervous system is intimately related to an animal's ecological niche and its natural behaviors. The connection between behavior and nervous system structure has led many researchers to the conclusion that a useful strategy in the study of sensory systems is to focus on attention on species exhibiting a strong ethological dependence on the sensory modality of interest. In the past 20 years, the neuroethological approach of combining the careful study of behavior with neurophysiology has been applied to the study of sensation time and time again in numerous species with great success. This approach has been successful in addressing the nature of structure-function relationships in the peripheral and central nervous systems in virtually all sensory modalities (*e.g.*, passive and active audition: Payne, 1971, Konishi et al., 1988, Suga, 1988; electrolocation: Heiligenberg 1988, 1991; Carr, 1990; vocal-motor learning: Konishi, 1985, Konishi, 1989; olfaction: Schneider, 1974; vision: Wehner, 1989).

A review of the recent work in the field of neuroethology reveals two consistent findings. First, with respect to sensory processing, the neuroethological approach has been remarkably successful in helping us to understand how neural circuitry is related to sensation in

specific highly adapted or specialized animals. Second, despite the fact that these studies often focus on such specialized species, the findings are often of general applicability and serve to directly extend our understanding of sensory processing in non-specialized species. For example, the ethologically based studies of Carr and Konishi (1988) aimed at characterizing the brain structures underlying the sound localization abilities of the barn owl, *Tyto alba*, provided the first direct physiological and anatomical evidence of a neural coincidence detector in the auditory system. The brainstem coincidence detector described by Carr and Konishi makes use of axonal delay lines to transform the temporal code of the auditory nerve into a place code in which the location of sounds sources is represented by the spatial distribution of neuronal activity. The existence of such a circuit was first hypothesized by Jeffress in 1948, and experiments in other species (Rose et al., 1966; Goldberg and Brown, 1969) provided indirect evidence of coincidence detection. It was the neuroethologically guided studies of the barn owl that provided the first clear understanding of the physiological and anatomic substrates for coincidence detection. Most interestingly, despite the fact that the barn owl is a specialized species, with an auditory system highly adapted to its ethological role as a nocturnal predator, subsequent studies later described similar circuits in other, non-specialized species (cats: Yin and Chan, 1990; hamsters: Sanes, 1990; chickens: Overholt et al., 1992). This example serves as a reminder of the general applicability of neuroethological methods beyond the study of specialized species.

A basic finding in the field of neuroscience has been the discovery that superficially different sensory systems can utilize common neural mechanisms and implement similar computational algorithms at the level the central nervous system. Kuffler's (1953) work on the mammalian retina and Barlow's (1953) on the retina of the frog described visual receptive fields organized in a circularly symmetric "center-surround" fashion. These receptive fields, which first appear in the retina at the level of the bipolar cell (Werblin and Dowling, 1969), have spatial receptive fields composed of a circular central region and annular surround. Center-surround neurons are excited by light striking the center region and inhibited by light in the surround (center-on), or vice versa (center-off). Twenty-five years later Knudsen and Konishi (1978a), described auditory neurons in the avian inferior colliculus with spatial receptive fields similarly arranged in a center-surround fashion. Sound sources positioned

in the center of a neuron's auditory receptive field excited such cells, while sources in the surround generated inhibition. Knudsen and Konishi's observations provided striking evidence that center-surround organization was not unique to the visual system, but was instead a general feature of sensory integration.

The experiments described in this text focus on understanding the neural substrate of the barn owl's ability to localize sounds. Specifically, they address the relationship between structure and function in the owl's inferior colliculus. It is important to keep in mind that the goal is not to understand how the owl localizes sounds *per se*, but rather to understand in more detail the general nature of the relationship between neural circuitry and the computational requirement of natural behavior. The intention is to take a step towards trying to understand the basic principles, independent of species and modality, which relate structure to function in the central nervous system.

1.1 A Brief Introduction to Sound Localization

One of the functions performed by the auditory system is the spatial localization of sound sources in an organism's environment. In other sensory modalities, such as vision, localization of environmental features is inherent in the spatial distribution of neuronal activity at the level of the transduction organ. In the case of the vertebrate visual system, photoreceptors are arranged in a sheet-like monolayer positioned at the back of the eye. The optics of the eye serve to focus and project an image of the visual field directly onto the sensory epithelium. When light projected through the eye strikes a photoreceptor, the event is signaled by the receptor to the central nervous system (CNS). Because the pattern of light falling on the retina is a direct projection of the visual field, the spatial pattern of photoreceptor activity in each eye is sufficient to present a spatial representation of the visual field to the central nervous system.

The auditory system, in contrast, transmits not spatial but spectral relationships to the CNS. The vertebrate organ of auditory transduction, the cochlea, consists of a bank of narrow band filters that decompose incoming sound waves into their individual narrow band components. The physical organization of the cochlear filters and their efferent projections

to the central nervous system preserve the spectral relationships present in environmental sounds. Information about spatial relationships in the auditory system must be extracted from the spectral representation by higher brain areas. Though different species utilize different neural circuits to extract this information, the cochleotopic representation provides three basic cues that can be used by an organism to localize sounds.

Interaural time differences (ITDs) arise when the path lengths, and corresponding travel times, between a sound source and each ear are not equal. When a source is displaced from the midline to the left, sounds arrive at the left ear before the right, as shown in figure 1.1A. Likewise, sound waves from a source displaced to the right arrive at the right ear first. It is important to note here that there are two independent ITD cues present for laterally displaced sources. There is an ongoing time disparity, corresponding to the instantaneous time or phase difference which is available for the duration of sound (referred to here simply as ITD). In addition, there is also a transient disparity (transient-ITD) caused by the rise and fall of the sound's envelope. Under natural conditions, transient disparity cues are usually present only at the onset and offset of a sound. In most animals ITD cues (ongoing and/or transient) are used for localization in the horizontal plane (Heffner and Heffner, 1992). Moiseff and Konishi (1981) demonstrated that in the barn owl, the ongoing-ITD alone was sufficient for accurate horizontal localization.

In the most vertebrates, interaural level differences (ILDs) provide a second cue about the azimuthal position of a sound source. When a source is located laterally, the head lies between the source and the far ear. The head, being acoustically opaque at high frequencies, acts to shadow the far ear. This results in an intensity or level difference between the near and far ears, with the intensity developing at the near ear greater than that at the far ear (figure 1.1B). The magnitude of the ILD caused by shadowing is a function of the azimuthal position of the sound source; in humans this can be as large as 35dB (Middlebrooks et al., 1989).

Attenuation caused head shadowing depends upon both the azimuth and frequency of the sound source. The frequency dependence results from the physical relationship between the wavelength of a sound and the size of the object (in this case the head) interfering with the sound field. While the physics of sound propagation which underlie this relationship are

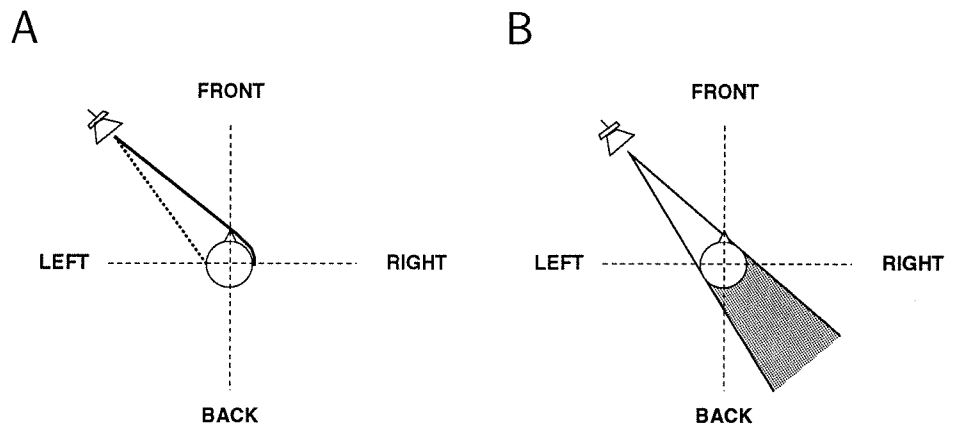

Figure 1.1: Time and level difference cues. (A) Sounds displaced to one side or the other of the midline generate interaural time differences. A source on the left, as shown, arrives at the left ear (dotted line) before the right (solid line). The sound wave "creeps" around the head to reach the right ear (Kuhn, 1977). (B) In symmetrically eared animals, lateral displacements also lead to interaural level differences. This occurs because the head acts to attenuate sounds reaching the far ear. The shaded area indicates the region falling in the acoustic shadow of the head when the sound source is located to the left.

beyond the scope of this discussion, the result is a frequency dependent interaural level difference (Δfi) that can provide additional information about source location in the horizontal plane (Heffner and Heffner, 1992; Makous and Middlebrooks, 1990; Middlebrooks and Green, 1991). Level difference cues, then, exist in two forms: Δfi and simple ILD, where the simple level difference refers to the overall difference in the sound pressure levels at the two ears, independent of frequency (*i.e.*, RMS level).

ITD, ILD and Δfi cues are all binaural, meaning that they depend upon a comparison of information from both ears. In most species these cues provide information only about azimuthal position. In most animals studied to date, with the notable exception of the barn owl, localization in the vertical plane makes use of monaural spectral cues. These spectral cues are caused by the frequency and elevation dependent filtering effects of the external ears or pinnae (Fisher and Freedman, 1968; Makous and Middlebrooks, 1990; Heffner and Heffner, 1992; Carlile and King, 1994). The pinnae, with their complex physical structure, act as both collectors and filters for sounds arriving at the ears. The shape of the pinnae serve to reflect and focus sound waves from the environment into the auditory canal. Be-

cause the pinnae usually have multiple reflecting surfaces, each located at a different distance from the ear canal, the reflections from each surface enter the ear and arrive at the tympanic membrane at slightly different times (Batteau, 1967; see Blauert, 1983, chapter 2, for review). The superposition of several time delayed reflections leads to characteristic peaks and notches of the power spectrum known as comb filtering (shown in figure 1.2). The exact location of these peaks and notches in the frequency domain are a function of the sound source's location in the vertical plane. Psychophysical and modeling studies have demonstrated that the spectral peaks and notches provide the primary cue for vertical localization in most species, including man (Blauert, 6970; Fuzessery, 1986; Middlebrooks and Green, 1991; Zakarauskas and Cynader, 1993).

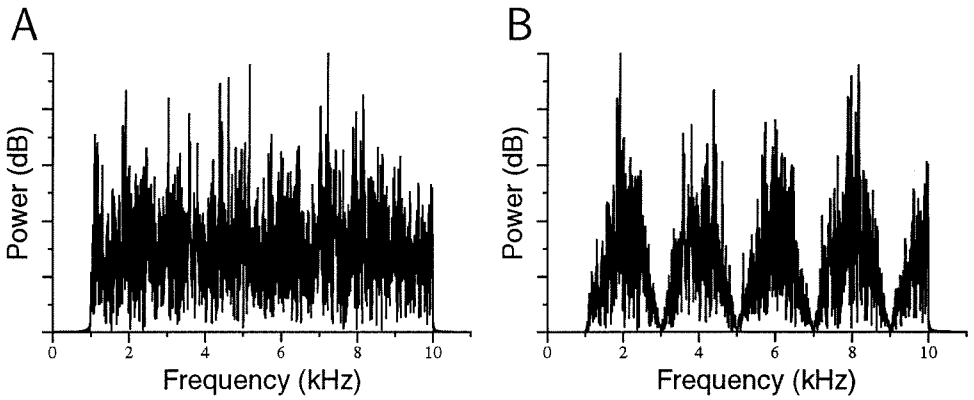

Figure 1.2: Simulated comb filtering like that caused by pinna reflections. (A) Power spectrum of a broadband (1-10kHz) noise signal. (B) A reflection was simulated by adding a time delayed (500 μs) version of the signal shown in A to itself. The power spectrum of the two wavefront signal exhibits peaks and notches characteristic of reverberation. The periodicity of the comb filter is a function of the echo delay. Note that the 500 μs delay used here is far greater than naturally occurring delays. However, it serves to clearly demonstrate the spectral effect of multiple reflecting surfaces.

In 1907 Rayleigh suggested that the cue used by humans for sound localization in the horizontal plane was a function of frequency. He proposed that low frequency sounds were localized using phase differences and high frequency sounds using level differences. These observations, which were more rigorously tested in the 1930's by Stevens and Newman, formed the basis of what is now known as the "duplex theory" of sound localization. To date, experimental studies have demonstrated that the duplex theory holds for virtually all

terrestrial vertebrates. The duplex theory appears to be a consequence of both the frequency dependence of ITD and ILD cues due to the physics of sound propagation and the operation of the neural structures which extract localization cues (Heffner and Heffner, 1992).

As mentioned above, at low frequencies the effect of head shadowing is minimal. Simply put, ILD cues are not available at low frequencies. At high frequencies, the time cues measured by the auditory system are ambiguous. This ambiguity occurs because most species do not actually measure time differences, but instead measure interaural phase differences (IPDs). This situation is a direct consequence of the cochlear decomposition of sounds into narrow band frequency channels. The relationship between ITD (or true azimuthal position) and IPD is a periodic function, with a period corresponding the center frequency of the narrow band channel. Figure 1.3 shows the ITD-IPD relationship for two different frequencies (a: 1kHz; b: 2kHz). The shaded area represents the range of ITDs experienced by human listeners under normal physiological conditions. At 1kHz IPD uniquely defines ITD over the physiological range. At 2kHz (and above), different ITDs have the same IPD. This means an animal or neuron sensitive to IPD alone will be unable to unambiguously localize high frequency sounds in the horizontal plane using temporal cues.

1.2 Sound Localization in the Barn Owl

The barn owl is notable in its deviation from the basic vertebrate plan for sound localization. Like other species, the barn owl uses interaural time difference to localize in the horizontal plane. In contrast to other species, including other owls (Volman and Konishi, 1989; Beitel, 1991), the barn owl relies on interaural level difference cues instead of monaural spectral cues for vertical plane localization.

The duplex theory states that low frequencies are localized using time cues, while high frequencies are localized using level cues. The sound localization abilities of the barn owl are not well described by the duplex theory, because the owl uses both time and level cues over the same frequency range. Behavioral studies by Moiseff and Konishi (1981) demonstrated that the owl uses only ITD cues for localization in the horizontal plane and only ILD cues in the vertical plane. Earlier work by Knudsen and Konishi (1979), demonstrated that

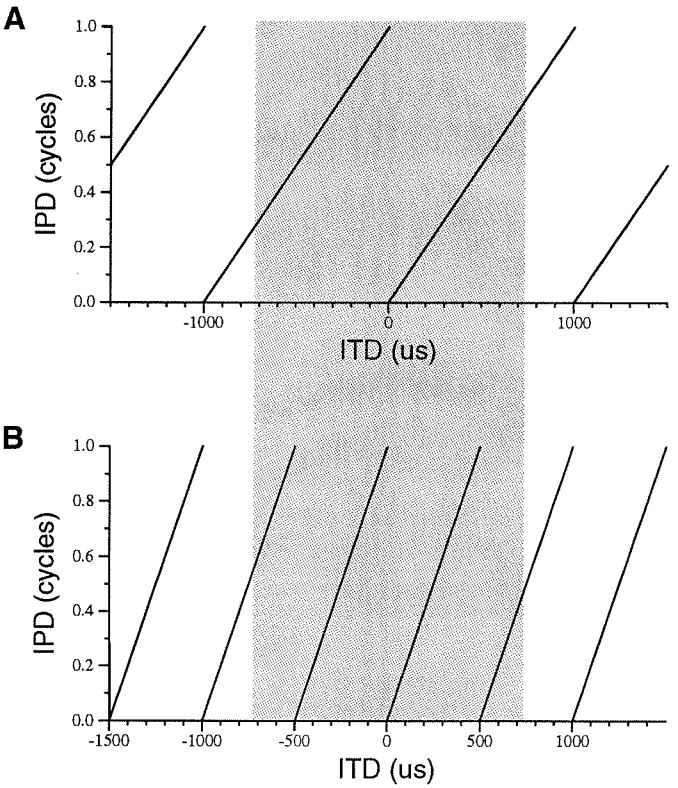

Figure 1.3: Phase ambiguity in humans. (A) IPD in cycles plotted as a function of ITD in μs for a 1kHz sound. (B) Same for a 2kHz sound. The shaded area indicates the physiological range of ITD for humans (about $\pm 750\,\mu s$).

the owl could accurately localize in both the horizontal and vertical places over the same frequency range. This leads to the unavoidable conclusion that the owl is making use of both ITD and ILD cues over the same frequency range, placing it in direct conflict with the duplex theory. These early studies posed two interesting questions: (1) how can the owl use ILD cues for vertical localization when other species can not? and (2) if the owl relies on ITD cues at high frequencies, how does it circumvent the problem of phase ambiguity?

The answer to the first question is that the barn owl, and a few distantly related owl species, have evolved a peripheral asymmetry of the external ears that makes the two ears maximally sensitive to sounds from different elevations. In the barn owl, the asymmetry is superficial and limited to the preaural flaps (analogous to pinnae) and the opening of the ear canal (shown in figure 1.4); other asymmetric species, such as the saw-whet owl (*Aegolius acadicus*), have a left-right asymmetry in the skull. The result of this ear asymmetry is that sounds louder in the left ear signal sources below the horizontal meridian while sounds louder in the right signal sources from above. Interaural level difference in asymmetrically eared owls is directly related to sound source elevation.

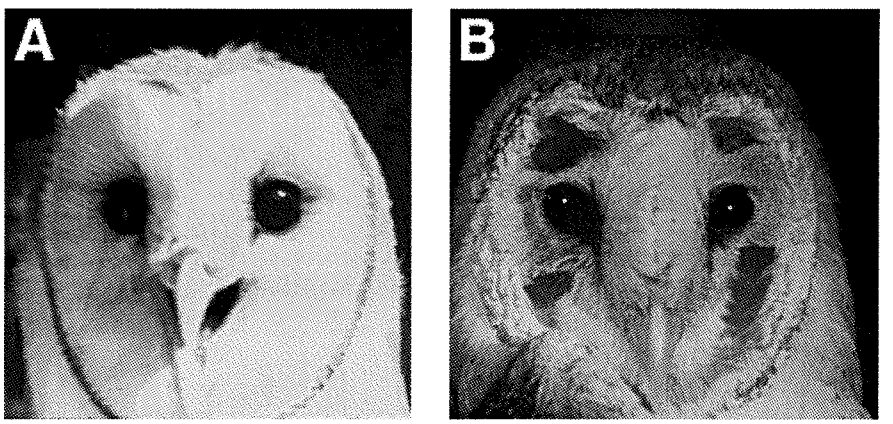

Figure 1.4: Asymmetrical ears in the barn owl. (A) Barn owl with the facial disk intact. (B) The fine feathers of the facial disk have been removed here to reveal the asymmetry in the owl's external ears. The preaural flaps, located laterally of either eye, show a marked vertical asymmetry. The openings of the ear canals (not visible from the front) lie immediately behind the the preaural flaps.

The answer to the second question (how does the owl resolve phase ambiguity at high

frequencies?) lies deep in the neural circuitry of the owl's auditory midbrain. The mechanism which allows the owl to avoid the ambiguity inherent in IPD measurements centers around the integration of multiple narrow band frequency channels to transform the neural representation of IPD into one of ITD. Figure 1.5A shows the response of a model IPD sensitive neuron (also known as a coincidence detector or a narrow band correlator) with a best IPD of 0 cycles and a best frequency of 7kHz; The shaded area indicates the physiological range of ITDs for the owl. The presence of multiple peaks within the shaded region indicates that the output of this neuron can not unambiguously signal interaural time difference. ITDs of -143, 0 and +143 μs, corresponding to sounds from the far left, midline and far right, all generate a maximal response in this neuron.

The response curves shown in figure 1.5B represent the ITD tuning curves for two phase ambiguous auditory neurons with different best frequencies. Inspection of these curves reveals that only one of the multiple peaks in each curve is common to both neurons. This common peak, referred to as the characteristic delay (the delay for which neuronal response is independent of frequency, Rose et al., 1966), represents the true interaural time difference. By comparing the output of two or more coincidence detector neurons, with different best frequencies, higher brain can resolve phase ambiguity. The answer to the second question is that the secret to the owl's ability to resolve phase ambiguity, or transform IPD to ITD or azimuth, lies in the integration of multiple frequency channels.

Of all the species in which sound localization has been studied, phase ambiguity is a behaviorally significant problem only in owls. Most species appear to simply switch to ILD cues when the IPD becomes ambiguous. Interestingly, despite the fact that under natural listening conditions phase ambiguity is not a significant problem for humans, there is psychophysical evidence that humans do have the ability to resolve IPD ambiguity (Trahiotis and Stern, 1989), albeit under non-physiological conditions (*i.e.*, ITDs well beyond the $\pm 700\,\mu s$ naturally experienced by humans).

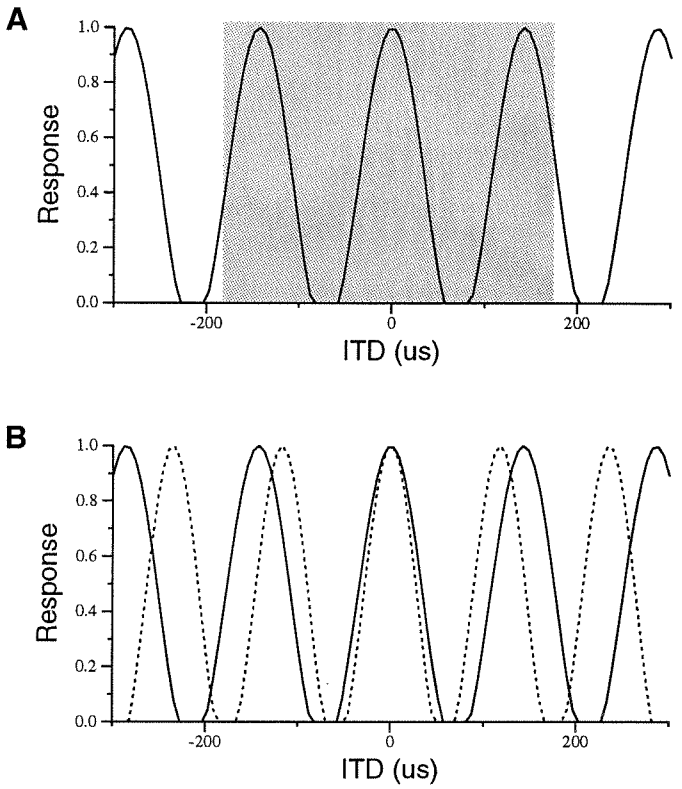

Figure 1.5: Phase ambiguity in ITD processing. (A) ITD tuning for a narrow band cross correlator (*i.e.*, IPD sensitive neuron) with a best frequency of 7.0kHz. The shaded area the range of ITDs experienced by the owl under physiological conditions ($\pm 180\,\mu s$). Multiple peaks in the ITD tuning curve within the physiological range makes the output of this correlator ambiguous with respect to azimuthal location. (B) ITD tuning for 7kHz (solid curve) and 8.5kHz (dotted curve) correlators. Note that only the peak at $0\,\mu s$ is common between the two tuning curves. By comparing the output of the two correlators, ITDs of $0\,\mu s$ can be distinguished from the other phase ambiguous peaks.

Parallel Processing

Sound localization in the barn owl is based on anatomically and physiologically distinct auditory pathways. One pathway is dedicated to the processing of temporal cues, which provide information about the horizontal location of sound sources. The other pathway processes interaural level cues, which, in the owl, are the primary cue for vertical localization. This means that information about the horizontal and vertical position of sound sources is processed separately by the central nervous system. The owl's nervous system combines the output of these two pathways for form space-specific auditory neurons which have spatially restricted receptive fields and are sensitive to both interaural time and level cues.

The remaining chapters of this thesis explore the nature of the neural substrates which underlie the integration of parallel processing streams. In particular, the experiments described here examine how different auditory stimulus features are integrated at the level of the inferior colliculus of the barn owl. In the owl, the inferior colliculus is the site of convergence for at least three parallel auditory processing streams. It is in the colliculus where the pathways responsible for processing time, level, and frequency information converge for the first time to form space-specific auditory neurons.

Chapter 2 The Integration of Parallel Processing Streams in the Lateral Shell Division of the Central Nucleus of the Inferior Colliculus

> True, the compiler of a lexicon or of a system of natural history must be prepared to undertake labor as wearying and as stubborn as the plowman's, but one must not suppose that his work is of secondary importance or that it is in any way as dry and mechanical as it looks when we have it before us in black and white. In this, as in any other sort of scientific work, it is necessary to establish every fact by careful observation, to verify and collate each one, and to separate what is important from what is not.
>
> – Hermann von Helmholtz, *The Relation of the Natural Sciences to Science in General*

The auditory system of the barn owl, *Tyto alba*, displays both peripheral and central evolutionary specializations that allow the owl to accurately localize environmental sounds and to function efficiently within its ethologically defined niche. The barn owl is a nocturnal predator capable of detecting and capturing prey solely on the basis of auditory cues (Payne, 1971). The adaptations of the owl's auditory system are consistent with its natural dependence on sound localization for survival. These adaptations enable the owl to localize sounds over a broad range of frequencies in both the horizontal and vertical planes with a high degree of accuracy (Konishi, 1973b; Knudsen and Konishi, 1979).

The owl, unlike other hearing vertebrates, relies exclusively on binaural cues for sound localization. Interaural time differences (ITDs) are used for localization in the horizontal plane and interaural level differences (ILDs) in the vertical plane. While most vertebrates appear to use ITD for horizontal localization (Heffner and Heffner, 1992), the owl is the only species in which behavioral evidence has been provided for the use of ILD cues in vertical plane localization (Knudsen and Konishi, 1979; Moiseff, 1989). Other vertebrates use both ITD and ILD for horizontal localization, with monaural spectral cues providing vertical plane information. The barn owl is one of a small number of owl species that have evolved a peripheral ear asymmetry that enables them to use level differences for vertical localization (Volman and Konishi, 1990).

In symmetrically eared animals, when a sound source is displaced laterally from the midline, the head shadows the far ear from the source and causes a level difference between the

ears (figure 2.1A). The result of head shadowing is a nearly linear relationship between ILD and azimuthal position at high frequencies. At low frequencies, when wavelength exceeds head diameter, the head does not cause significant attenuation and ILD cues can not be used for horizontal localization.

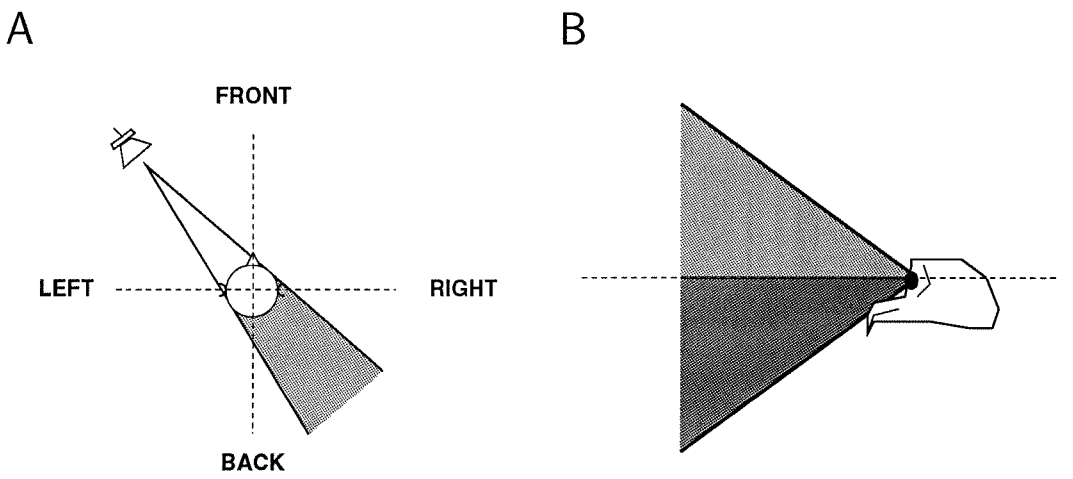

Figure 2.1: ILD in symmetrically and asymmetrically eared animals. (A) The figure shows the geometry and acoustics of a horizontally positioned sound source for a symmetrically eared animal, as viewed from the top. In these conditions, a sound source displaced horizontally from the midline places the far ear in an acoustic shadow formed by the volume of the head, indicated by the shaded region. (B) In the barn owl, an asymmetry in the external location of the ear flaps and auditory meatus have the result that ILDs primarily occur when the sound is displaced vertically. The side view of the barn owl's head, without feathers, indicates the region of maximum sensitivity for the left (dark grey) and right (light grey) ears.

In the barn owl an ear asymmetry exists in the preaural flaps (analogous to the mammalian pinnae) and the superficial location of the entrance to the ear canal. In all hearing animals, the ears act as efficient and somewhat directional sound collectors. The left-right asymmetry in the owl changes the axis of maximum sensitivity for each ear making the left ear maximally sensitive to sounds from below and the right ear sensitive to sounds from above the horizontal meridian, as shown in figure 2.1B. By comparing sound intensities between the two ears, each with their different acoustic foci, the owl is able to accurately localize in elevation (Payne, 1971; Konishi et al., 1988; Knudsen et al., 1991).

Much of the midbrain and brainstem circuitry subserving sound localization in the owl

has been described at the anatomical and physiological levels. Sound source location is represented in the external nucleus of the inferior colliculus (ICx) in the form of a topographic map of auditory space, as first described by Knudsen and Konishi (1978b). This "centrally synthesized" map is similar to the topographic maps in the visual or somatosensory systems in that the sounds are systematically represented in the map by the spatial locus of neural activity (Konishi, 1986). The map is, however, in many ways more analogous to maps of orientation tuning in the visual forebrain areas (Hubel et al., 1978; Pettigrew and Konishi, 1976) because, like orientation in the visual system, information about spatial location is not present in the primary representation of incoming sounds. This information must be computed by the central nervous system from the spectral representation presented by the cochlea.

Spatial representations in the visual system are inherent in the representation presented by the retina to the visual areas of the central nervous system. In contrast, the cochlea decomposes incoming sounds into individual frequency components using a bank of narrow band hydromechanical filters arranged lengthwise along the basilar membrane. The representation of sounds provided to the nervous system is one based on frequency, and not on space. The distribution of activity along the basilar membrane represents an approximation of the power spectrum for sound signals impinging on the ears and not spatial position.

Information about spatial position, however, is available in the cochlear output, but it is encoded in the firing patterns of individual auditory nerve (nVIII) fibers and must be computed downstream by the central nervous system. Spatial information is represented using rate and time codes in the peripheral auditory system, instead of the place code used by the peripheral visual and somatosensory systems. The term "centrally synthesized" refers to the fact that the central nervous system must derive source location computationally by analyzing the temporal structure in the action potential trains carried by the eighth nerve.

In the case of the barn owl, the synthesis of an auditory space map is the result of a two step process, each of which can itself be considered as a central synthesis operation. The first step consists of deriving ITD and ILD from the spiking patterns of the auditory nerve; this operation is fairly well understood at both anatomical and physiological levels. The auditory nerve bifurcates and forms two independent pathways, one for processing time cues and

one for level cues. In recent years, the anatomical connectivity of the time and intensity pathways has been well described (Takahashi et al., 1984; Takahashi and Konishi, 1988a, 1988b; Adolphs, 1993a, see Konishi et al., 1988 for a complete review), and a complete connectivity diagram of the two pathways is shown in figure 2.3.

Interaural phase difference (IPD) is computed using a coincidence detection circuit, as first proposed by Jeffress (1948). The coincidence detector transforms the phase locked action potentials of the auditory nerve from a time code into a place code. Carr and Konishi (1990) demonstrated that in the barn owl, the site of coincidence detection is nucleus laminaris (NL, homologous to the mammalian medial superior olive, MSO). NL is a bilaterally innervated brainstem structure which receives afferent input from both the ipsi- and contralateral ears via nucleus magnocellularis (NM). Like the auditory nerve fibers, NM neurons phase lock to auditory stimuli. Each laminaris neuron fires maximally when the arrival times of ipsi- and contralateral inputs are simultaneous. Axonal delay lines are used to systematically delay the arrival time of impulses from one ear. Delaying input from the left ear makes the response in NL maximal when the sound at the left ear leads that at the right ear by an amount equal to the length of the delay line. The length of these delay lines are organized systematically along the dorsal-ventral axis of laminaris (Carr and Konishi, 1990) resulting in a systematic map of IPD within laminaris.

Interaural level differences are computed by an anatomically separate circuit originating with the other branch of the auditory nerve (Takahashi and Konishi, 1988a). Neurons of nucleus ventralis lemnisci lateralis, pars posterior (VLVp) receives excitatory input from nucleus angularis (NA), which encodes sound intensity in the form of spike rate and inhibitory input from the contralateral VLVp (Takahashi and Keller, 1992). This combination of excitatory input from the ipsilateral ear and inhibitory input from the contralateral VLVp provides the substrate for computing interaural level difference (Manley et al., 1988; Adolphs, 1993b; Mogdans and Knudsen, 1994).

Both NL and VLVp project to the inferior colliculus, where the second step, the integration of interaural phase/time and level information, occurs to generate spatially restricted auditory receptive fields. This integration process is somewhat complicated by the fact that single NL and VLVp neurons are incapable of uniquely representing the azimuth and ele-

vation of a sound source.

Laminaris neurons operate as time-domain coincidence detectors with a narrow input bandwidth; because of the narrow input bandwidth, single NL neurons can only signal interaural phase differences. This means that they respond equivalently to time delays differing by integer multiples of their best frequency. In spatial terms, this means the output of single NL neurons can not unambiguously encode the azimuthal location of a sound source (figure 2.2A). Further computation is required to convert IPD sensitivity into tuning for single azimuthal positions.

A similar limitation exists in the output of single VLVp neurons. These neurons do not directly encode the elevation of a sound source, but only coarsely signal its limits. VLVp neurons have sigmoid ILD tuning curves, corresponding to spatial receptive fields sensitive to sounds from above or below a particular elevation (figure 2.2B). Space specific neurons in ICx respond to a restricted range of ILDs, corresponding to a single elevation (Knudsen and Konishi, 1978b).

The generation of proper space-specific cells, selective for the combination of a single azimuth and single elevation, therefore, requires additional computations beyond the simple combination of time and intensity information. The output of NL must be "post-processed" to eliminate phase ambiguity, and the sigmoid ILD tuning observed in VLVp must be transformed into the peaked ILD tuning associated with the space-specific cells of ICx. Those post-processed outputs must then find their way to single ICx neurons. These computational steps are depicted schematically in figure 2.2C.

The phase ambiguous neurons of nucleus laminaris make an efferent projection to the Core division of the central nucleus of the inferior colliculus. Core neurons exhibit the same tuning properties and IPD sensitivity observed in NL (Fujita and Konishi, 1991). The phase ambiguous time pathway and sigmoid-tuned ILD pathway converge in the lateral shell of the central nucleus of the inferior colliculus (LS) which receives projections from both Core and VLVp. LS neurons are the first auditory neurons to receive both time and intensity input. LS projects primarily to the space specific neurons in ICx, though there is a weak ascending projection to the auditory thalamus, nucleus ovoidalis (Proctor, 1993). The role performed by LS is threefold. First, LS neurons eliminate phase ambiguity by integrating the activity

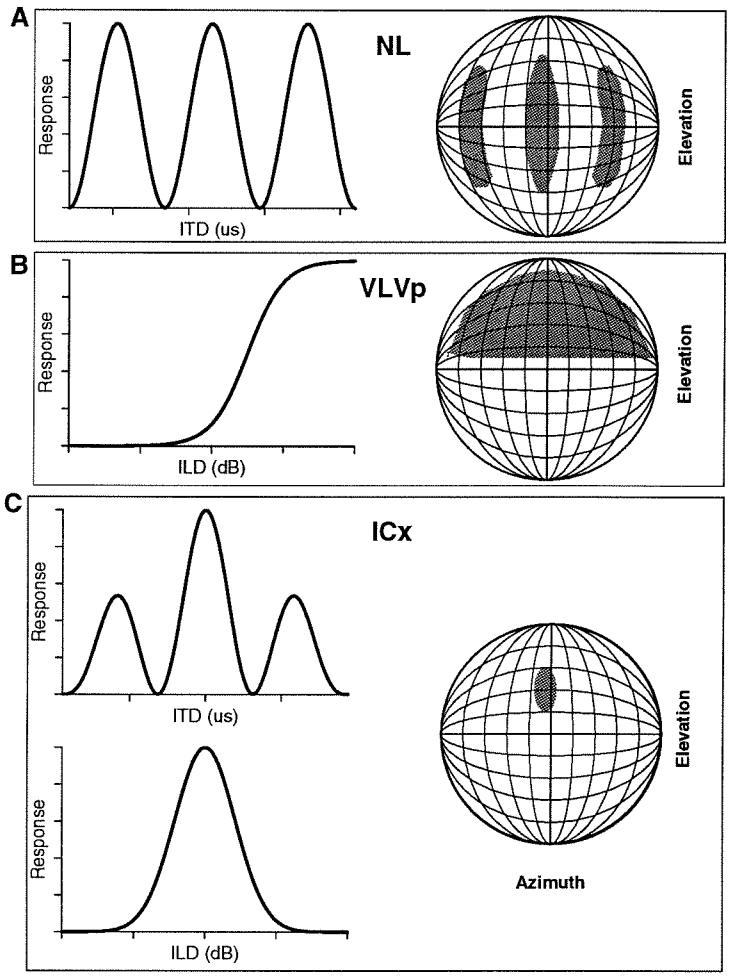

Figure 2.2: Schematic ITD and ILD tuning properties for ICx and afferent nuclei. Each plot on the left indicates either an ITD or ILD tuning curve typical of the indicated nucleus. Globes on the right represent the auditory space around the owl's head. Shaded areas indicate spatial receptive fields for neurons with tuning curves like those shown on the right. (A) ITD tuning in NL is phase ambiguous, meaning that a single neuron can not unambiguously encode a particular ITD. This corresponds to a multi-lobed spatial receptive field. (B) ILD tuning in VLVp is sigmoid, which means that the activity of a single neuron potentially represents a large range of ILD values. Spatially, this corresponds to a receptive field signaling sounds from above or below a particular elevation; the actual elevation is related to the 50% point of the sigmoid ILD tuning curve. (C) ICx neurons encode true interaural time differences and have peaked ILD tuning curves, resulting in selectivity for a single position in space.

of the narrow band, IPD sensitive Core neurons across frequency channels. The process of combining multiple frequency channels to eliminate phase ambiguity is commonly referred to as sidepeak suppression (SPS), since it has the effect of reducing the height of the phase ambiguous side peaks in ITD tuning curves (compare ITD tuning curves in figures 2.2a and c). Second, the LS transforms the sigmoid ILD tuning curves observed in VLVp into peaked tuning curves (compare figures 2.2b and c). Finally, the two processing streams are combined with the final result being single neurons with receptive fields restricted in both azimuth and elevation.

For some time now, the computational requirements of LS have been fairly well understood (Wagner et al., 1987). The details of the neuronal substrates subserving these computations have yet to be fully characterized. Traditionally, LS has been considered to be a simple non-linear relay station in the localization system. In this model, it receives phase ambiguous IPD and sigmoid ILD inputs and combines them using a neuronal circuit analogous to an AND gate. A simple model of this sort of one-step integration leading to sidepeak suppression is shown in figure 2.4A. In this model, a large number of narrow band Core neurons synapse onto single LS neurons, whose outputs are a non-linear, though relatively simple, combination of the inputs.

The physiological data presented here and elsewhere (*e.g.*, Takahashi and Konishi, 1986) indicate that the operation performed by LS is not a simple one-step integration, but instead that the output of LS is computed by extensive local circuitry within the shell. This local circuitry appears to be arranged in a hierarchically fashion, both physiologically and anatomically. Sidepeak suppression, for example, does not occur in an all-or-none fashion, but rather appears to emerge as the result of a series of processing steps arranged across the mediolateral axis of LS (figure 2.5). A model of this hierarchical organization for the time pathway is shown in figure 2.4B for comparison to the one-step model. The final output of this circuit is similar to that of the one-step model; however, it postulates a class of intermediate neurons, with tuning properties intermediate between those observed in Core and ICx. Moreover, the model makes predictions as to what the tuning properties of these intermediate neurons should be, providing a testable hypothesis.

The approach described here relies upon conventional electrophysiological mapping tech-

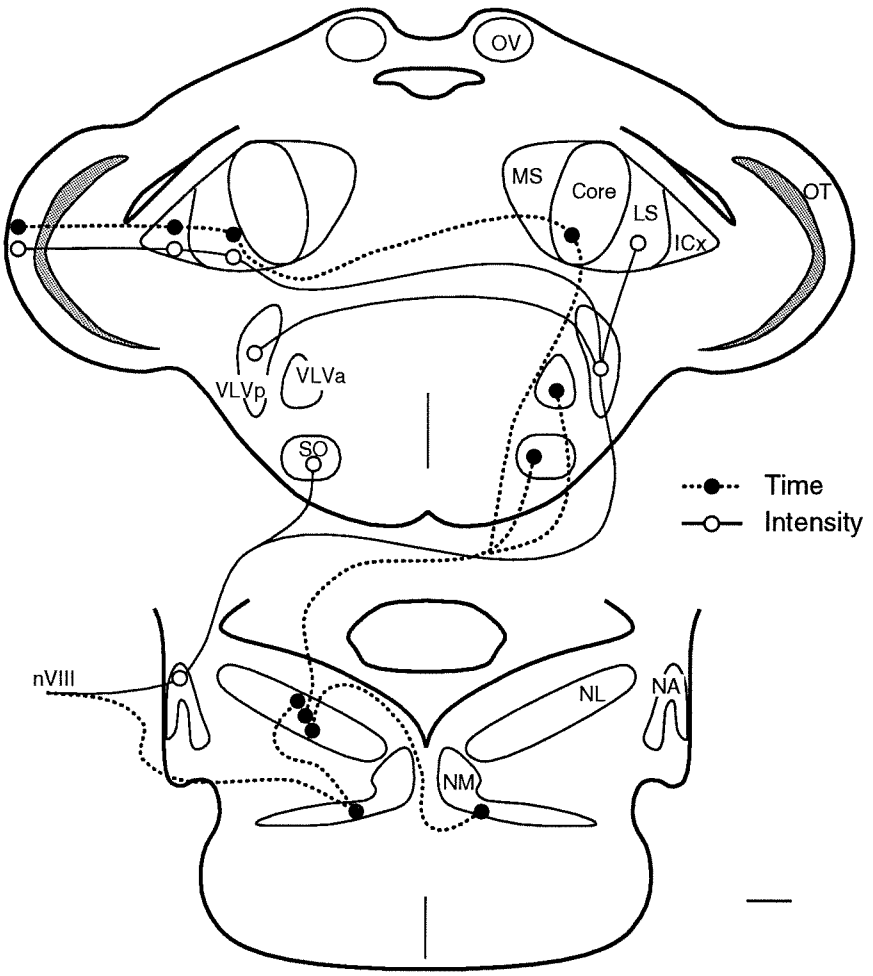

Figure 2.3: Gross anatomy of the time and intensity pathways. The two parallel pathways for computing time and intensity processing (dashed and solid lines, respectively) are shown on camera lucida drawings of transverse sections from the owl's midbrain (top panel; anterior) and brainstem (bottom panel; posterior). Scale bar in lower right is 1mm. Only one of each pair of bilaterally symmetric nuclei is labeled. Abbreviations: nVIII, auditory nerve; NL, n. laminaris; NM, n. magnocellularis; MS, medial shell of the central n. of the inferior colliculus (ICc); Core, core division of ICc; LS, lateral shell division of ICc; ICx, external n. of the inferior colliculus; OT, optic tectum; OV, n. ovoidalis.

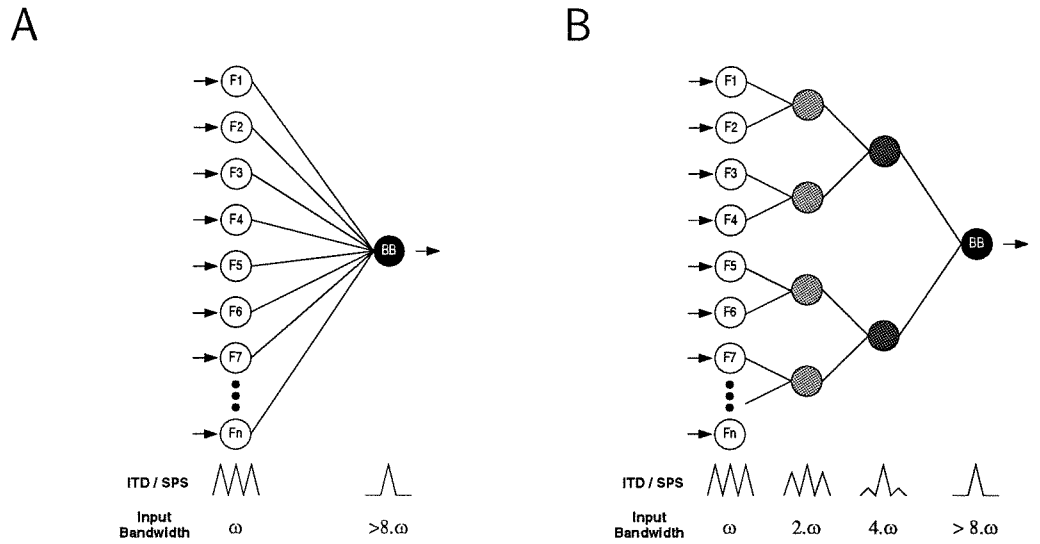

Figure 2.4: Models of frequency convergence for the elimination of phase ambiguity. Lower inset graphs schematically represent sidepeak suppression in the form of ITD tuning curves. ω indicates the bandwidth of the afferent inputs to LS, which generally have frequency tuning widths of about 1.5-2kHz. (A) One-step model: A large number of narrow band, phase ambiguous inputs Core (F1..Fn), with a large distribution of best frequencies synapse onto a single LS or ICx neuron with broadband frequency tuning (BB) which, as a result of this cross-frequency integration, is sidepeak suppressed. (B) Cascade model: Small clusters of narrow band neurons project to "higher" level neurons, which in turn cluster and project to the next level. At each level both input bandwidth and sidepeak suppression increases. The final output, as in A, has broadband frequency sensitivity and is sidepeak suppressed.

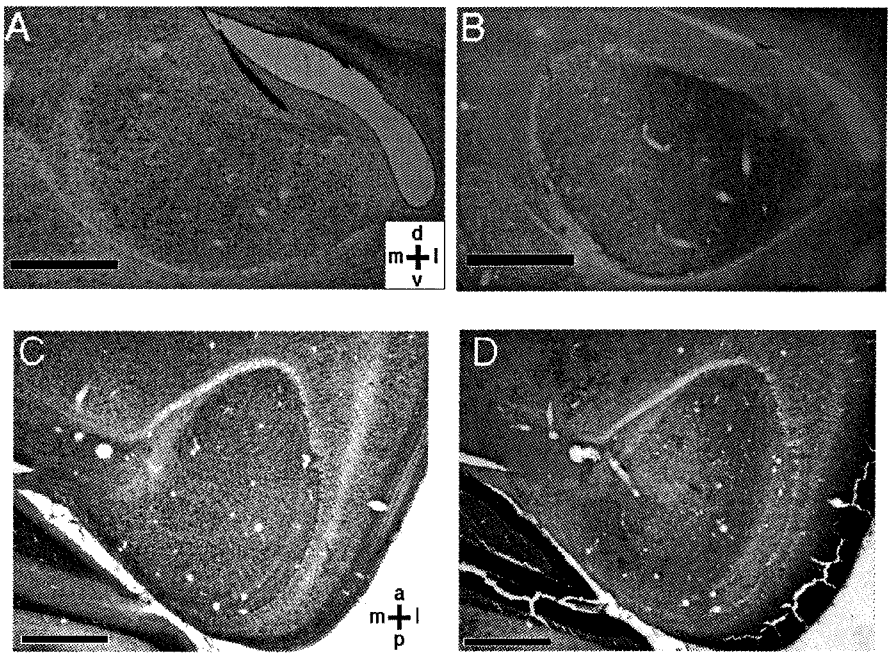

Figure 2.5: Anatomical localization of the lateral shell. Acetylcholinesterase (AChE) activity is a marker for the intensity pathway in the barn owl (Adolphs, 1993a). AChE delineates the border between Core and LS, with Core being AChE-negative and LS being AChE-positive. (A) Cresyl violet stained transverse section through IC. (B) Adjacent section stained for AChE. (C) Cresyl violet stained horizontal section through IC. (D) Adjacent section stained for AChE. (scale bars = 1mm)

niques using single neuron recordings to examine the relationship between the tuning properties of LS neurons related to sound localization and anatomical location of these neurons within the inferior colliculus. The ultimate goal of this work is to define the nature of the lateral shell's neural circuitry and to understand how this circuitry subserves the computational requirements of generating auditory neurons with spatially restricted receptive fields.

2.1 Methods

2.1.1 Surgical Procedures

Eight adult barn owls weighing 450–550g were used for this study. Owls were housed individually in cages before and after all experiments.

Prior to the first recording session, animals were prepared for electrophysiology. Animals received no food for 12 hours prior to any procedure requiring general anesthesia. Animals were anesthetized by intramuscular injections of Ketamine-HCl (25mg/kg; Ketaset, Fort Dodge) and Diazepam (1.3mg/kg; Steris) into the pectoral muscles. This initial dose was supplemented, if necessary, with additional Ketamine (15mg/kg/h). The owl was wrapped in a soft leather jacket and the feathers covering the top of the head were removed with scissors. The owl was placed in a custom made stereotaxic frame with the palatine ridge tilted 45° downward from horizontal. The scalp was cleaned with alcohol wipes and treated with topical anesthetic (Xylocaine, Astra). A 3cm incision in the scalp was made over the midline and the skin and fascia retracted. A flat surface was made using rongeurs at the anterior extent of the incision in order to affix a stainless steel headplate. The headplate was attached to the skull with dental acrylic (Perm Rebase Corp.) and a small metal pin (0.25mm diameter) was attached to the bone with methyl acrylic glue at the intersection of the midline and the interaural axis to serve as a reference mark. The exposed bone was cleaned, antibiotic ointment (Bacitracin-Neomycin, Fougera) was applied, and the wound was closed with sutures around the headplate.

The owl was gently restrained in a soft towel and returned to a dark, heated cage for recovery. Each owl was monitored continuously until it was able to maintain balance on a perch, at which point heat was removed and fresh food supplied. Food intake was monitored carefully following surgery, and owls usually began eating within 5 hours of recovery; all ate within 1-2 days.

Recording sessions began a minimum of 3-5 days after headplate implantation. Anesthesia was induced and maintained as described above. Animals were weighed and given subcutaneous fluids (5% Dextrose in Lactated Ringers, 20ml/kg). Owls were placed in a stereotaxic apparatus and secured by the headplate. Body temperature was maintained at 40C with a heating jacket (Baxter). Custom made earphone assemblies (see below) were inserted into the auditory meatus to a depth of approximately 0.5cm. Following application of topical anesthetic, sutures were removed and the scalp retracted. A small (12x12mm) craniotomy was made overlying IC. A microelectrode was positioned relative to the reference pin with an accuracy of $\pm 10\mu m$. The *dura mater* directly below the microelectrode was punctured with a sharp needle and the electrode was advanced into the brain by an electronically controlled stepper motor (μD-100, Beckman Electronics).

Recording sessions lasted 8-15 hours, following which the craniotomy was sealed with a layer of dental acrylic. Antibiotic ointment was applied to the exposed skull, the wound was sutured closed and topical anesthetic was applied to the area around the incision. The owl was returned to its cage and monitored as described above. The health of each animal was determined by monitoring daily food intake, activity levels, general appearance and body weight. Experiments were repeated an average of every 4-6 days, over a period of several weeks. The interval between experimental sessions was extended if the animal exhibited any form of anorexia or a significant reduction in body weight.

In two of the eight owls the forebrain immediately overlying the inferior colliculus was removed by aspiration at the beginning of the final experimental session. At the beginning of these experiments, a suction probe, made from a 21G needle was used to remove a column of forebrain approximately 1-2mm in diameter, and 10mm deep. This exposed the optic lobe directly over the colliculus, allowing for direct visualization of the electrode positions (relative to the midbrain). This allowed for more accurate electrode positioning and enabled

a more complete electrophysiological coverage of LS and ICx during the subsequent mapping.

2.1.2 Acoustic Stimuli

Experiments were performed in either a double walled sound-attenuating chamber or a double walled anechoic chamber (Industrial Acoustics Corp.).

Acoustic stimuli consisted of pure tone, broadband (0-13kHz) and band limited noise bursts of variable ILD and ITD. Stimuli were 100ms in duration, 5ms linear rise/fall times, presented 1 per second. Stimuli were synthesized on a computer workstation (Sparc/IPX, Sun Microsystems), presented through a digital signal processor equipped with a 16bit, 48kHz data acquisition subsystem (S56X+ProPort-656, Berkeley Camera Engineering). Analog signals were attenuated with a pair of digitally controlled attenuators (PA4, Tucker Davis) to control ILD and overall stimulus level, amplified (Power Amp, Beckman Electronics), and presented to the owl dichotically through custom made earphone assemblies. ILD could be specified in 1dB increments and ITD in 5 μs increments.

Earphone assemblies consisted of level- and phase-matched earphones (Sony MDR-E535 or Koss LS/6) attached to a 3cm metal delivery tube (25mm ID). Each tube contained a small calibrated probe microphone (Knowles-3033) designed to measure sound pressure levels at the end of the delivery tube. At the beginning of each experimental session, the earphone assemblies were calibrated using the probe microphones. The calibration data were used during the experiment to adjust the computer output to effect a nominally flat frequency response ($\pm$6dB) from 0.5-13kHz.

In one owl, sound pressure levels were also measured close to the tympanic membrane using a calibrated 2mm probe tube attached to a $\frac{1}{2}$-inch condenser microphone (Brüel&Kjær-4133). A small hole was made on the ventral border of the squamosal bone and the probe tube inserted under visual guidance. The end of the probe tube was positioned 1–2mm from the tympanic membrane. The dichotic earphone assemblies were then inserted as described above. The calibration procedure was repeated using both the Knowles and Brüel&Kjær microphones. Differences between the two calibrations were limited to a frequency inde-

pendent attenuation indicating that calibrations based solely on the Knowles microphone were sufficient for the purposes of this experiment.

2.1.3 Data Collection

Isolated neurons were recorded from extracellularly in LS and ICx with either tungsten or glass microelectrodes (tungsten, 250 μm, 12MΩ, AM Systems; glass, 10–15 μm tip diameter, 4M K-Acetate, 0.5-1.5MΩ). Signals from the electrode were amplified (100–1000 times), filtered (0.3–10kHz) and discriminated with a level detector (μA-200, Beckman Electronics). The level detector output was recorded by the computer system (21 μs resolution). In some cases, analog records were also recorded (48kHz, 16bits) and an online spike sorting algorithm (Lewicki, 1994) was used to extract single unit data from multi-unit clusters.

Broadband noise (ILD=0dB, ITD=0 μs) was used as a search stimulus. LS and ICx were located stereotaxically. LS and ICx neurons were classified as such based on a combination of stereotaxic position and physiological tuning properties (Takahashi and Konishi, 1986; Wagner et al., 1987).

Isolated cells were first characterized manually to determine approximate values for best ILD, ITD and frequency. Tuning curves for ILD, ITD and frequency were then collected holding the non-varying stimulus parameters constant, usually at optimal values. Tuning curves were measured at a constant average binaural intensity (ABI, $(I_L + I_R)/2$) of 20dB above threshold and averaged over 4-6 repetitions.

In addition to ILD tuning curves at constant ABI, for some neurons a "fixed-ILD" tuning curve was also collected. For fixed-ILD curves the intensity at one ear was held constant, while the intensity at the other ear was varied. Unless otherwise noted, ILD tuning curves presented here are of the constant-ABI variety.

For generating tuning curves, neuronal responses were calculated as the number of action potentials occurring in a time window extending from stimulus onset to 20ms after stimulus offset. Spontaneous activity was characterized by counting the number of action potentials occurring in the same time window for "spontaneous trials" (no stimulus occurring),

which were randomly interleaved with stimulus trials.

For the purposes of computing response latencies, a 100ms window of undriven activity, immediately preceding the onset of each stimulus, was used to characterize spontaneous activity.

At the end of a set of experiments, small electrolytic lesions were made (-2 μA, 10-15s) in order to identify recording sites. Lesions were usually made only on the last or second to last recording session, because it is difficult to recover small electrolytic lesions in owls after survival periods longer than 7–10 days. In a few owls, small iontophoretic tracer injections of biotin-dextran (10kD, Sigma) or flourscent-dextran (3kD, Molecular Probes) were place physiologically in the lateral shell for anatomical studies, usually during the last experimental session. Tracer injections provided additional histological confirmation of recording sites.

2.1.4 Data Analysis

Latency Measurements. The response latency of each neuron was calculated using a procedure similar to that described by Maunsell and Gibson (1992). In brief, for each neuron, a compound peristimulus time histogram (PSTH) was computed by collapsing all available tuning curves into a single PSTH (0.5ms bins) aligned with the stimulus onset. The number of trials incorporated into a compound PSTH depends upon how many tuning curves were collected for a particular neuron. At least two tuning curves were collected for all cells reported here, corresponding to a minimum of 128 trials of 300ms duration per compound PSTH.

For each compound PSTH, the distribution of spike rates in the 100ms prior to stimulus onset was used to compute two criterion levels ($p < 0.01$ and $p < 0.05$). Response latency was defined as the first bin following stimulus onset in which that bin and the following bin exceeded the $p < 0.01$ criterion and the next following bin exceeded the $p < 0.05$ criterion. This defines response latency as the first time at which the spike rate exceeds the spontaneous rate with statistical confidence for a duration of 1.5ms.

Frequency Tuning. Frequency tuning curves were characterized by their half-width

(denoted $F_{1/2}$) and best frequency (BF). $F_{1/2}$ is defined to be the range of frequencies over which the cell's response was greater than or equal to half the maximal tone response. Best frequency is usually defined to be the frequency that elicits the maximal response in an iso-intensity frequency tuning curve. However, ICx cells often exhibit broad frequency tuning with no clear single peak. For this reason, best frequency (BF) was defined to be the center of the range described by $F_{1/2}$ (figure 2.6A). For symmetric, peaked tuning curves the definition used here is essentially the same as the traditional one. In the case of broadly tuned non-peaked, or asymmetric, curves, the definition used here provided a better estimate of the center of the frequency range capable of driving a cell. This is similar to the median frequency (MF) described by Yin et al. (1986) for synchronization-rate tuning curves.

ITD Tuning. Three parameters were extracted from ITD tuning curves: best ITD, ITD tuning width ($ITD_{1/2}$) and degree of side peak suppression (%SPS) in response to broadband noise stimuli (figure 2.6B).

The best ITD or main peak (MP) is defined as the time difference required for a broadband noise stimulus to generate a maximal neuronal response. For phase ambiguous neurons the best ITD was defined by the neuron's characteristic delay (CD). CDs were estimated by collecting ITD tuning curves using pure tone stimuli of several different frequencies spanning the neuron's input bandwidth. These pure tone responses were used to estimate the neuron's characteristic delay as described by Rose et al. (1966). Sharpness of ITD tuning, $ITD_{1/2}$, was determined by calculating the width of the main peak at the half-maximal response level.

An index of side peak suppression (%SPS) was calculated as:

$$\%\text{SPS} = 100 \times (MP - \overline{SP})/(MP),$$

where MP is the response at the main peak and $\overline{SP}$ is the mean of the responses at both the left and right flanking side peaks. %SPS ranges from 0, for phase ambiguous cells, to 100 for cells exhibiting complete suppression.

ILD Tuning. ILD sensitive neurons fell into one of three categories: peaked (P), open-peaked (OP) or sigmoid (SIG). ILD tuning curves representative of each category are shown

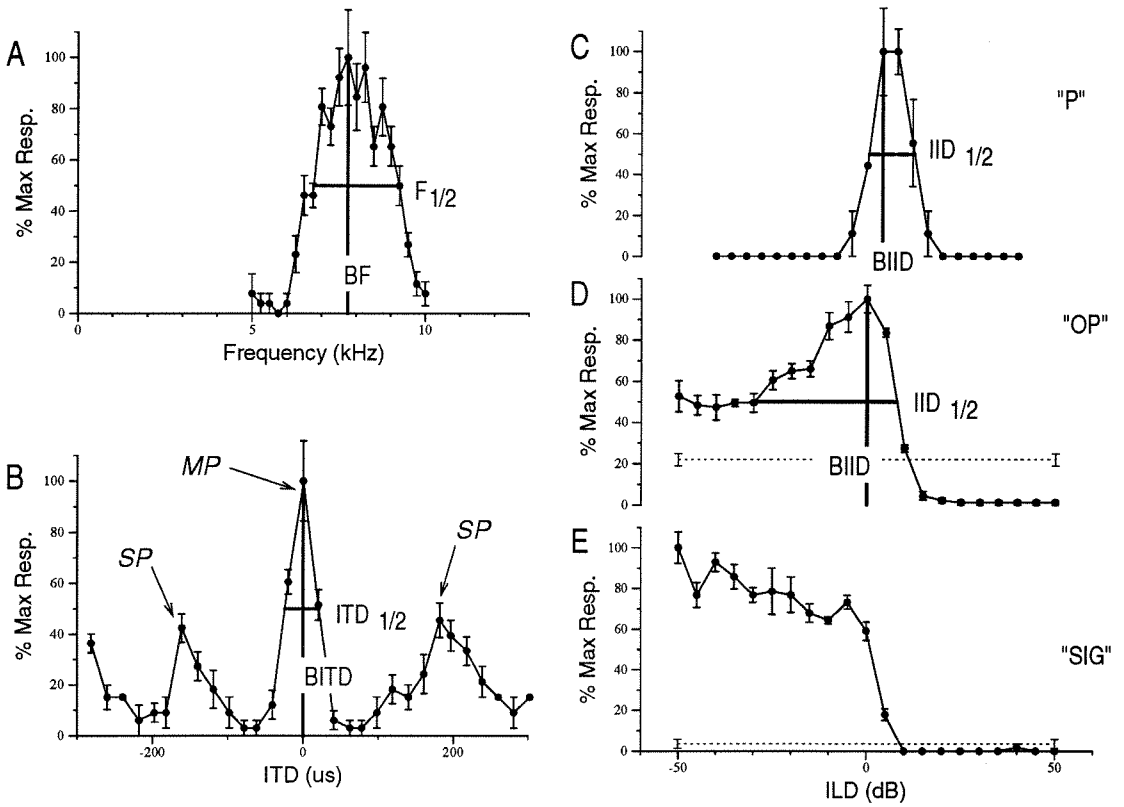

Figure 2.6: Typical tuning curves from IC. Each panel represents a typical tuning curve from cells described below along with a representation of the metrics used to parameterize each curve. Solid lines and filled circles indicate mean neuronal responses, with error bars indicating the standard error of the mean (SEM). Dashed horizontal lines show the mean level spontaneous activity and the heavy lines indicated metrics described in the text. (A) Iso-intensity frequency tuning curve with BF and $F_{1/2}$ indicated. (B) Interaural time difference tuning curve. *MP* and *SP* arrows indicate the positions of the main and side peaks, respectively, used to compute %SPS. A-E Three classes of interaural level difference tuning: (C) peaked, (D) open-peaked and (E) sigmoid.

in figures 2.6c-e. For peaked and open-peaked neurons, the best ILD and width at half-height ($ILD_{1/2}$) were calculated as shown in figures 2.6c and d.

For most cells, the shape of the ILD tuning curve was further quantified by computing a symmetry index, *S*, which represents the difference in areas under the left and right halves of each ILD tuning curve (relative to the best ILD), normalized by the total area under the ILD curve. The value of S can be expressed analytically as the ratio:

$$S = \frac{|\sum_{i<0} R(i) - \sum_{i>0} R(i)|}{\sum_{i} R(i)},$$

where $R(i)$ is the ILD tuning curve of a neuron fit with a smooth cross-validated spline function (Splus, StatSci). For a peaked tuning curve resembling a Gaussian the symmetry value (S) will be zero, while for a sigmoid or step function S is 1.

2.1.5 Histology

Following recording sessions and tracer injections, owls were overdosed with pentobarbital (60mg/kg; Nembutal, Abbott Laboratories) and then perfused transcardially with 0.9% saline in 0.1M phosphate buffer (PBS, pH 7.3) at 40C followed by ice-cold 4% paraformaldehyde in 0.1M PBS containing 18g/l L-Lysine and 2.2g/l $NaIO_4$ (pH 7.3) for fixation. Following fixation, the brain was blocked stereotaxically in a plane parallel to that of the electrode penetrations. The brain was removed and placed in a 30% sucrose/paraformaldehyde solution to sink. Brains were then embedded in a 30% sucrose/gelatin block and 30 μm transverse sections were cut frozen on a sliding microtome. Every third section was stained with cresyl violet. In most owls, one set of intermediate sections was also stained for acetylcholinesterase (AChE) activity to delineate the anatomical boundary between Core and LS (Karnovsky and Roots, 1964; Adolphs, 1993a).

2.2 Results

The results reported here were collected from 423 well isolated single neurons located in the LS and ICx regions of the inferior colliculus. For some of the 423 neurons, not all tuning parameters were collected. As a result, the number of cells in the distributions described here can contain less than 423 neurons; in such cases, the number of neurons used to compute each histogram or statistic is reported with the results.

Response Latency. The distribution of response latencies for neurons in LS and ICx is shown in figure 2.7A. Of the 423 cells described here, accurate latency measurements were possible for all but three neurons, in which the magnitude of the auditory response was insufficient to exceed the $p < 0.01$ criterion of Maunsell and Gibson (1992). Of the remaining 420 neurons, response latency ranged from 2.5ms to 22.0ms, with only 2 neurons having latencies greater than 16ms. The distribution is unimodal with a median value of 6.2ms (7.1ms mean). A slight tendency towards latencies longer than the median is visible in the histogram.

Response latency increases monotonically as a function mediolateral position in the colliculus. Medially positioned neurons, corresponding to neurons close to the Core/LS boundary, exhibit the shortest latencies, while neurons on the LS/ICx boundary have the longest latencies. This relationship is shown in figure 2.7B.

Figure 2.7C shows the distribution of recording sites across the mediolateral axis of the colliculus. There is a slight sampling bias favoring neurons located more laterally. Though from 3.5-6.0mm, an area which covers most of the LS, the distribution is relatively uniform.

Frequency Tuning. Figure 2.8A shows the distribution of best frequencies recorded throughout LS. The histogram shows a distribution with a median best frequency of 6.8kHz (7.0kHz mean). Of all neurons studied here 62.6% had BF values between 6.0 and 8.0kHz. This corresponds to the frequency range in which the barn owl's localization behavior is the most accurate (Konishi, 1973b).

The width of a neuron's iso-intensity frequency tuning curve, $F_{1/2}$, reflects the excitatory input bandwidth of the neuron. $F_{1/2}$ ranged from 0.3 to 7.9kHz, with a median value of 2.3kHz (2.6kHz mean, figure 2.8B). This represents an increase in input bandwidth over

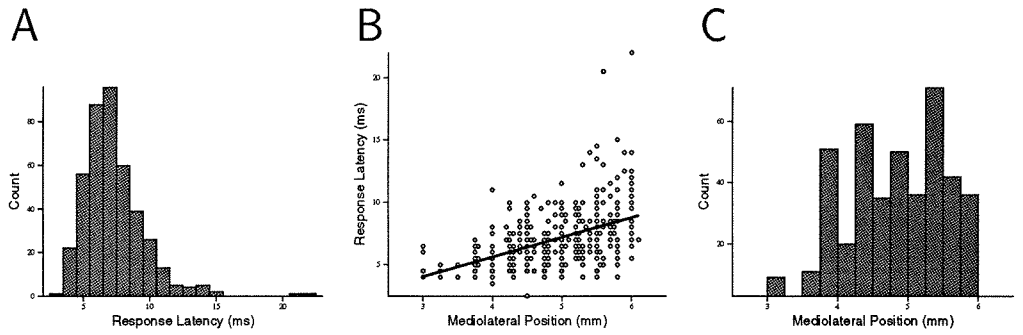

Figure 2.7: Response Latencies in LS and ICx. (A) Histogram indicates the distribution of response latencies observed in the population of LS and ICx neurons (n=420, binwidth 1 ms). (B) Response latencies are plotted as a function of mediolateral (ML) position of the recording site (n=420). ML position is defined as the distance from the midline. The solid line indicates linear regression ($r = 0.49$, $p < 0.0001$). (C) Histogram shows the distribution of recording sites across the mediolateral aspect of the colliculus (binwidth 0.25 mm).

NL and Core neurons, where the average $F_{1/2}$ values are about 1.5kHz (Fujita and Konishi, 1991).

There is a weak, though statistically significant correlation between BF and $F_{1/2}$ ($r = 0.01$, $p = 0.0114$). A correlation between BF and $F_{1/2}$ is expected for a system based on constant-Q filters, in which the ratio of BF to $F_{1/2}$ is constant. There is evidence that the auditory system operates in this fashion from psychophysical studies of the mammalian auditory system (Greenwood, 1961). There is also evidence that the arrangement of the owl's auditory filters may be somewhat different from that observed in mammals (Klumpf and Köppl, unpublished observations).

Best frequency is not correlated with mediolateral position within IC (figure 2.9A). In contrast, $F_{1/2}$ is highly correlated with ML location (figure 2.9B). Though there is a considerable amount of scatter visible in figure 2.9B, it is clear that close to the medial margin of LS broadly frequency tuned neurons are rare, while more laterally, towards ICx, broadband neurons appear more frequently. The observed correlation between $F_{1/2}$ and mediolateral position is consistent with a model in which laterally located broadband neurons receive synaptic connections from several medial narrow band neurons with different best frequencies.

Interaural Time Differences. In order to combine the data collected in both the right

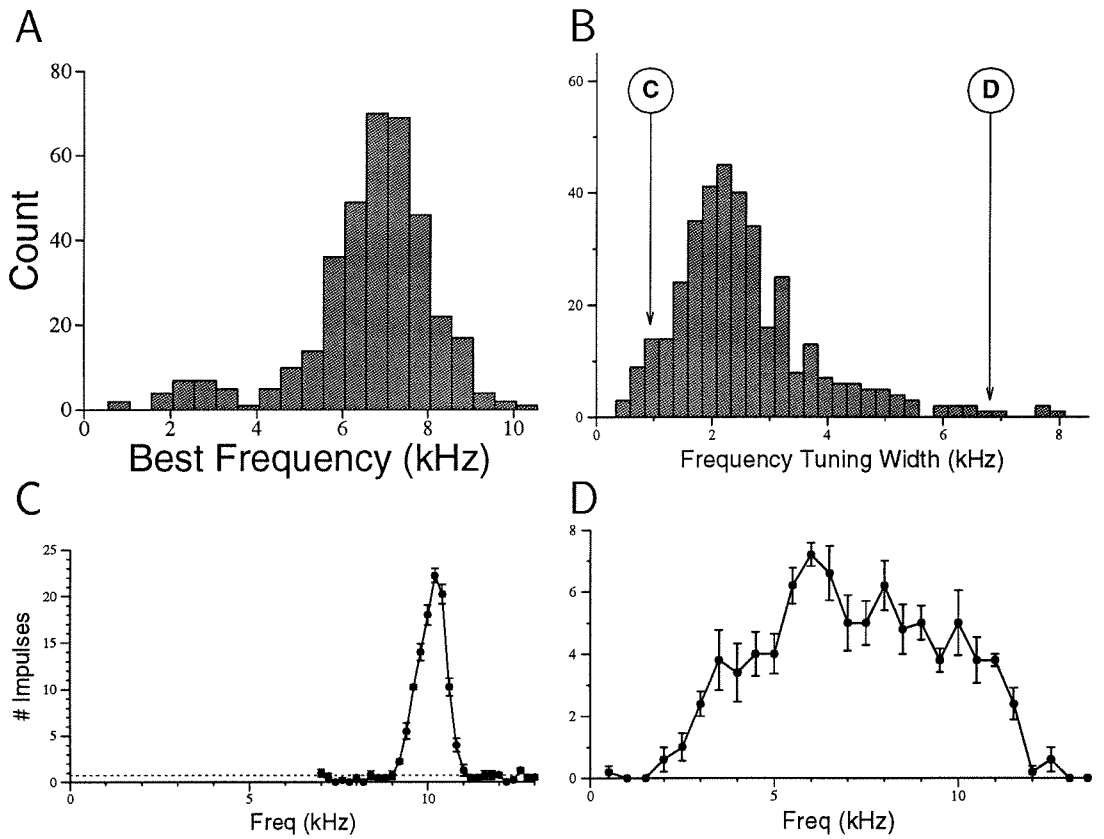

Figure 2.8: Distribution of frequency tuning. (A) Best frequency (n=374, binwidth 0.5 kHz). (B) $F_{1/2}$, tuning width at half maximal response (n=374, binwidth 0.25 khz). Circled letters mark locations in the distribution of the frequency tuning curves shown in C and D. (C) Iso-intensity frequency tuning curve for a narrow band neuron (BF=10.0kHz, $F_{1/2}$=0.94kHz). (D) Broadband neuron (BF=7.6kHz, $F_{1/2}$=6.9kHz).

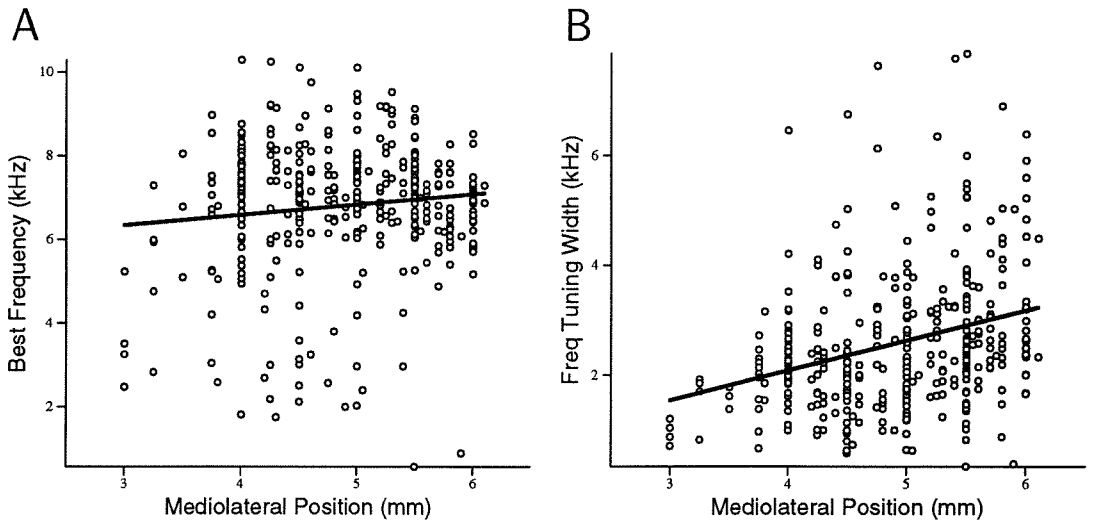

Figure 2.9: Frequency tuning as a function of mediolateral position. (A) Correlation between BF and ML position ($r = 0.11$, $p = 0.028$, n=372). (B) Correlation between $F_{1/2}$ and ML position ($r = 0.32$, $p < 0.0001$, n=368). In both panels, solid line indicates linear regression.

and left colliculi, best ITDs were normalized so that negative ITD values correspond to contralateral ear leading and positive ITDs to ipsilateral ear leading.

Best ITD values ranged from -298 to +146 μs with a mean of -10 μs (figure 2.10A. The maximum ITD experienced by the barn owl, under natural conditions, is approximately $\pm 180\,\mu s$, corresponding to an interaural separation of about 6cm. The range of best ITDs observed here is largely confined to $\pm 100\,\mu s$ with 93.6% of the neurons having best delays within this range. This is consistent with previous work demonstrating that the auditory space map contains an over representation of frontal space (Knudsen and Konishi, 1978b). $ITD_{1/2}$ ranged from 27–299 μs (56 μs median, 64 μs mean) with the complete distribution shown in figure 2.10B.

The distribution of sidepeak suppression values from -32 to 88% with a mean value of 31% SPS is shown in figure 2.10C. Sidepeak suppression was distributed bimodally, as can be seen in the distribution histogram; 13% of all cells where phase ambiguous, with %SPS values between 0 and 5, with the remainder showing some degree of suppression. Of the 349 neurons for which %SPS was measured 18 exhibited suppression values less than zero. In 16 of the 18, the negative %SPS values were the result of large trial-to-trial response vari-

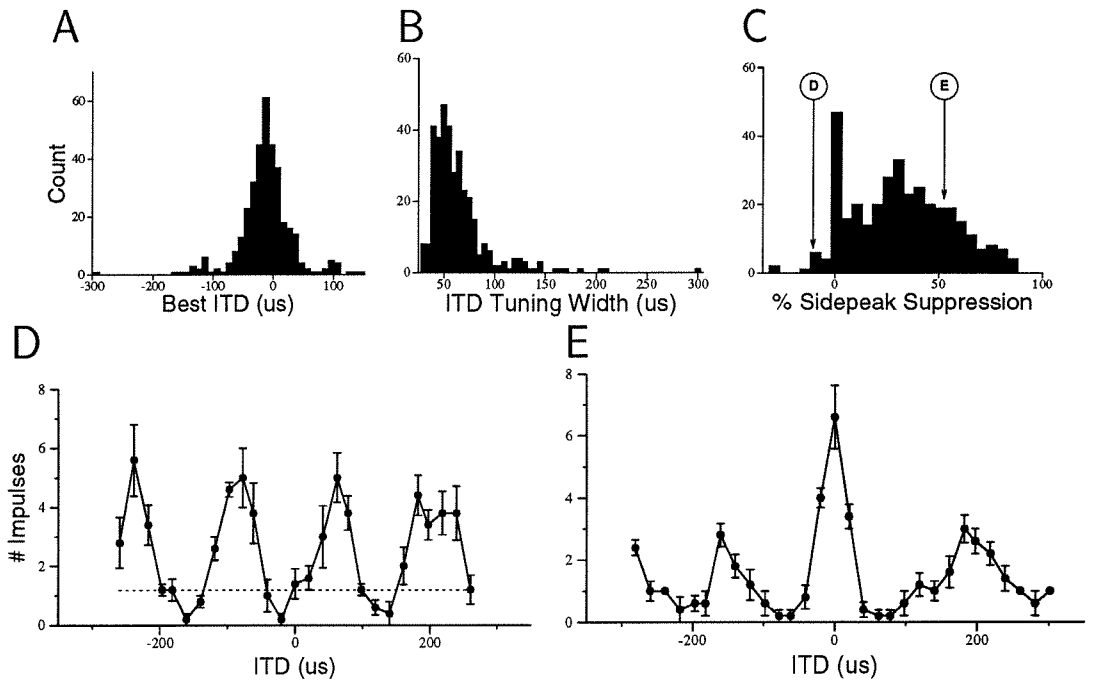

Figure 2.10: ITD tuning. (A) Range of Best ITDs. Negative ITDs correspond to contralateral ear leading (n=358, binwidth 10 μs). (B) $ITD_{1/2}$, tuning width at half-maximal response for the main peak (n=356, binwidth 5 μs). (C) Percent Sidepeak Suppression (%SPS), (n=350, binwidth 5%). Circled letters refer to the ITD tuning curves shown below in C and D. (D) ITD tuning curve with -6% SPS in response to broadband noise. (E) 56% SPS.

ance and the negative %SPS values were not significantly different from 0 (unpaired t-test, $p > 0.05$). In the remaining two cells, the main peak was qualitatively defined by the characteristic delay (CD), derived from at least two pure tone ITD tuning curves (Rose et al., 1966). In both cases one side peak was significantly higher than the response at the CD, while the response at the other side peak was not (unpaired t-test, $p < 0.01$). It is possible that in these neurons the CD does not represent the main peak (*i.e.*, suppression is not symmetric about the CD). Moiseff and Haresign (1992) previously reported the occurrence of such neurons, whose best delays are not the same as the characteristic delay, in the inferior colliculus of the owl.

Best ITD is independent of mediolateral position (figure 2.11A); however, both $ITD_{1/2}$ and %SPS show a significant correlation with ML position (figures 2.11b,c). ITD tuning curves have a maximum half width medially; $ITD_{1/2}$ decreases at a rate of 11 μs/mm towards the lateral margin and into ICx. %SPS, in contrast, is positively correlated with ML position, with phase ambiguous cells most common medially and side peak suppression increasing towards ICx (figure 2.11C). It is important to note that some phase ambiguous neurons were observed at virtually all mediolateral positions; however, the relative frequency of phase ambiguity is substantially higher medially. Similarly, side peak suppression is rarely observed at medial locations, and when it does appear medially, the degree of suppression is substantially lower than that observed laterally.

Best frequency and $ITD_{1/2}$ are correlated. When $ITD_{1/2}$ is expressed in μs, high frequency neurons have sharper ITD tuning curves than low frequency neurons (figure 2.12A), indicating a negative correlation. However, when $ITD_{1/2}$ values are plotted in units of cycles (relative to the neuron's best frequency, figure 2.12A), the correlation between best frequency and $ITD_{1/2}$ is positive. The mean ITD tuning width, relative to neuronal best frequency, was 0.39 ± 0.01 cycles.

Interaural Level Differences. As described in the methods, neurons sensitive to ILD were classified as either P, OP or SIG neurons. The relative frequency of each ILD tuningclass is shown in figure 2.13A. Best ILDs were distributed between -44 and +45dB (1.3dB mean, see figure 2.13B). Like the distribution of best ITDs, the range of best ILDs also reflects an overrepresentation of frontal space, consistent with previous reports (Knudsen and

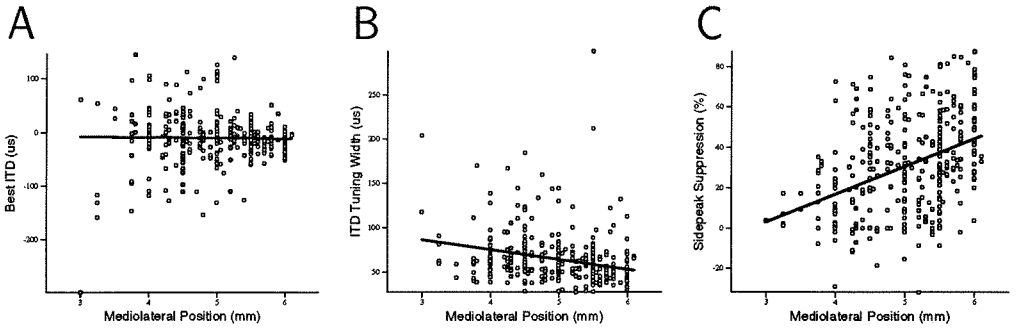

Figure 2.11: ITD tuning as a function of mediolateral (ML) position. (A) No correlation exists between best ITD and ML position ($r = -0.018, p = 0.737$, n=357). (B) $ITD_{1/2}$ is inversely correlated with ML position ($r = -0.230, p < 0.0001$, n=354). ITD tuning width increases across the mediolateral aspect of IC. (C) %SPS is positively correlated with ML position ($r = 0.399, p < 0.0001$, n=349). Phase ambiguous neurons are more frequent close to the Core/LS boundary, and maximal sidepeak suppression occurs in ICx or near the LS/ICx boundary.

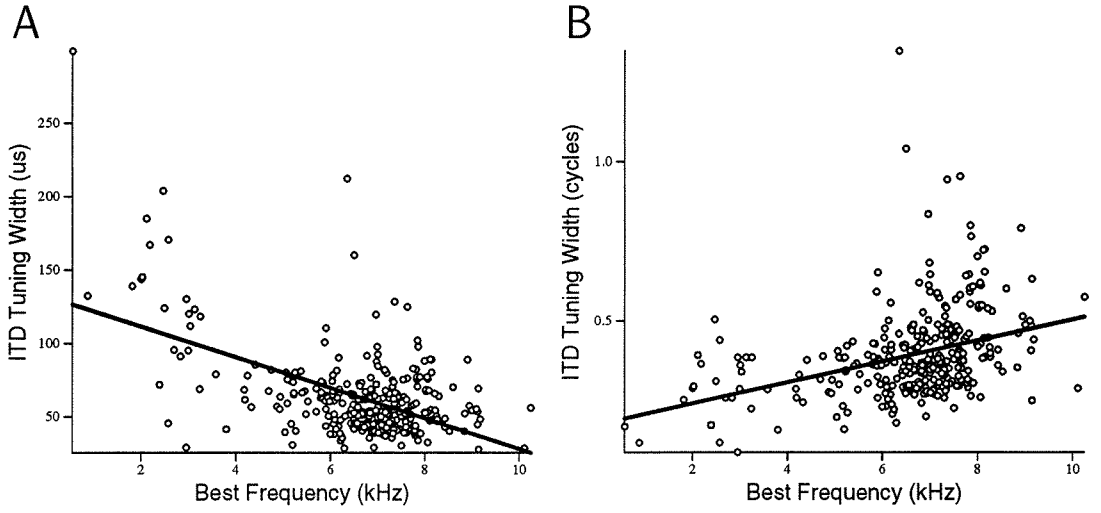

Figure 2.12: $ITD_{1/2}$ vs. Best Frequency. (A) There is strong negative correlation between $ITD_{1/2}$, measured in μs, and best frequency ($r = -0.531$, $p < 0.0001$, n=312). (B) The same dataset shown in A has been transformed by dividing $ITD_{1/2}$ values the period of each neuron's best frequency, so that $ITD_{1/2}$ is now plotted in cycles of the best frequency. When plotted in this way, there is no correlation between $ITD_{1/2}$ and best frequency ($r = 0.352$, $p = 0.0001$, n=312).

Konishi, 1978b). The range of $ILD_{1/2}$ values observed for ILD sensitive neurons is shown in figure 2.13C; the distribution ranges from 7 to 64dB with a mean of 26dB.

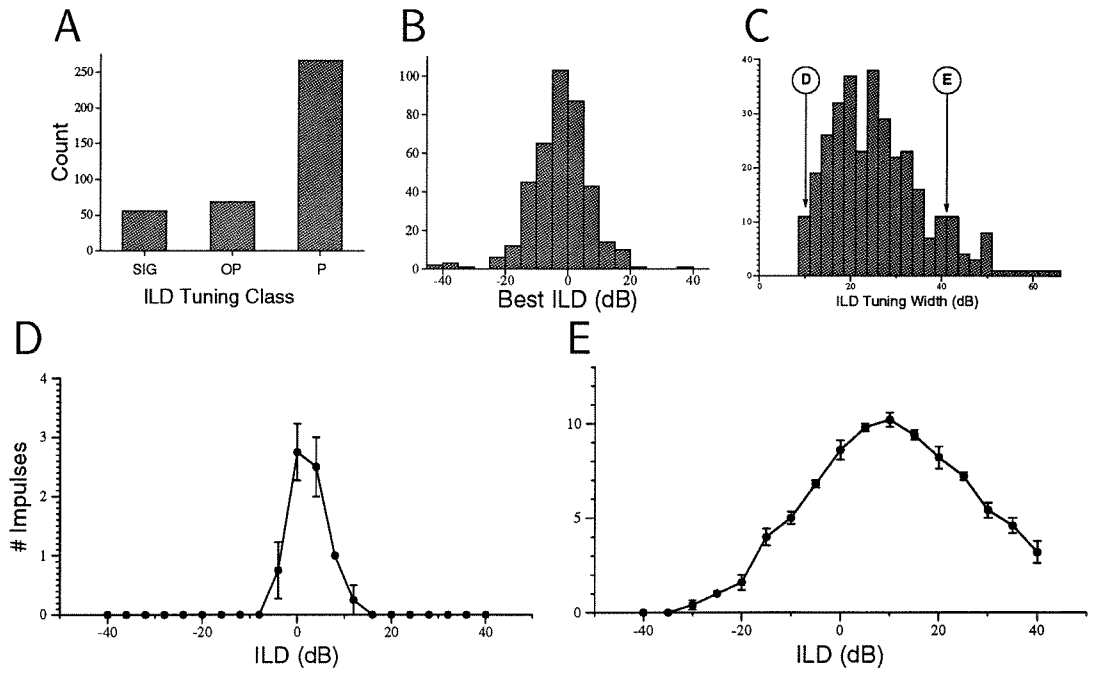

Figure 2.13: ILD tuning. (A) Distribution of ILD tuning classes: sigmoid, open-peaked, peaked (n=390). (B) Best ILD values for all neurons with a clearly defined best ILD. Negative values correspond to contralateral ear louder (n=394, binwidth 5 dB). (C) $ILD_{1/2}$, tuning width at half-maximal response for P and OP neurons (n=336, binwidth 0.5 dB). Circles and arrows refer D and E below. (D) Narrow ILD tuning (Best ILD +2.1dB, $ILD_{1/2}$=9.8dB). (E) Broad ILD tuning (Best ILD +11.1dB, $ILD_{1/2}$=41.6dB).

There is a weak positive correlation between best ILD and ML position (figure 2.14A), with more positive ILDs (sounds originating above the horizon) occurring more frequently at lateral recording sites. $ILD_{1/2}$ shows a weak, though statistically significant negative correlation with mediolateral position (figure 2.14B). The symmetry of ILD tuning (*S*) also shows a weak negative correlation with mediolateral position (figure 2.14B), with higher symmetry values, indicative of SIG and OP neurons, occurring medially, and smaller symmetry values, or peaked neurons, laterally.

ITD and ILD tuning. Most neurons (388/423, 92%) were sensitive to both time and

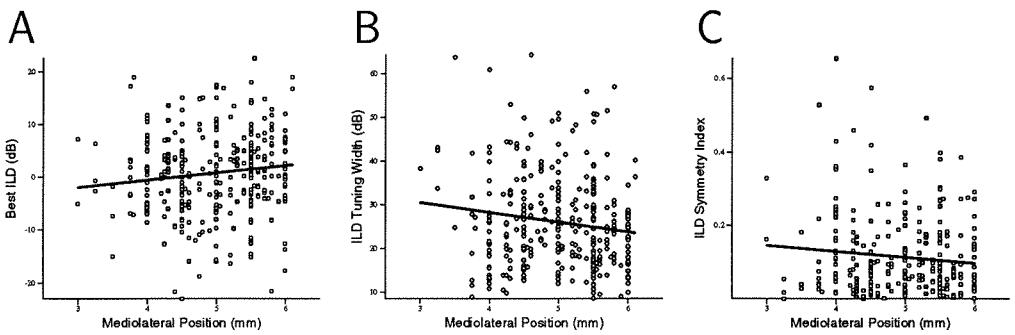

Figure 2.14: ILD tuning as a function of mediolateral position. (A) Best ILD ($r = 0.122$, $p = 0.027$, n=328). (B) ILD tuning widths ($r = -0.144$, $p = 0.010$, n=317). (C) ILD Symmetry Measurements ($r = -0.105$, $p = 0.082$, n=274).

intensity differences (see figure 2.15). Twenty-seven neurons (6% of all neurons) were ILD tuned but insensitive to time differences. By ILD tuning class, 17/27 had sigmoid ILD tuning, 8/27 where open-peaked and 3/27 were peaked. Eight neurons (2%) were ITD tuned but insensitive to ILD. There was no pattern to the anatomical distribution of the 35 neurons insensitive to either ITD or ILD.

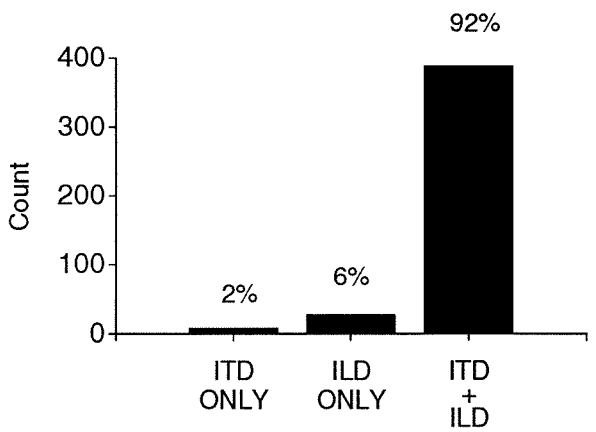

Figure 2.15: Conjunction of ITD and ILD sensitivity. Most of the 423 LS neurons were sensitive to both time and intensity cues (ITD+ILD). A small number were sensitive to time, but not intensity (ITD only) or vice versa (ILD only).

Correlation Among Tuning Properties

Because correlation is a transitive operation, it logically follows that if tuning property A is correlated with B and B with C, that A is also correlated with C. However, if the correlation is not perfect (*i.e.*, $r < 1.0$) this may not be true. Even if the correlation is transitive, it is not always obvious from inspection what the magnitude of the new correlation or the slope and significance of the regression line will be. For these reasons, the correlations between different tuning properties discussed above are presented explicitly here.

Response Latency. As discussed above, response latency increases from medial to lateral locations within the shell. Response latency is (weakly) correlated with both $F_{1/2}$ and ILD tuning widths (see figures 2.16a,b). The correlation with $F_{1/2}$ is positive: increases in excitatory input bandwidth correspond to an increase in latency. An increase in sharpness of ILD tuning is positively correlated increases in response latency, with the sharpest ILD sensitive neurons having latencies of around 14-15ms.

One example of the problem discussed above, with respect to the transitivity of correlations, occurs in the relationship between $ITD_{1/2}$ and latency. Despite the fact that both latency and $ITD_{1/2}$ are both independently correlated with mediolateral position (see figures 2.16b and 2.11B), they are not themselves strongly correlated with each other as shown in figure 2.16C.

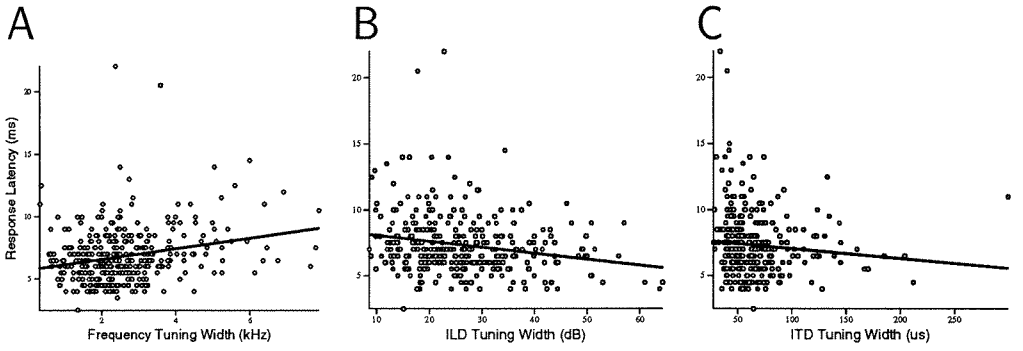

Figure 2.16: Tuning properties vs. response latency. (A) $F_{1/2}$ ($r = 0.245$, $p < 0.0001$, n=367). (B) $ILD_{1/2}$ ($r = -0.211$, $p = 0.0001$, n=323). (C) $ITD_{1/2}$ ($r = -0.095$, $p = 0.077$, n=348).

Of all the properties examined, sidepeak suppression is most strongly correlated with

response latency (figure 2.17). There is a systematic increase in %SPS of almost 22% for every additional ms of response latency, suggesting that increases in sidepeak suppression require increased computation time. This is consistent with a model in which sidepeak suppression arises from a feed-forward synaptic convergence, with multiple levels of convergence, and a corresponding increase in computation time, leading to further increases in sidepeak suppression.

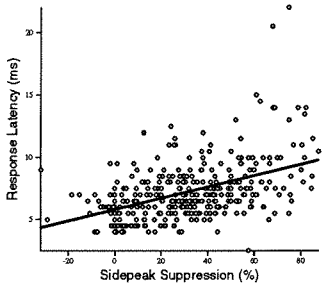

Figure 2.17: %SPS vs. latency. Increases in sidepeak suppression correlate with increases in response latency ($r = 0.475$, $p < 0.0001$, n=346).

Sidepeak Suppression. Sidepeak suppression is negatively correlated with both ITD and ILD tuning widths (figure 2.18A,B). Phase ambiguous neurons tend to have broader ITD and ILD tuning curves, while space-specific, sidepeak suppressed neurons have sharper time and level difference tuning. There is a weak positive correlation between SPS and input bandwidth, with broad frequency tuning predictive of more complete sidepeak suppression (figure 2.18C); however, this correlation is weaker than that observed between $ITD_{1/2}$ and $ILD_{1/2}$.

Summary of Correlations

Table 2.1 summarizes the significant correlations between individual tuning properties and anatomical position along the mediolateral axis of the inferior colliculus. In addition, the table shows the significant correlations that exist between pairs of tuning properties.

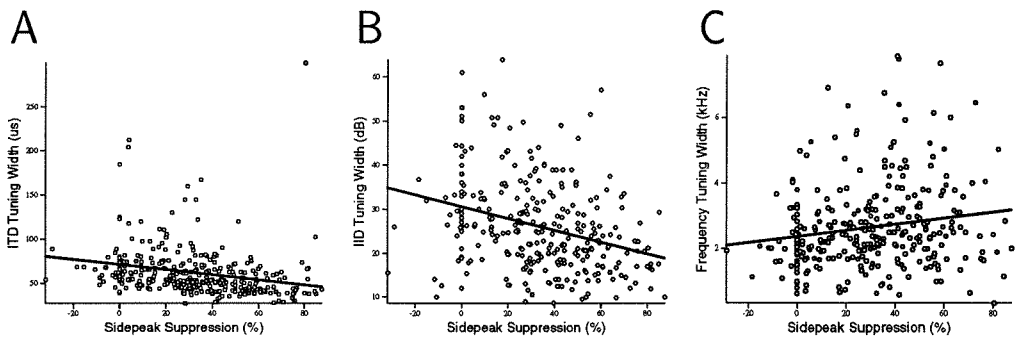

Figure 2.18: Sidepeak suppression vs. tuning properties (A) $ITD_{1/2}$ ($r = -0.245$, $p < 0.0001$, n=338). (B) $ILD_{1/2}$ ($r = -0.309$, $p < 0.0001$, n=287). (C) $F_{1/2}$ ($r = 0.172$, $p = 0.0023$, n=312).

	Latency	$F_{1/2}$	$ITD_{1/2}$	%SPS	$ILD_{1/2}$
Mediolateral Location	***	***	***	***	**
Latency	–	***	NS	***	***
%SPS	***	**	***	–	***

Table 2.1: Summary of Physiology Data. The statistical significance of correlations between pairs of measured tuning properties and mediolateral position is indicated in each cell of the table (*** $p < 0.0001$; ** $p < 0.01$; NS, not significant).

Histology

Figure 2.19 shows a transverse section through the owl's inferior colliculus indicated the anatomical location of several recording sites. The series of vertical electrode penetrations running from medial to later shown are characterized by a systematic increase in $F_{1/2}$, %SPS and a transition from sigmoid to peaked ILD tuning (figure 2.19, plots). The data from an individual set of penetrations reflects, to some extent, the pooled data collected from eight owls.

2.3 Discussion

The data presented here are consistent with the systematic emergence of spatial tuning across the mediolateral axis of the lateral shell. Medially located LS neurons exhibit tuning properties similar to those found in the afferent neurons of VLVp and Core. Medial neurons have phase ambiguous ITD tuning, relatively narrow band excitatory frequency tuning and broad or sigmoid ILD tuning. More laterally, neurons gradually acquire the tuning properties associated with the space specific neurons of the owl's auditory space map: sidepeak suppression, an increase in frequency tuning width and a decrease in the width of ILD tuning. This successive refinement of ITD and ILD tuning ending with space specificity is consistent with a hierarchically organization of LS. In such a model, LS neurons are arranged as a feed-forward network systematically distributed from medial to lateral across the shell. This results in a continuous progression of tuning properties towards the spatially restricted fields required for accurate sound localization.

Latency. Raman et al. (1994) examined the time course of synaptic conductances in the avian (chick) brainstem *in vitro* and found that excitatory postsynaptic currents in the auditory nuclei were extremely fast, often in the sub-millisecond range. The change in latency observed between the medial and lateral edges of the shell is about 5ms (5-10ms), setting an upper limit, based on the data of Raman et al., about five synapses between the afferent input to LS and final output to ICx neurons. It is important to keep in mind two caveats about these observations: First, Raman et al. did not actually study collicular neurons, but

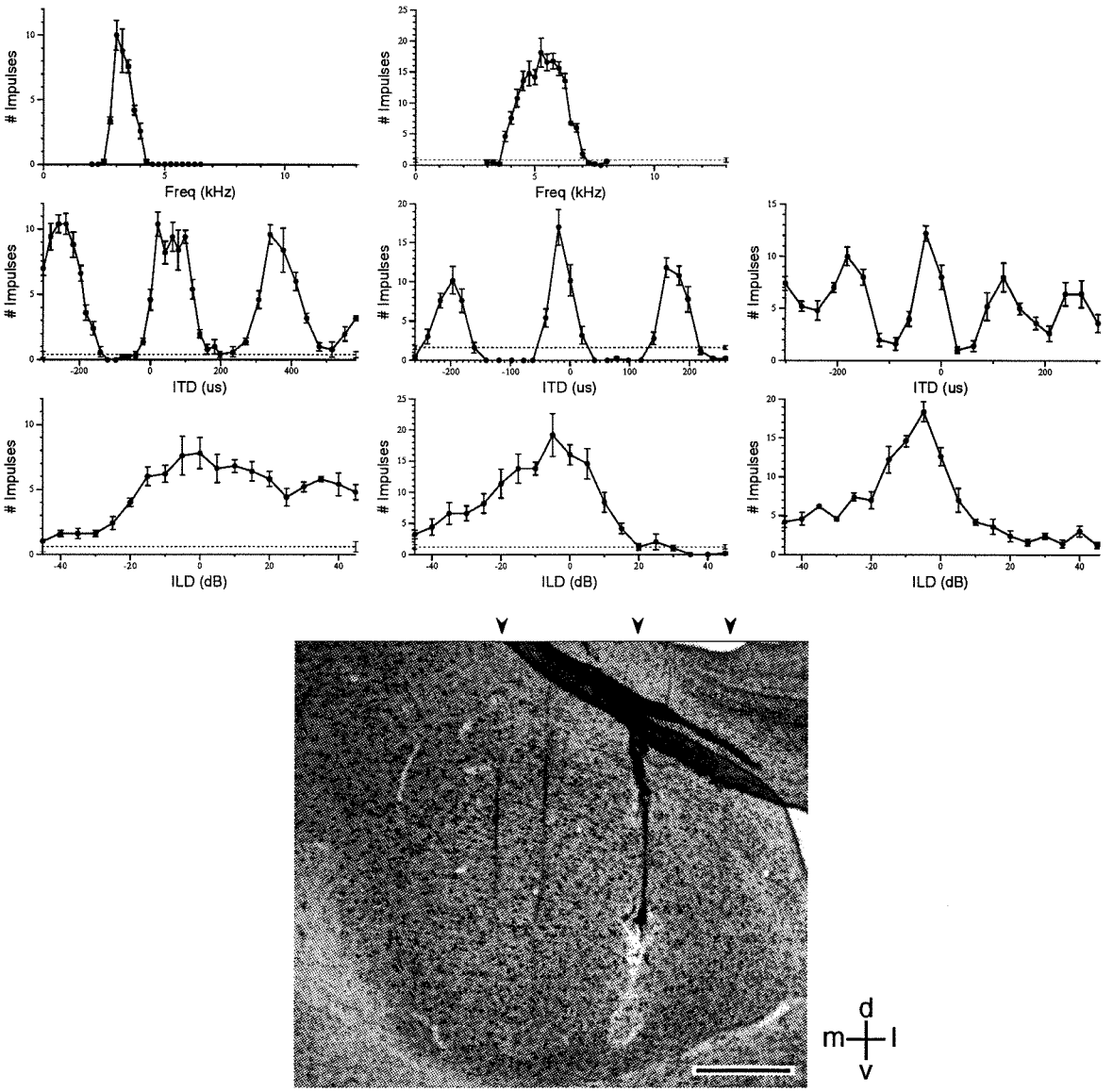

Figure 2.19: Tuning properties in histologically verified penetrations. Each column of plots come from a single dorsal-ventral penetration. Electrode tracks from dorsal-ventral passes are visible in the cresyl violet stained transverse section below. Arrowheads at the top of the section indicate the ML positions of electrode tracks. Scale bar = 500 μm. No frequency tuning data was available for the lateral-most pass. However, mean $F_{1/2}$ was 2.2±0.6kHz in the pass located 0.25mm medial of the final pass.

rather other auditory brainstem and midbrain neurons, and, second, measurements made *in vitro* do not always accurately reflect the *in vivo* conditions.

The relationship between position and latency (figure 2.7B) is not simply linear, but is rather triangular in appearance. Long latency neurons occur with higher frequencies at lateral locations. Of the 44 neurons with latencies longer than 10ms, 85% are located beyond 5.0mm laterally. However, there are also a substantial number of short latency neurons occurring at such lateral positions. One possible explanation for this is that afferent projections to LS contact both medial and lateral targets. This is also consistent with the observation that phase ambiguous neurons are found to some extent at all mediolateral positions.

ITD Tuning Widths and Cross Correlation Models.

Neurons in nucleus laminaris operate as coincidence detectors and transmit information about interaural phase differences (Carr and Konishi, 1990) to the Core. To a first approximation, ITD tuning curves in both NL and Core resemble cosine functions, which is expected for IPD sensitive neurons (Goldberg and Brown, 1969; Wagner et al., 1987; Colburn et al., 1990). Also consistent with the idea that NL neurons act as narrow band coincidence detectors is the observation that NL and Core neurons exhibit periodic ITD tuning, with no sidepeak suppression, even in response to broadband noise stimuli (Fujita and Konishi, 1991).

At levels beyond Core, the ITD sensitivity in the system begins to show properties not expected for a simple correlator. The cosine-like ITD tuning of a narrow band correlator predicts that $ITD_{1/2}$ measured in μs should decrease as a function of $1/BF$. This is because the period of the ITD tuning curves is a function of BF. As BF increases, the tuning curves will have sharper ITD tuning curves, as shown in figure 2.20. In terms of cycles, relative to best frequency, tuning widths should remain constant; for a simple correlator $ITD_{1/2}$ should remain constant at 0.5 cycles, independent of best frequency.

Fujita and Konishi (1991) compared $ITD_{1/2}$ values in NL, Core, LS and ICx. They found that in all the nuclei of the time pathway, ITD tuning curves were, on average, sharper than the 0.5 cycles expected for a correlator. In NL and Core neurons $ITD_{1/2}$ in cycles was observed to be independent of best frequency; however, in LS (n=30) and ICx (n=20) they observed a positive correlation between BF and $ITD_{1/2}$, with low frequency having sharper

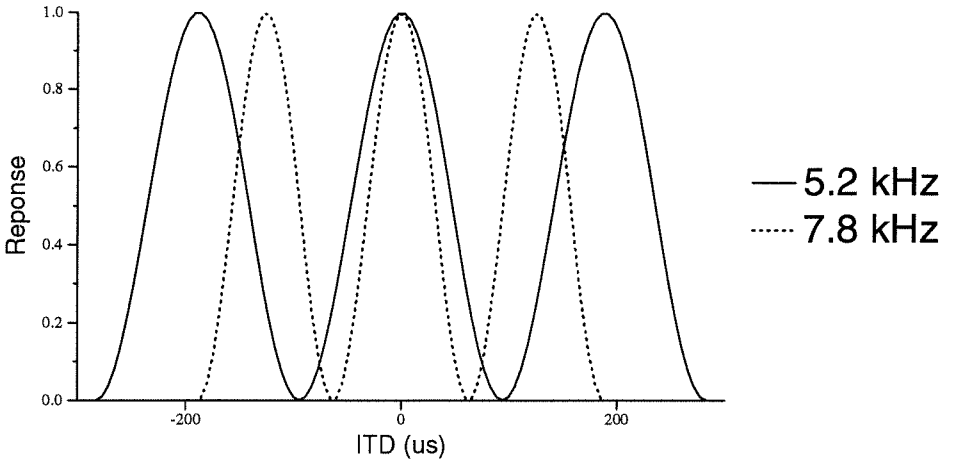

Figure 2.20: The relationship between $ITD_{1/2}$ and best frequency. Two simulated pure tone ITD tuning curves for neurons with different best frequencies, one low frequency (solid) and one high frequency (dotted). The higher frequency neuron exhibits sharper ITD tuning in units of time, though in units of cycles (with respect to best frequency), the tuning widths are both 0.5 cycles of the neuronal best frequency.

ITD tuning than high frequency neurons (essentially the same relationship reported here in figure 2.12B).

These observations signify a consistent difference between the physiological coincidence detection circuit in the owl's brainstem and the operation of a simple theoretical cross correlator. ITD tuning curves in the owl, throughout the time pathway, are uniformly sharper than expected for a simple correlator, with LS and ICx neurons exhibiting a maximum deviation from the model (about 20% sharper than expected).

Fujita and Konishi (1991) also demonstrated that the differences between auditory neurons and the cross correlation model are at least partially the result of local inhibition. In Core, LS and ICx local iontophoretic application of the $GABA_A$ antagonist bicuculine methiodide (BMI) broadened ITD tuning curves. In Core and LS, $ITD_{1/2}$ in the presence of BMI were close to the predicted 0.5 cycles. In ICx BMI also had the effect of broadening ITD tuning, but $ITD_{1/2}$ in the presence of BMI reached 0.5 cycles in only one of the reported cases.

Based on the data described here and the proposed model of hierarchical convergence, it is possible that the limited effect of BMI on ICx neurons is due to the fact that the LS neu-

rons projecting to ICx are already significantly different than a simple correlator. Though it wasn't tried, simultaneous application of BMI in both LS and ICx, if the model presented here is correct, might restore ICx neurons to the 0.5 cycle tuning widths expected for a coincidence detector.

ILD Tuning and Lateral Inhibition. Takahashi and Keller (1992) demonstrated that the sigmoid ILD tuning in VLVp arises as a result of result of excitatory input from one ear, via nucleus angularis, and inhibition from the contralateral VLVp. Adolphs (1993b) further demonstrated that peaked ILD tuning in the colliculus is the result of inhibitory projections from VLVp to the colliculus. Sigmoid ILD sensitivity can be transformed into peaked ILD tuning curves by combining the output of several sigmoid neurons with slightly different best ILDS (or 50% points). Figure 2.21A shows a simple model of excitatory and inhibitory synaptic interaction that can lead to the peaked ILD curves observed in LS.

When the excitatory and inhibitory synaptic inputs are unequal in strength, ILD curves are open-peaked, as indicated in figure 2.21C. Full closure of such curves can be achieved by increasing the strength of the inhibitory sigmoid input or by inhibitory inputs from sigmoid cells onto open-peaked neurons. In either case, the final result is fully-closed, peaked ILD tuning, as observed in most LS neurons and space-specific neurons in ICx.

Once peaked ILD tuning is generated, it can be further refined or sharpened by lateral inhibition (see figure 2.22A–C). In this context, lateral inhibition provides a mechanism for decreasing $ILD_{1/2}$ widths by using inhibitory connections from neighboring cells with slightly different best ILDs, but of similar tuning widths. A schematic model of this circuit and its operation are shown in figure 2.22A–C. Each neuron, with its different best ILD, sends either an excitatory or inhibitory projection to the output neuron.

While the traditional formulation of lateral inhibition has inhibitory neurons projecting directly to neighbors in the same processing layer, the model here shows excitatory and inhibitory synapses on a common output cell. Computationally there is little difference between these two formulations; however, the data presented here, both for the evolution of peaked ILD tuning and the observed sharpening of ILD tuning curves, describe a correlation between anatomical location and ILD tuning (figure 2.14B) consistent with a feed-forward network. This feed-forward aspect is combined with lateral inhibition by considering the

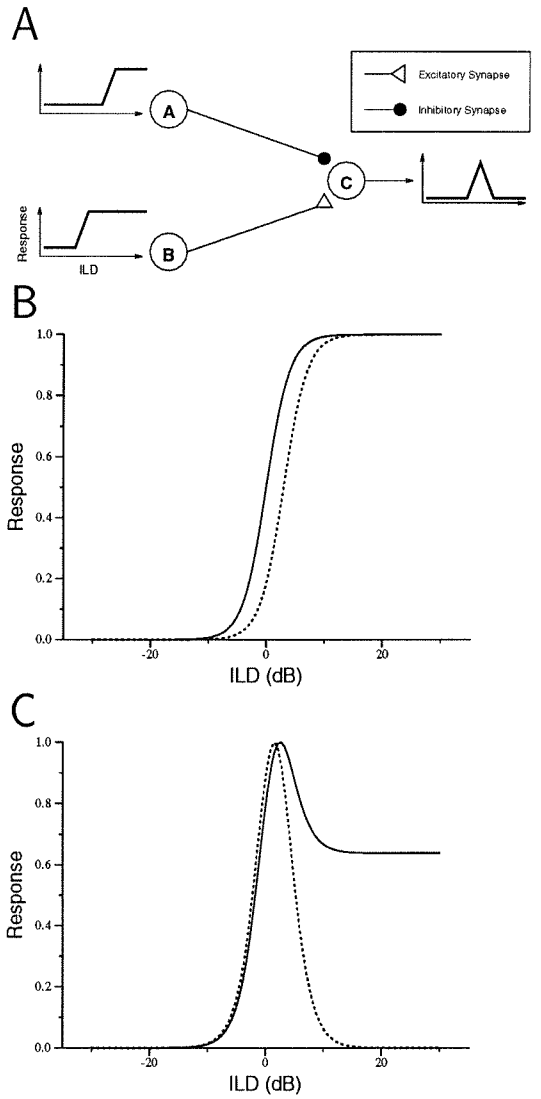

Figure 2.21: Generating Peak ILD tuning from Sigmoid Inputs. (A) A combination of excitatory and inhibitory connections from ILD sensitive, SIG class neurons can lead to P and OP class neurons. Neurons A and B are both sigmoid, with different 50% points. Neuron C exhibits peaked ILD tuning as a result of inhibitory input from neuron A. (B) Two simulated of sigmoid ILD tuning curves for neurons A and B. (C) Neuron C can be either peaked (P) or open-peaked (OP), depending upon the synaptic strength of the inhibition from neuron A. If the inhibitory connection is weaker than the excitatory connection, then C will display OP class tuning (solid line), if the two inputs are equal, then C will be peaked (dashed line). The width of the peaked ILD tuning curve is a function of the displacement of the two sigmoid tuning curves along the ILD axis.

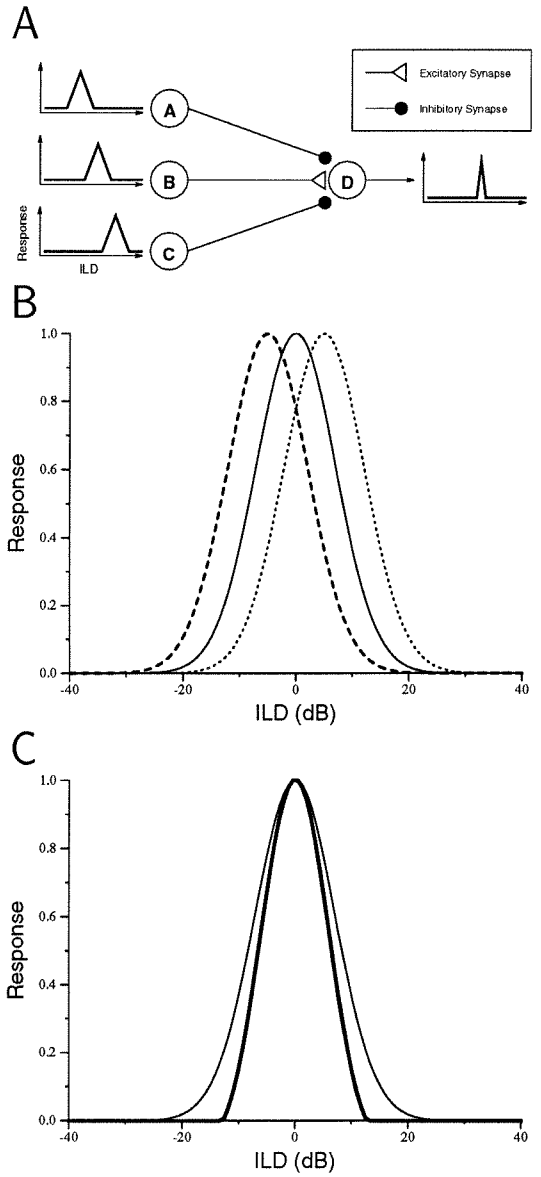

Figure 2.22: ILD sharpening by lateral inhibition. (A) A synaptic model of lateral inhibition leading to ILD sharpening. Three ILD selective, broadly tuned neurons (A, B and C) synapse onto a single cell (D). All three neurons have slightly different preferred ILDs. Neuron B excites output neuron D, while A and C are inhibitory. (B) ILD tuning curves for neurons A (dashed), B (solid) and C (dotted) in the model circuit. (C) The output of neuron D (heavy line) has the same best ILD as neuron A (solid line), but has a narrower ILD tuning curve.

output neuron of each "micro-circuit" shown in figures 2.21A and 2.22A to be located laterally, with the input neurons located medially.

A Model of ITD and ILD Integration. The observation that more than 90% of the neurons studied here are selective for both ITD and ILD suggests that the integration of time and intensity processing first occurs early, or medially, in lateral shell. Taken together, the data presented here support a model based on a hierarchy or cascade of neural processing, with afferent-like tuning properties occurring near the Core/LS boundary. Clusters or bands of medial neurons act as small processing units and integrate their outputs onto more laterally located neurons (see figure 2.23). These neurons in turn cluster and project even more laterally. This process continues across the mediolateral dimension of the lateral shell. The final outputs of this processing hierarchy are the auditory space neurons in ICx.

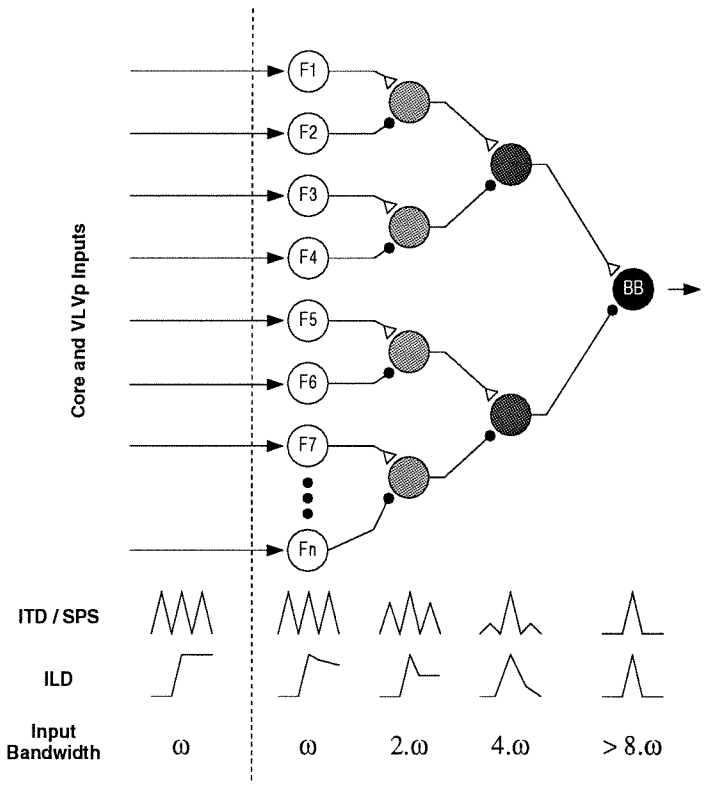

Figure 2.23: Mixed model of frequency, time and intensity integration in LS. Open triangles indicate excitatory synapses, filled circles indicate inhibitory synapses. Afferent input to LS arrives from the left (left of dashed line). At the bottom is indicated ITD, ILD and Frequency tuning at each stage of processing. ω indicates $F_{1/2}$ on the order of 1kHz, corresponding the tuning width observed to NL/Core neurons.

With respect to ITD processing, the model can be framed in a spatial context by considering the LS's integration of the output pattern from nucleus laminaris. The output of laminaris can be considered as a joint representation of IPD and frequency, as shown in figure 2.24. LS neurons can be considered to have receptive fields in this delay-frequency domain analogous to the spatial filters that generate orientation tuning in visual areas (monkey visual cortex: Hubel et al., 1978; owls: Pettigrew and Konishi, 1976).

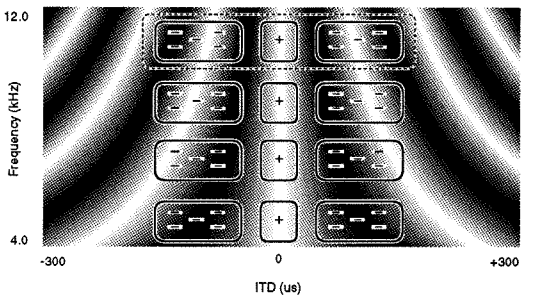

Figure 2.24: Spatial interpretation of LS receptive fields. The hierarchical integration observed in LS is in many ways to the spatial filters used to generate orientation tuning in mammalian visual cortex. The receptive fields of LS neurons are depicted on a surface representing the activity pattern of NL or Core in response to a broadband noise stimulus with an ITD of $0\,\mu s$. Solid lines indicate inhibitory (-) and excitatory (+) receptive fields that span multiple frequency channels. Dashed line indicates a receptive field corresponding to lateral inhibition across IPD channels.

Comparison to Other Models. Stern and his colleagues (Stern et al., 1988; Trahiotis and Stern, 1994) described a computational model to account for the observed relationship between stimulus bandwidth and azimuthal localization reported by human psychophysical studies. The model addresses the resolution of phase ambiguity in humans, and in other species with large head sizes relative to the barn owl. The model represents the binaural temporal structure of auditory signals by computing the maxima in the delay-frequency space represented in nucleus laminaris (see figure 2.25 for an example).

In brief, the model suggests that the auditory system uses two mechanisms to resolve phase ambiguity: a "straightness" constraint, which corresponds closely to integrating or summing across frequency channels to locate the ITD range with maximum activity across all frequency channels, and a "centrality" constraint, which weights the output of the model towards central locations (ITDs near zero) when the straightness constraint is insufficient

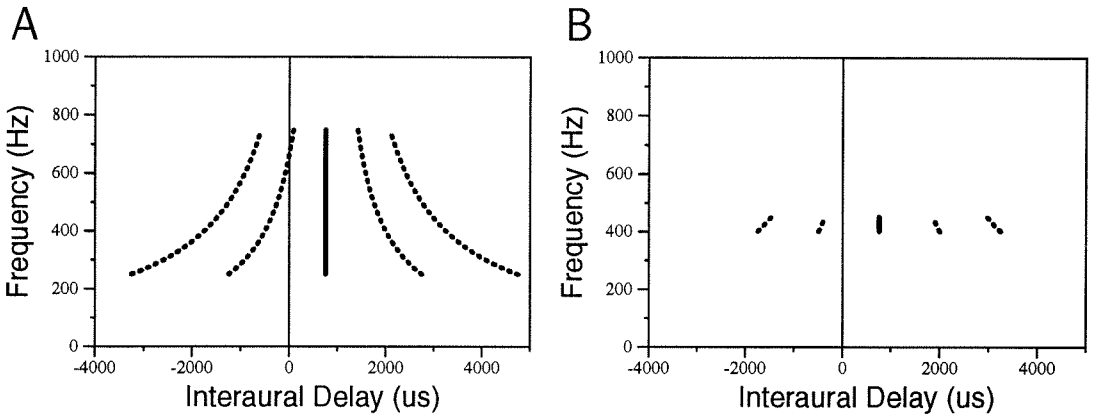

Figure 2.25: Weighted-Image model. ITD or IPD as a function of frequency are represented by the maxima of the cross correlation function for each narrow band frequency channel, simulating a cochlear narrowband filter followed by subsequent NL- or MSO-like coincidence detection. The multiple bands in the plot represent phase ambiguity. The true ITD in both plots is 750 μs, and is represented by the solid lines. (A) "Broad" band input (250–750 Hz). (B) Narrow band input (400–450 Hz). After Stern et al. (1988).

for disambiguation. When the input signal is broadband, as shown in figure 2.25A, the algorithm correctly identifies the vertical band as the true interaural delay. For narrow band signals (figure 2.25B) there is insufficient data to accurately choose the correct ITD based on straightness and the algorithm chooses the locus of activity closest to the midline. In figure 2.25B, this would lead to an incorrect decision of -500 μs.

The fact that the model makes errors at narrow bandwidths should not be considered to be a problem with the model, since psychophysical experiments by Trahiotis and Stern (1989) demonstrated that human listeners make the same type of errors when localizing narrow band signals. In fact, this error, which is caused by the centrality constraint, is one of the key results this model was intended to replicate. Nonetheless, one must carefully evaluate the relevance of this model to ITD processing in the barn owl, since there are several important differences between human and owl sound localization behavior.

In humans, the range of physiological interaural delays is about $\pm 750\,\mu s$ (Kuhn, 1977). This means that phase ambiguity only occurs above about 650Hz. Numerous psychophysical studies have demonstrated that in human subjects, ITD processing is largely limited to frequencies below about 1.5kHz (see Middlebrooks and Green, 1991 for review). There-

fore, only from 650–1.5kHz, corresponding to a relatively narrow portion of the normal human hearing range, the bias towards localizing to central locations can potentially lead to behavioral errors where localizing narrow band stimuli.

The owl, however, relies on ITD cues well beyond the range at which phase ambiguity occurs. In owls, the physiological range of ITDs is $\pm 180\,\mu s$, which corresponds to a lower frequency limit for phase ambiguity of about 4kHz. Behavioral and physiological studies have demonstrated that the owl relies on ITD cues for horizontal localization up to around 9kHz (Moiseff and Konishi, 1981; Sullivan and Konishi, 1986). The assumption of centrality in the owl, therefore, would lead to localization errors over about half of its hearing range, including the spectral range over which the owl shows maximal localization acuity (Knudsen and Konishi, 1979).

One other caveat that should be kept in mind when considering Stern et al.'s model is the fact that the trajectories shown in figure 2.25 represent the steady state relationship between internal delay (*i.e.*, IPD) and frequency for a single sound source. The dynamic aspects of this delay-frequency representation are considerably more chaotic (Takahashi and Keller, 1994), as is the situation in the presence of multiple independent or uncorrelated sound sources (Mazer, unpublished observations). It is not clear that Stern et al.'s weighted-image model will suffice to determine ITD under more complex situations. (See Blauert, 1983, chapter 3, for a complete review of multiple sound source localization issues.)

In general, the idea of using straightness in the delay-frequency representation to disambiguate azimuthal locations is similar to what is thought to occur in the barn owl. However, the neural substrate proposed by Stern et al.is significantly different than that proposed here. In a later papers (Stern and Trahiotis, 1992; Trahiotis and Stern, 1994) they suggested a physiological implementation of the model requiring a second order coincidence detector, similar to that proposed in 1959 by Licklider as a neural circuit for pitch perception (Licklider, 1959). Unfortunately, there is no evidence to date for coincidence detection in the barn owl's beyond nucleus laminaris.

Shackleton et al. (1992) proposed a model similar to Stern and Trahiotis's weighted-image model with two notable differences. First, this model is more physiologically accurate and uses a more realistic model of the peripheral auditory system, and second, the

formulation of the ITD estimator is presented as a sort of oriented spatial filter in delay-frequency space. They described two possible estimators (the heart of the model) that operate on the linear summation of each delay band across all frequency channels. One P_{peak} simply locates the largest peak in the broadband ITD curve, and the other P_{av} computes the weighted average of all the peaks. Unfortunately, this model fails to address an important issue raised in the owl literature. While the model is functionally capable of explaining many of the behavioral observations in both humans and owls, the use of simple linear summation is largely inconsistent with the results of Takahashi (1989) which demonstrated that ITD tuning curves in ICx are the result of a non-linear integration across frequency bands.

While the algorithm underlying the hierarchical model of cross-frequency channel integration proposed here (see figures 2.4B and figure 2.23) bears little outward resemblance to the models of Stern et al. and Shackleton et al., two common features are that (1) all three models depend on frequency channel integration to eliminate phase ambiguity and (2) to a first approximation, they all generate similar output patterns or make similar predictions about behavior, with one exception. The model proposed here simply predicts phase errors when localizing narrow band stimuli, consistent with the response properties of space specific neurons in ICx. While studies have not yet been done to examine the relationship between bandwidth and behavioral responses, there is a hint in the literature (Knudsen and Konishi, 1979; Wagner, 1993) that the localization errors made by owls do not reflect the central bias predicted by the weighted-image model.

This study has largely considered integration of frequency channels within a single ITD column as described by Wagner et al. (1987); however, that need not be the case. Preliminary experiments with frequency modulated (FM) sweep stimuli suggest that the inputs to a LS neuron may be a function of both best ITD and best frequency. ITD tuning curves collected using FM sweep stimuli show that at different ITDs, many LS and ICx neurons respond to different portions of the FM sweep. This is consistent with a model in which input to a single lateral shell neuron can originate in several ITD columns as well as several frequency laminae in NL, as shown in figure 2.26.

Figures 2.27 and 2.28 show two examples of the LS responses to FM sweep stimuli. Figure 2.27 compares the response of a LS neuron to broadband noise stimuli with that ob-

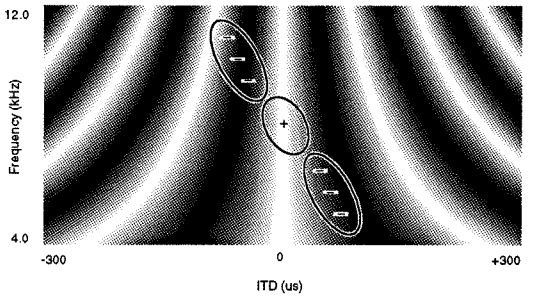

Figure 2.26: Frequency-dependent ITD channel integration. The grey scale surface represents the spatial distribution of activity in NL or Core, with the ellipsoid regions indicating excitatory (+) and inhibitory (-) connections to the lateral shell. Oriented receptive fields of this type correspond to integration of different frequency channels for each ITD (see text for details).

tained using an FM sweep covering the same spectral range. Figure 2.27D demonstrates that the latency to first spike appears to be a function of both the instantaneous frequency and the interaural time difference. At each ITD sampled, the neuron responds to a different frequency band. Figure 2.28 shows the responses of another LS neuron to three different sweeps, varying in both sweep bandwidth and sweep rate.

Conclusions. The physiological description of the lateral shell presented here is inconsistent with the idea that lateral shell neurons act as a simple AND gates integrating time and level processing channels in a single synaptic step. Instead, the data support a model of hierarchical convergence consistent with the observed heterogeneous, yet systematic, arrangement of neuronal tuning properties across the width of the shell. The serial computations that arise as a result of this organization lead to a successive refinement of the tuning properties associated with sound localization. In many ways, this process resembles that which leads to the formation of visual neurons with complex receptive fields, *e.g.* simple, complex and hypercomplex cells in striate cortex (Hubel et al., 1978) or "face-neurons" in inferotemporal cortex (Desimone et al., 1984). In marked contrast to the visual system, however, the auditory integration process described here is confined to a single neuroanatomically homogeneous structure with no gross anatomical correlate of the integration process.

In the case of the barn owl, the auditory space map found in the external nucleus of the inferior colliculus can be considered as an emergent property of the lateral shell. The shell

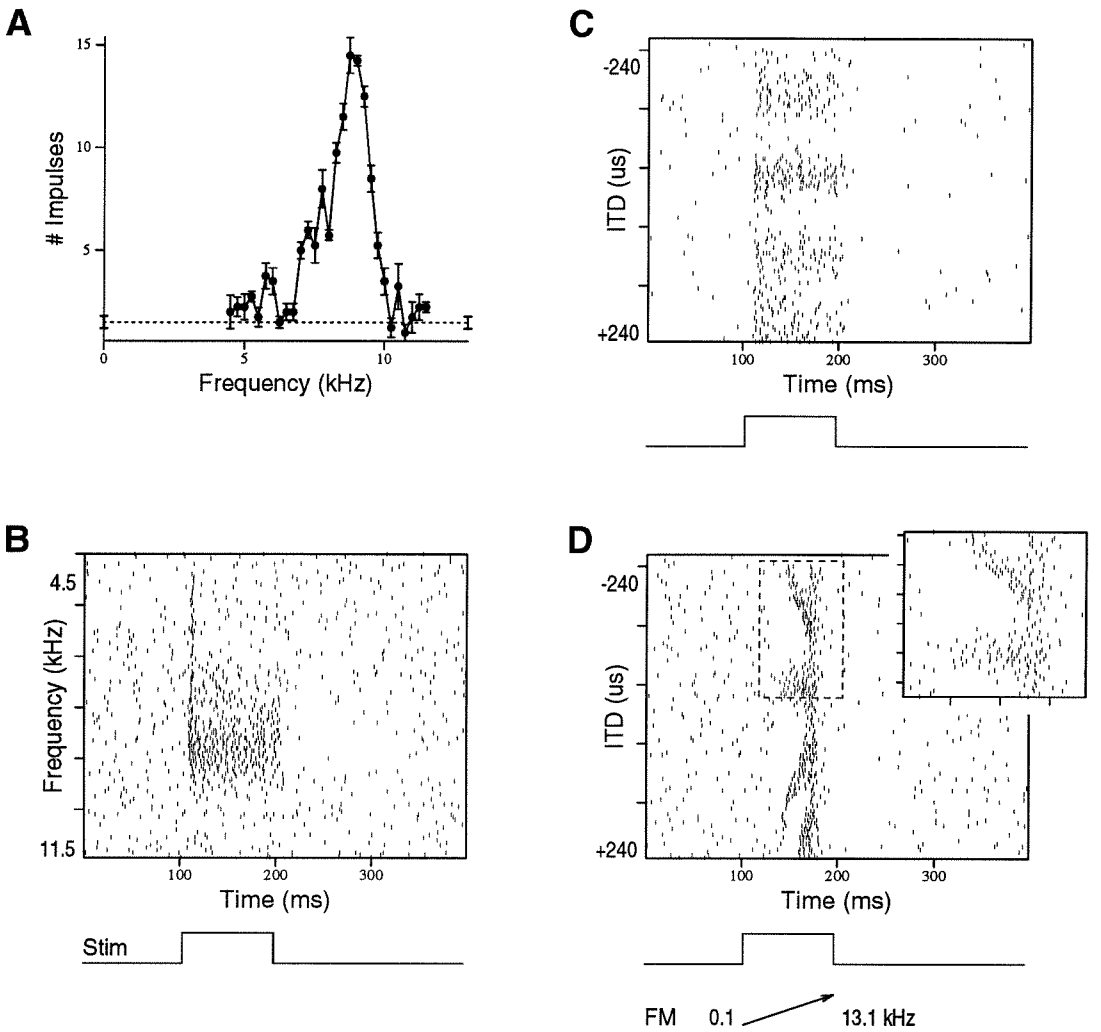

Figure 2.27: Comparison of LS responses to broadband noise and FM sweeps. (A) Frequency tuning of LS neuron (#495.40, BF=8.8kHz, $F_{1/2}$=1.5kHz). Error bars indicate SEM. (B) Raster plot from frequency tuning curve shown in A. Note consistent onset response at high stimulus frequencies. (C) Raster plot for an ITD tuning curve using a broadband (0.1-13kHz) noise stimulus. (D) Raster plot for an ITD tuning curve using an FM sweep (0.1-13kHz) stimulus; all other parameters the same as in C. Insert shows enlarged view of the boxed region.

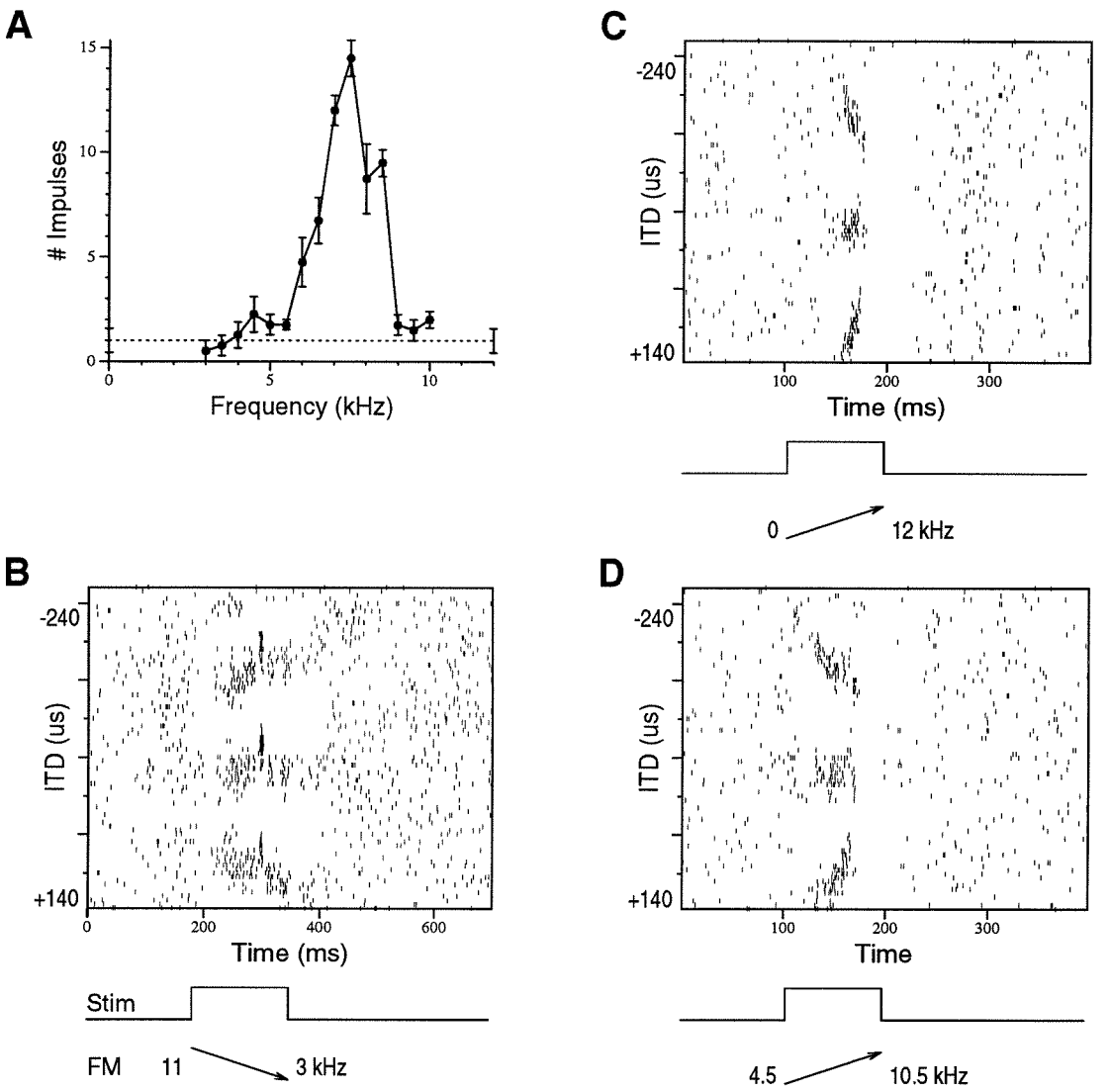

Figure 2.28: LS responses to different FM sweeps. (A) Frequency tuning (#495.35, BF=7.6kHz, $F_{1/2}$=2.1kHz). Error bars indicate SEM. (B) Raster plot of ITD tuning curve using an FM signal sweeping down from 11–3 kHz (80kHz/s). Note the trajectory of the bands in the raster. (C) FM signal sweeping up from 1–12 kHz (120kHz/s). (D) FM signal sweeping up from 4.5–10.5 kHz (60 kHz/s). The trajectories of the bands visible in these rasters is a function of both the direction and speed of the FM sweep. The neuron appears to respond to a single frequency band when the stimulus has a particular ITD.

provides a neural substrate for this property in the form of a feed-forward neural network which uses local circuit interactions to transform raw sensory input into a highly regular sensory map. The mechanisms described here integrate three independent processing channels (time, level and frequency) to provide the owl with a centrally synthesized representation of auditory space. While this study has focused exclusively on the barn owl and spatial localization, it seems clear that parallel processing and the integration of parallel streams by downstream regions of the central nervous system represent common structural motifs that cuts across the boundaries defined by species and sensory modality.

Chapter 3 The Effects of Signal Bandwidth on Processing of Interaural Time Difference in Barn Owls

Interaural time difference (ITD) provides an important cue for the localization of sounds in the horizontal plane for mammals and owls (Heffner and Heffner, 1992; Konishi, 1973a; Moiseff and Konishi, 1981). Interaural time differences arise when the path from a sound source to the left ear differs in length from the path to the right ear. Jeffress (1948) was the first to propose a neural circuit consisting of axonal delay lines and neural coincidence detectors which could encode ITD. Subsequently, studies in several species have provided experimental evidence for this model (*e.g.*, dog, Goldberg and Brown, 1969; cat, Yin and Chan, 1990; owl, Carr, 1990; chicken, Overholt et al., 1992). In mammals, the location of the coincidence detector is the medial superior olivary nucleus (MSO). In the barn owl, nucleus laminaris (NL), thought to be the avian homologue of MSO, is the site of coincidence detection.

Individual NL and MSO neurons respond to more than one time difference. ITD tuning curves, in which neuronal response is plotted as a function of ITD, exhibit a characteristic cyclical pattern of peaks and troughs. The period of these cycles corresponds to either the period of the stimulus tone, or in the case of broadband noise, the period of the neuron's best frequency. This phenomenon is referred to as "phase ambiguity."

Phase ambiguity is a direct consequence of the way in which timing information is encoded by the auditory nerve (Rose et al., 1966). Both MSO and NL receive input from the cochlear nuclei in the form of impulses phase-locked to the stimulus. A laminaris neuron fires maximally when these impulses arrive simultaneously from the left and right cochlear nuclei. Selectivity for particular time differences is achieved by axonal delay lines that delay the impulses such that they reach the coincidence detector neuron at the same time. As a result, when the axonal delay corresponds to the real ITD, the coincidence detector fires maximally. Coincidence also occurs, however, when the interaural time differences is increased or decreased by an amount equivalent to an integer multiple of the stimulus period (figure 3.1), resulting in a characteristic cycling of ITD tuning curves in response to pure tone stimuli in which ITD tuning curves exhibit peaks separated by multiples of the stimulus period.

While phase ambiguity can occur at any frequency, under natural conditions it is only a problem at high frequencies, when the wavelength of the sound is less than half the inter-

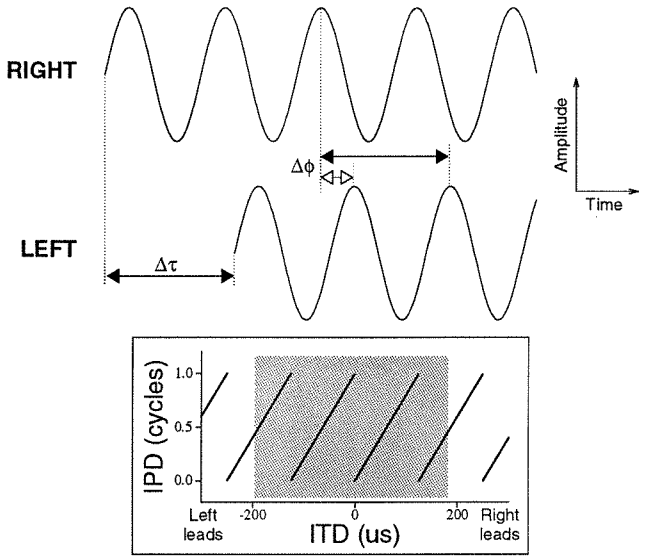

Figure 3.1: This diagram illustrates the basic problem of phase ambiguity when measuring ongoing interaural time disparities (*i.e.*, at steady state). In the top part of the figure the waveforms marked RIGHT and LEFT represent the sound waves arriving at the right and left ears. The line on the left with filled arrow heads ($\Delta\tau$) represents the interaural *time* difference; the right ear leads by just over one period of the waveform, corresponding to a sound source on the right. The two lines on the right ($\Delta\Phi$) indicate two equivalent interaural *phase* differences (*i.e.*, differing by exactly one cycle). Only the IPD indicated with filled arrows actually corresponds to the true interaural *time* difference. However, as described in the text, a cell sensitive to IPD will respond to both $\Delta\phi$'s, as well as any other $\Delta\tau$ differing by an integral multiple of the stimulus period. The inset graph at the bottom represents the relationship between ITD and IPD for an 8kHz sound. The shaded area is the range of ITDs experienced by the barn owl under natural conditions ($\pm 180\,\mu s$). Different ITDs with the same IPD within the shaded area indicates phase ambiguity occurs under natural listening conditions for the owl.

aural distance (Kuhn, 1977). One solution, taken by most mammalian species, is to rely on ITD cues only for low frequencies and to use interaural level differences (ILDs) for high frequencies (Heffner and Heffner, 1992). Barn owls, however, use ITD over a frequency range of 4 to 9 kHz, well beyond the limit imposed by phase ambiguity (Konishi, 1973b; Knudsen and Konishi, 1979).

One method for resolving phase ambiguity is to determine the true interaural time difference by comparing the phase ambiguous information across several frequency channels (Takahashi and Konishi, 1986; Wagner et al., 1987; Mori et al., 1991). The anatomical and neural substrates for this operation have been described in the barn owl (Konishi et al., 1988) and are illustrated in figure 3.2. NL projects to the Core subdivision of the central nucleus of the inferior colliculus (ICc; Takahashi and Konishi 1988a, 1988b, Fujita and Konishi 1991, Adolphs 1993). Core neurons show narrow frequency tuning and phase ambiguous ITD tuning, similar to that observed in NL (Wagner et al., 1987). The Core projects to the lateral shell (LS) of the contralateral ICc (Takahashi et al., 1989), which, in turn, connects to the external nucleus of the inferior colliculus (ICx). LS is the first site in the sound localization pathway where neurons exhibit broad frequency tuning, indicating the convergence of different spectral processing channels. Tuning width increases in ICx, where many neurons have frequency tuning widths greater than 5 kHz. LS and ICx neurons are phase ambiguous when stimulated with tones, but these same cells, in response to broadband noise, show ITD tuning curves with one dominant peak, corresponding to the real ITD. This phenomenon is referred to as side peak suppression.

The use of coincidence detection and integration across frequency channels to determine interaural time difference is similar to cross correlating the acoustic waveforms arriving at the left and right ears. Like the output of LS and ICx neurons, the cross-correlation of periodic signals, *e.g.*, tones, is periodic, while that of non-periodic signals, *e.g.*, broadband noise, yields a single value, corresponding to the true time difference. The periodicity, or side peak suppression, in the output of a cross-correlator is dependent on signal bandwidth in a characteristic fashion. These experiments test the hypothesis that LS and ICx neurons operate as cross-correlators of the input waveforms to the two ears by examining the relationship between side peak suppression and signal bandwidth in comparison to that of a

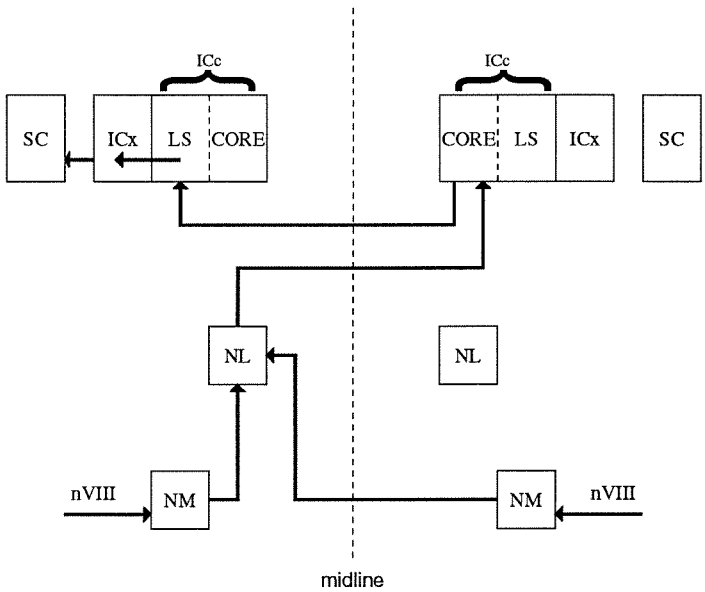

Figure 3.2: A block diagram showing the connectivity of the brainstem and midbrain nuclei involved in processing interaural time differences in the barn owl. The circuit is bilaterally symmetric, only one half of the circuit is shown here (abbreviations: **nVIII**, Auditory Nerve; **NL**, Nucleus Laminaris; **NM**, Nucleus Magnocellularis; **ICc**, Central Nucleus of the Inferior Colliculus; **LS**, Lateral Shell of ICc; **CORE**, Core of ICc; **ICx**, External Nucleus of the Inferior Colliculus; **SC**, Superior Colliculus).

simple analytical cross correlator.

3.1 Methods

3.1.1 Surgical Procedures

Five adult barn owls weighing 450-500g were used for this study. Owls were housed individually in cages before and after all experiments.

Prior to the first recording session, animals were prepared for electrophysiology. Animals received no food for 12 hours prior to any procedure requiring general anesthesia. Animals were anesthetized by intramuscular injections of Ketamine-HCl (25mg/kg; Ketaset, Fort Dodge) and Diazepam (1.3mg/kg; Steris) into the pectoral muscles. This initial dose was supplemented, if necessary, with additional Ketamine (15mg/kg/h). The owl was wrapped in a soft leather jacket and the feathers covering the top of the head were removed with scissors. The owl was placed in a custom made stereotaxic frame with the palatine ridge tilted 45° downward from horizontal. The scalp was cleaned with alcohol wipes and treated with topical anesthetic (Xylocaine, Astra). A 3cm incision in the scalp was made over the midline and the skin and fascia retracted. A flat surface was made using rongeurs at the anterior extent of the incision in order to affix a stainless steel headplate. The headplate was attached to the skull with dental acrylic (Perm Rebase Corp.) and a small metal pin (0.25mm diameter) was attached to the bone with methyl acrylic glue at the intersection of the midline and the interaural axis to serve as a reference mark. The exposed bone was cleaned, antibiotic ointment (Bacitracin-Neomycin, Fougera) was applied and the wound was closed with sutures around the headplate.

The owl was gently restrained in a soft towel and returned to a dark, heated cage for recovery. Each owl was monitored continuously until it was able to maintain balance on a perch, at which point heat was removed and fresh food supplied. Food intake was monitored carefully following surgery, and owls usually began eating within 5 hours of recovery; all ate within 1-2 days.

Recording sessions began 3-5 days after headplate implantation. Anesthesia was in-

duced and maintained as described above. Animals were weighed and given subcutaneous fluids (5% Dextrose in Lactated Ringers, 20ml/kg). Owls were placed in a stereotaxic apparatus and secured by the headplate. Body temperature was maintained at 40C with a heating jacket (Baxter). Custom made earphone assemblies (see below) were inserted into the auditory meatus to a depth of approximately 0.5cm. Following application of topical anesthetic, sutures were removed and the scalp retracted. A small (12x12mm) craniotomy was made overlying IC. A microelectrode was positioned relative to the reference pin with an accuracy of $\pm 10\mu$m. The *dura mater* directly below the microelectrode was punctured with a sharp needle and the electrode was advanced into the brain by an electronically controlled stepper motor (μD-100, Beckman Electronics).

Recording sessions lasted 8-15 hours, following which the craniotomy was sealed with a layer of dental acrylic. Antibiotic ointment was applied to the exposed skull, the wound sutured closed and topical anesthetic applied. The owl was returned to its cage and monitored as described above. Depending on the owl's weight and speed of recovery, experiments were repeated every 4-6 days for a period of 4-6 weeks.

3.1.2 Acoustic Stimuli

Experiments were performed in either a double walled sound-attenuating chamber or a double walled anechoic chamber (Industrial Acoustics Corp).

Acoustic stimuli consisted of pure tone, broadband (0-13 kHz) and band limited noise bursts of variable ILD and ITD. Stimuli were 100ms in duration, 5ms linear rise/fall times, presented 1 per second. Stimuli were synthesized on a computer workstation (Sparc/IPX, Sun Microsystems), presented through a digital signal processor equipped with a 16bit, 48 kHz data acquisition subsystem (S56X+ProPort-656, Berkeley Camera Engineering). Analog Signals were attenuated with a pair of digitally controlled attenuators (PA4, Tucker Davis) to control ILD and overall stimulus level, amplified (Power Amp, Beckman Electronics), and presented to the owl dichotically through custom made earphone assemblies. ILD could be specified in 1dB increments and ITD in 5 μs increments.

Earphone assemblies consisted of intensity- and phase-matched earphones (Sony MDR-

E535 or Koss LS/6) attached to a 3cm metal delivery tube (25mm ID). Each tube contained a small calibrated probe microphone (Knowles-3033) designed to measure sound pressure levels at the end of the delivery tube. At the beginning of each experimental session, the earphone assemblies were calibrated using the probe microphones. The calibration data were used during the experiment to adjust the computer output to effect a nominally flat frequency response ($\pm$6dB) from 0.5-13 kHz.

In one owl, sound pressure levels were also measured close to the tympanic membrane using a calibrated 2mm probe tube attached to a $\frac{1}{2}$-inch condenser microphone (Brüel&Kjær-4133). A small hole was made on the ventral border of the squamosal bone and the probe tube inserted under visual guidance. The end of the probe tube was positioned 1–2mm from the tympanic membrane. The dichotic earphone assemblies were then inserted as described above. The calibration procedure was repeated using both the Knowles and Brüel&Kjær microphones.

3.1.3 Data Collection and Analysis

Isolated neurons were recorded from extracellularly in LS and ICx with either tungsten or glass microelectrodes (tungsten, 250 μm, 12MΩ, AM Systems; glass, 10-15 μm tip diameter, 4M K-Acetate, 0.5-1.5MΩ). Signals from the electrode were amplified (100–1000 times), filtered (0.3–10 kHz) and discriminated with a level detector (μA-200, Beckman Electronics). The level detector output was recorded by the computer system (21 μs resolution). Broadband noise (ILD=0dB, ITD=0 μs) was used as a search stimulus. LS and ICx were located stereotaxically. LS and ICx neurons were classified as such based on a combination of stereotaxic position and physiological tuning properties, namely sidepeak suppression, ILD sensitivity and an increase in frequency tuning widths beyond that reported for Core neurons (Takahashi and Konishi, 1986; Wagner et al., 1987). Physiologically, the difference in tuning properties between LS and ICx, with respect to temporal processing, is continuous. No attempt is made here to distinguish between these two neuronal populations.

Isolated cells were first characterized manually to determine approximate values for best ILD, ITD and frequency. Tuning curves for ILD, ITD and frequency were then collected

holding the non-varying stimulus parameters constant, usually at optimal values. Tuning curves were measured at 20dB above threshold and averaged over 4-6 repetitions.

Neuronal responses were recorded as the number of spikes occurring in a time window beginning at stimulus onset and ending 20ms after stimulus offset. Spontaneous activity was characterized by counting the number of spikes occurring in the same time window for "spontaneous trials" (no stimulus) randomly interleaved with stimulus trials.

Frequency tuning was assayed using iso-intensity frequency response curves presented binaurally at the best ITD and ILD. Tones were presented at 20dB above threshold for each neuron's best frequency, as determined by hand. Each iso-intensity frequency response curve was characterized by its width, defined to be the range of frequencies over which the cell's response was greater than or equal to 50% of the maximal tone response, denoted W_{50}. Because ICx cells often exhibit broad frequency tuning with no clear single peak, best frequency (BF) was defined to be the center of this range. The traditional definition of BF is the frequency eliciting a maximal response in an iso-intensity frequency tuning curve. For symmetric, peaked tuning curves, the definition used here is essentially the same as the traditional one. In the case of broadly tuned non-peaked, or asymmetric, curves, the definition used here provided a better estimate of the center of the frequency range capable of driving a cell. This is similar to the median frequency (MF) described by Yin et al. (1986) for synchronization-rate tuning curves.

The best ITD, or main peak (MP), was defined as the time difference generating a maximal response with broadband noise stimuli. For those cells with pure tone ITD curves available at several different frequencies, the characteristic delay (Rose et al., 1966) was estimated qualitatively by determining ITD for which the neuronal response was the same across all frequencies. In all the cells reported here, the main peak and characteristic delay values were the same, though there are reports that this is not the case for all neurons (Moiseff and Haresign, 1992). The two peaks immediately adjacent to the MP were defined to be the side peaks (SPs).

An index of side peak suppression (%SPS) was calculated as:

$$\%\mathrm{SPS} = 100 \times (MP - \overline{SP})/(MP),$$

where MP is the response at the main peak and $\overline{SP}$ is the mean of the responses at both the left and right flanking side peaks. %SPS ranges from 0, for phase ambiguous cells, to 100 for cells exhibiting complete suppression.

The effect of bandwidth on side peak suppression was assayed by measuring a cell's response to ITDs corresponding to the MP and SPs over a range of stimulus bandwidths. Bandpassed noise was generated digitally using a rectangular filter (>100dB/octave) centered at the cell's BF (similar to the method described by Chan et al., 1987). The noise was nominally flat in the passband. Bandpassed stimuli were presented at a constant RMS level. In early experiments, full ITD tuning curves (usually $\pm 300\,\mu s$ in $20\,\mu s$ steps) were collected at a constant ILD for each stimulus bandwidth. During later experiments, only responses at the MP and the two flanking SPs were collected at each bandwidth in order to reduce the time required for data collection. In these later cases, the MP and SP values were determined from a preliminary ITD tuning curve using a broadband noise stimulus.

3.2 Results

The results reported here were collected from 37 well isolated neurons located in the LS and ICx divisions of the inferior colliculus.

Frequency Tuning. Side peak suppression is thought to be at least partially generated by the integration of multiple narrow band frequency channels originating in NL. Iso-intensity frequency tuning width, characterized by W_{50}, reflects the range of excitatory frequency channels providing input for cells in LS and ICx. Of the 37 neurons 29 had frequency tuning curves with a single clearly defined peak. The remaining 8 neurons were broadly tuned. BFs ranged from 4.5 to 9 kHz (figure 3.3A); this corresponds to the spectral range in which the owl most accurately localizes sounds (Knudsen and Konishi, 1979). W_{50} values ranged from 0.9 to 6.9 kHz (figure 3.3B).

ITD Tuning. The population of cells found in LS and ICx are spatially tuned for azimuths ranging from far contralateral to just ipsilateral of the midline, corresponding to best ITDs ranging from approximately $180\,\mu s$ contra ear leading to $40\,\mu s$ ipsi ear leading. This distribution is not uniform; the frontal region of space, corresponding to the behaviorally

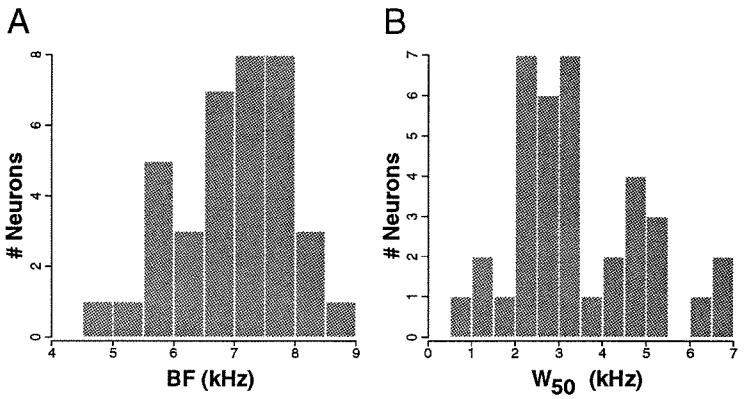

Figure 3.3: Distribution of frequency tuning parameters in the population of observed cells ($n = 37$): (A) Best frequency (7.0±1.5 kHz, mean±SEM). (B) Width of frequency tuning at 50% maximal response (2.4±0.2 kHz, mean±SEM).

observed region of maximum localization acuity, is over-represented (Knudsen and Konishi, 1978b). Acoustically, the frontal region corresponds to an area in which ITD is essentially linearly related to sound source azimuth (Olsen et al., 1989). The population of cells reported in this study are largely restricted to this frontal or linear region of space. The distribution of main peak values for the 37 cells reported here is shown in figure 3.4A.

Side peak suppression. In response to broadband noise (>10 kHz) cells showed %SPS values ranging from 26 to 87% (figure 3.4B). All 37 cells reported here demonstrated some degree of suppression in response to broadband noise; only 11% (4/37) were suppressed beyond 70%. This is consistent with the results of Takahashi and Konishi (1986), who reported a mean suppression value of 47±0.2 (mean±S.D.) for ICx neurons.

In all cells studied, suppression was monotonically related to stimulus bandwidth. All cells were phase ambiguous in response to pure tones ("zero bandwidth"), with ITD peaks repeating at the period of the stimulus, and all peaks of approximately equal magnitude. Suppression increased with increasing bandwidth until it reached an asymptotic value; the distribution of asymptotic or maximum suppression values is shown in figure 3.4B.

A typical cell's response as a function of stimulus bandwidth is shown in figure 3.5. Figure 3.5A demonstrates the basic finding that side peak height decline relative to the main peak as bandwidth increases. The absolute magnitude of response at the main and side

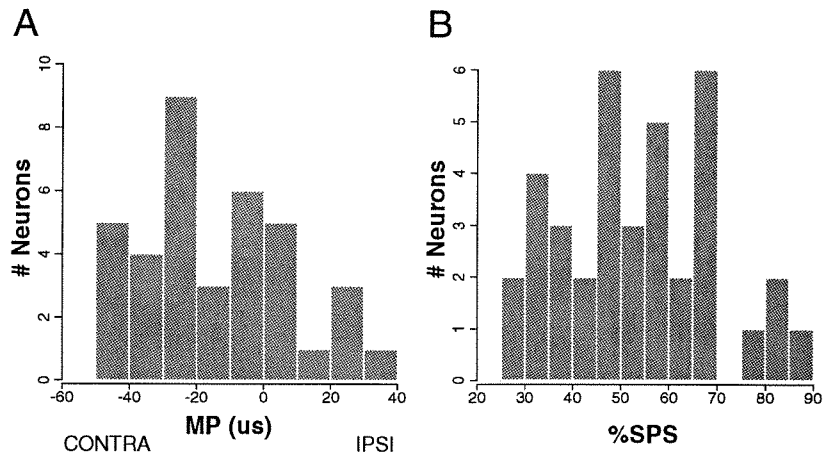

Figure 3.4: Distribution of ITD tuning parameters ($n = 37$): (A) Shows the range of MP values for the entire population of cells (-9.6±3.6 μs, mean±SEM). Negative ITDs (labeled CONTRA) correspond to contralateral ear leading. (B) Maximum percent side peak suppression (%SPS) in response to broadband (>10 kHz) noise (53±3%, mean±SEM).

peaks, as a function of stimulus bandwidth, is shown in (figure 3.5B). In this particular cell the increase in %SPS that occurs with greater bandwidths is largely due to an increase in the main peak response and not to a reduction in the responses at the sidepeaks.

Because the bandpassed stimuli were presented at constant RMS level, within any given narrow band, *e.g.*, the band defined by a cell's frequency tuning curve, the stimulus power is either constant or decreases as the stimulus bandwidth increases. The increase in response, therefore, can not be explained simply by sensitivity to stimulus intensity. This increase, however, is consistent with the idea that each increase in stimulus bandwidth recruits successively more frequency channels, each of which is relatively insensitive to absolute stimulus power. This relationship between bandwidth and response magnitude appears to be opposite in sign to that observed for some ICc cells in the cat (Yin et al., 1987).

In almost all 37 cells, the monotonic %SPS curves relating %SPS to signal bandwidth (ω) were well described by a sigmoid function of the form:

$$\%\mathrm{SPS}(\omega) = k/(1+\exp[-\sigma(\omega-\mu)]),$$

where the three parameters k, μ and σ correspond to maximum suppression, bandwidth at

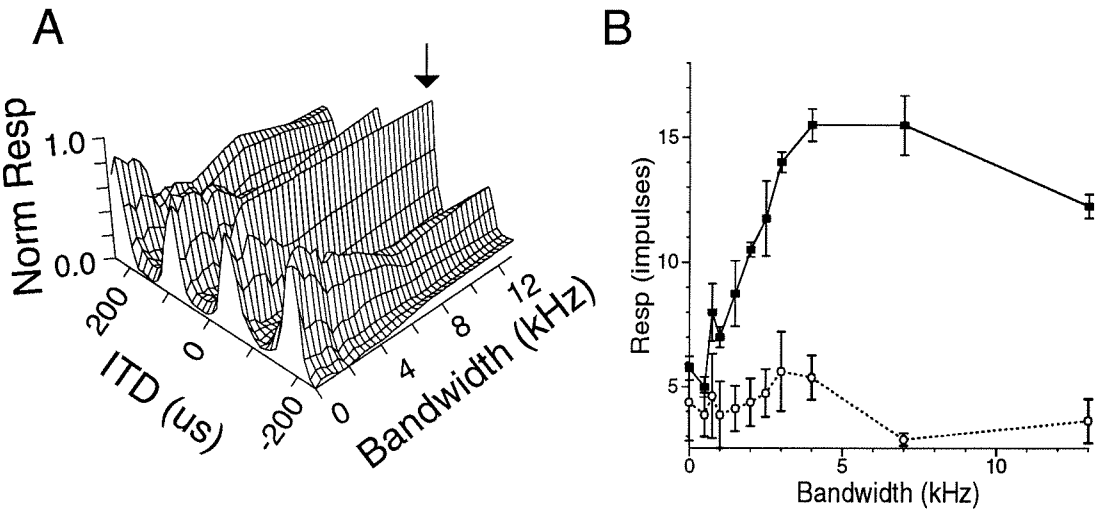

Figure 3.5: Response properties of a typical cell as displayed as function of increased stimulus bandwidth. (A) The surface represents a set of ITD tuning curves collected over a wide range of bandwidths (0–13 kHz). Each tuning curve has been individually normalized by dividing the maximum response for that curve. Note that side peaks decline relative to the main peak (indicated by arrow) as the stimulus bandwidth increases. (B) Comparison of the unnormalized responses to ITDs corresponding to the main and side peaks for the same cell as in A. Filled rectangles indicate mean main peak responses, and open circles indicate the mean of responses at the two side peaks flanking the MP. Error bars indicate the SEM.

50% maximum suppression and the slope of the %SPS curve respectively. The three parameters were chosen using an iterative curve fitting procedure designed to minimize mean squared error. Fitting the data with an analytic function allowed for accurate estimation of the signal bandwidth required to generate 50% suppression given the sparse nature of the %SPS data. The sigmoid fit for the cell shown in figure 3.5 is shown in figure 3.6, along with several representative ITD tuning curves at different stimulus bandwidths.

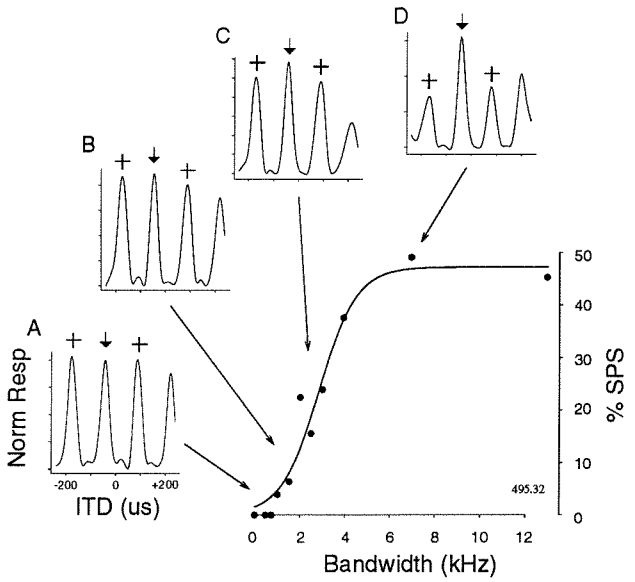

Figure 3.6: In the main plot (lower right) %SPS is shown as a function of stimulus bandwidth for the cell pictured in figure 3.5. Individual points represent measured %SPS values and the solid curve is the best fitting sigmoid. Inset graphs A–D are normalized (% maximum response) ITD tuning curves at particular stimulus bandwidths: (A) 0.75 kHz, (B) 1.5 kHz, (C) 2.5 kHz, and (D) 7.0 kHz. Arrows indicate the MP; crosses, the side peaks.

The sigmoid appearance of the %SPS curve was independent of maximum observed suppression. The cell shown in figure 3.7 was suppressed more than 80% in response to broadband noise, while the cell in figure 3.6 showed a maximum suppression of less that 50%. Despite the difference in maximal suppression levels, the shapes of the two tuning curves are qualitatively similar.

Typical %SPS curves, ranging from shallow to steep, are shown in figure 3.8A–C. Despite the variation in maximum %SPS and the steepness of tuning curves, all six cells exhibit a monotonically increasing relationship between %SPS and stimulus bandwidth. The shal-

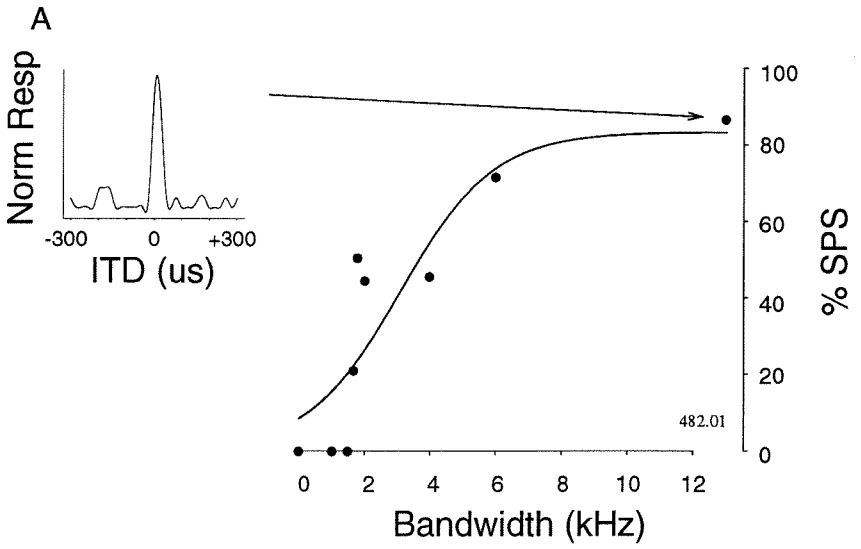

Figure 3.7: %SPS increases in this cell to over 80%, though the shape of the curve is still somewhat sigmoid. (A) ITD tuning curve at 13.0 kHz.

low curves in figure 3.8A are almost linear from 0 to 8 kHz, while the steeper curves (figure 3.8C) appear linear only over a narrow range of bandwidths (approximately 3-5 kHz).

In general, the sigmoid function fit the data less well at narrow bandwidths, primarily due to an increase in response variance in most cells for narrow band stimuli. Overall, however, the sigmoid provided a good fit for the %SPS curves of all cells presented here. Figure 3.9 shows an example of a cell with large variance at narrow bandwidths and the resulting sigmoid fit. There is no significant suppression below 3 kHz (figure 3.9A), however, several of the data points at low frequencies are not well fit by the sigmoid. In this case, and all others like it, the poor fit is largely due to the low discharge rate of the cell at narrow bandwidths. Below 4 kHz the distribution of responses at the MP and SPs are overlapping; as the bandwidth increases beyond 4 kHz, the MP response continues to increase, while the SP response saturates (figure 3.9B); note that in some cells the SP responses decline instead of saturating. The estimate of %SPS is sensitive to the variance of response. At low bandwidths response levels both for the MP and SP show high variance, resulting in a noisy estimate of %SPS. All possible combinations of main and side peak response patterns that can result in non-zero %SPS values were observed: MP saturates, SP declines (figure 3.10A);

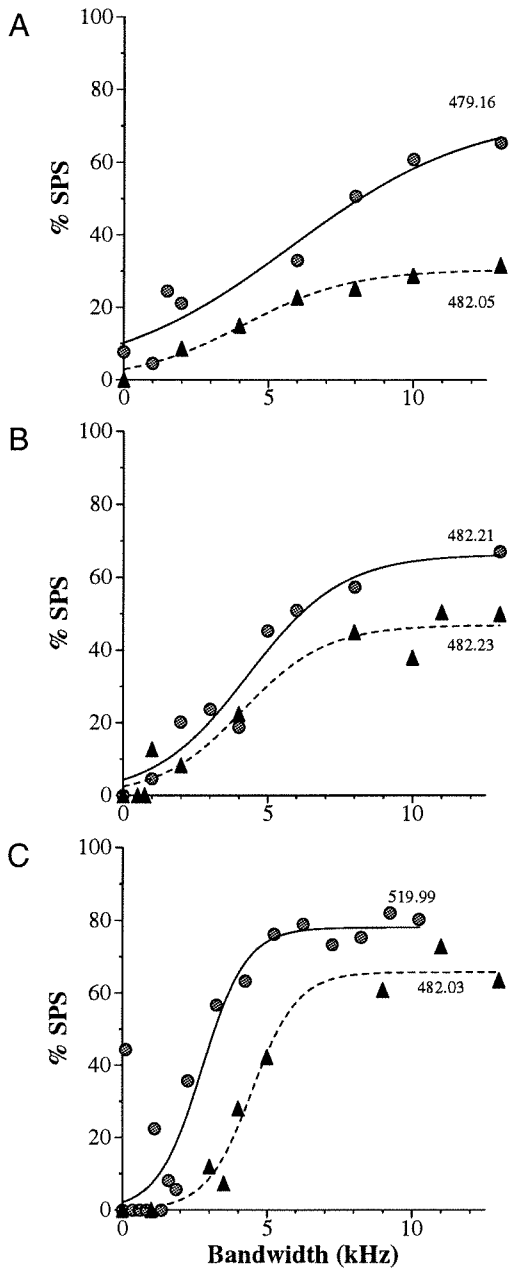

Figure 3.8: Representative %SPS curves. Each graph displays data from two cells; the curves indicate the best fitting sigmoid and the marks indicate the data points used to generate the curves (solid curves fit circles, dashed curves fit triangles). (A) "Shallow" tuning curves, below 8 kHz both cells exhibit an almost linear relationship between signal bandwidth and %SPS. (B) "Moderate" tuning curves. (C) "Steep" tuning curves.

MP increases, SP declines (figure 3.10B); and MP increases, SP saturates (figure 3.10C).

In order to test the validity of fitting with a sigmoid function, 50% suppression levels, estimated with the sigmoid, were compared to those calculated with a cross-validated smoothing spline fit (SPlus, StatSci) of the same data. The spline fit is less constrained than the sigmoid and is capable of fitting more of the variance present in the data, including the variance at low bandwidths observed in some cells. Despite the spline's ability to fit small perturbations in the tuning curves, the 50% SPS values estimated using the two fitting algorithms were highly correlated (figure 3.11B). Based on this finding, the remainder of this paper relies on the 50% values as determined from the sigmoid fit.

Models for side peak suppression based on across-frequency channel integration often suggest that suppression should be associated with an increase in frequency tuning width. However, comparison of the input bandwidth, as measured by W_{50}, and the stimulus bandwidth required for 50% of maximum side peak suppression obtained from the best fitting sigmoid, μ, showed no significant correlation (figure 3.12A). W_{50} was also uncorrelated with maximum observed side peak suppression (figure 3.12B).

In order to examine the overall effect of bandwidth on %SPS for the auditory localization system up to the level of the inferior colliculus, the combined data from all 37 cells were fit using the same fitting algorithms described above for single cells. The results of the sigmoid fit for all 37 cells are shown in figure 3.13A. The results of fitting the entire dataset with a single sigmoid function are shown in figure 3.13B. The shape of this "population curve" closely resembles the tuning curves observed in individual cells. The bandwidth required for 50% of maximum suppression is 3.1 kHz (3.2 kHz for spline fit).

3.3 Discussion

The shape of the cross-correlation functions (CCF) for band limited signals closely resembles the ITD tuning curves recorded from LS and ICx neurons in response to comparable signals. Figure 3.14 shows CCF functions computed for typical stimuli used in the physiological experiments described above. Correlation functions were computed using a simple

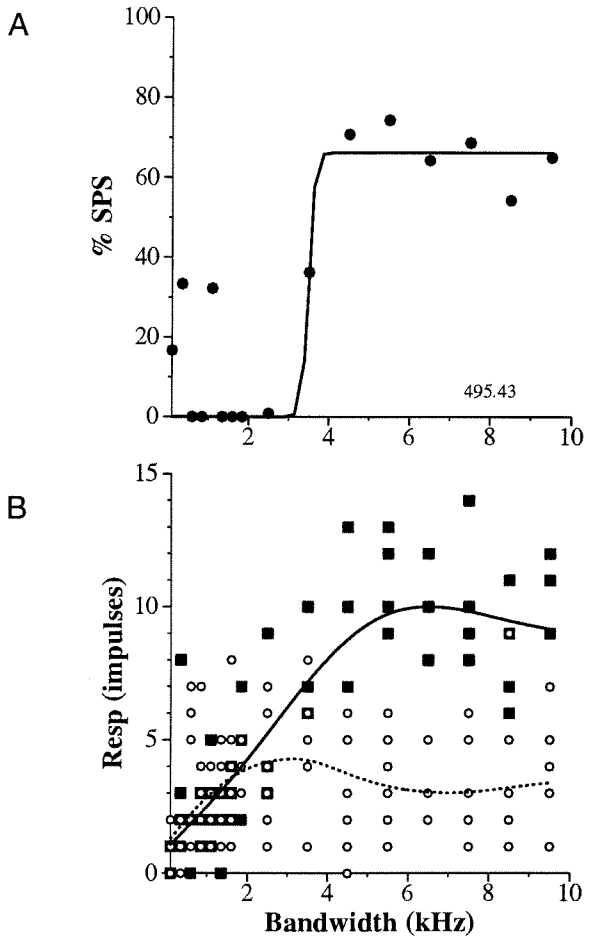

Figure 3.9: Sensitivity of %SPS estimates to variance at narrow stimulus bandwidths. (A) At narrow stimulus bandwidths (< 2 kHz), this cell shows considerable jitter in the estimate of %SPS. The narrow bandwidth points are not well fit by the sigmoid. These jitter or noise in these measurements is due to a high degree of response variability at narrow bandwidths. (B) The absolute response magnitude for the same cell shown in A at ITDs corresponding to the MP (solid rectangles) and SPs (open circles) is shown here over the same range of stimulus bandwidths. At low bandwidths, the MP and SP distributions are essentially overlapping, but as bandwidth is increased, the distributions separate. The solid and dotted lines represent cross validated splines fit the MP and SP distributions respectively.

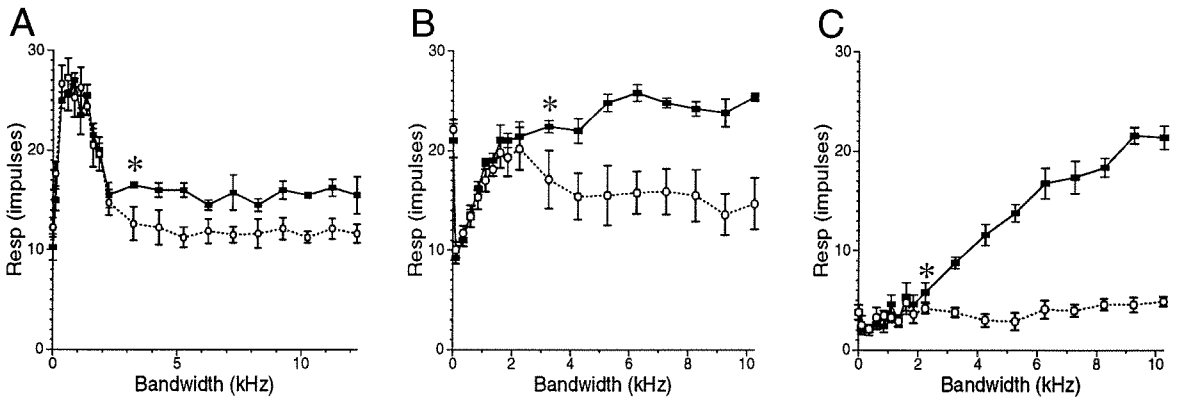

Figure 3.10: Graphs A–C illustrates three different examples of MP/SP response patterns as a function of increasing bandwidth (MP=solid rectangles, SP=open circles). The effect of increasing bandwidth on the MP response can be different from the effect on the SP response. $*$ indicates the minimum stimulus bandwidth for which the MP and SP responses significantly differ (t-test, $p < 0.05$); the MP-SP difference is significant at all bandwidths at and beyond the $*$. Error bars indicate the SEM for each measurement. (A) At low bandwidths ($\leq$2 kHz) the MP and SP responses are the same. However, beyond 2 kHz the MP response saturates, while the SP response declines. (B) Beyond 2.5 kHz the MP response continues to increase, while the SP response declines. (C) Up to 10 kHz, the MP response increases monotonically, while the SP response is essentially constant.

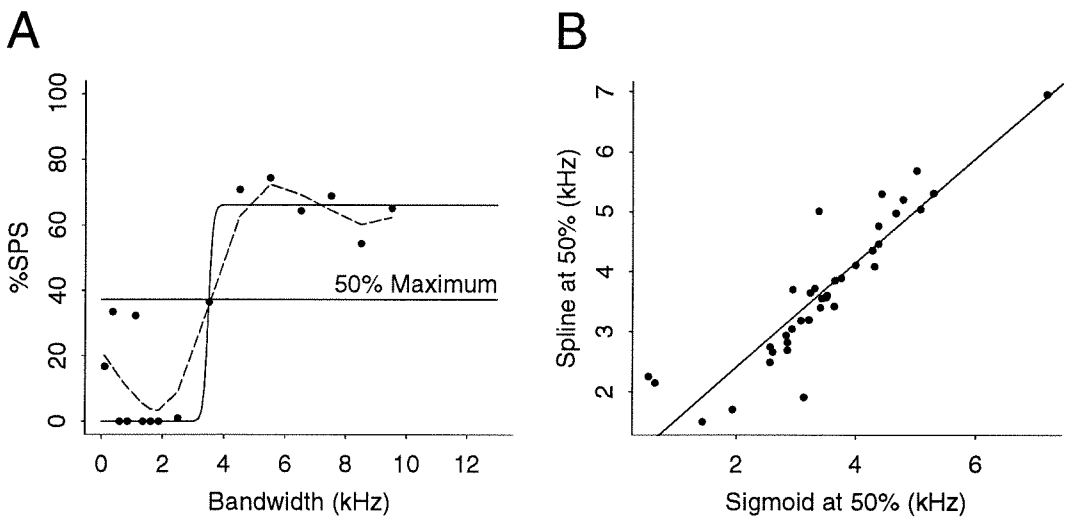

Figure 3.11: Comparison of curve fitting methods: (A) This cell shows considerable jitter at low bandwidths that is not well described by a sigmoid function (solid line). In contrast, the cross-validated spline function (dashed line) fits small deviations in the noisy low bandwidth measurements. The horizontal line indicates 50% maximum suppression (for this particular cell); both the sigmoid and the spline fits give almost exactly the same bandwidth for 50% suppression. (B) 50% values estimated by the two methods were highly correlated (solid line) for the entire population of 37 cells ($r = 0.904$, $p < 0.001$).

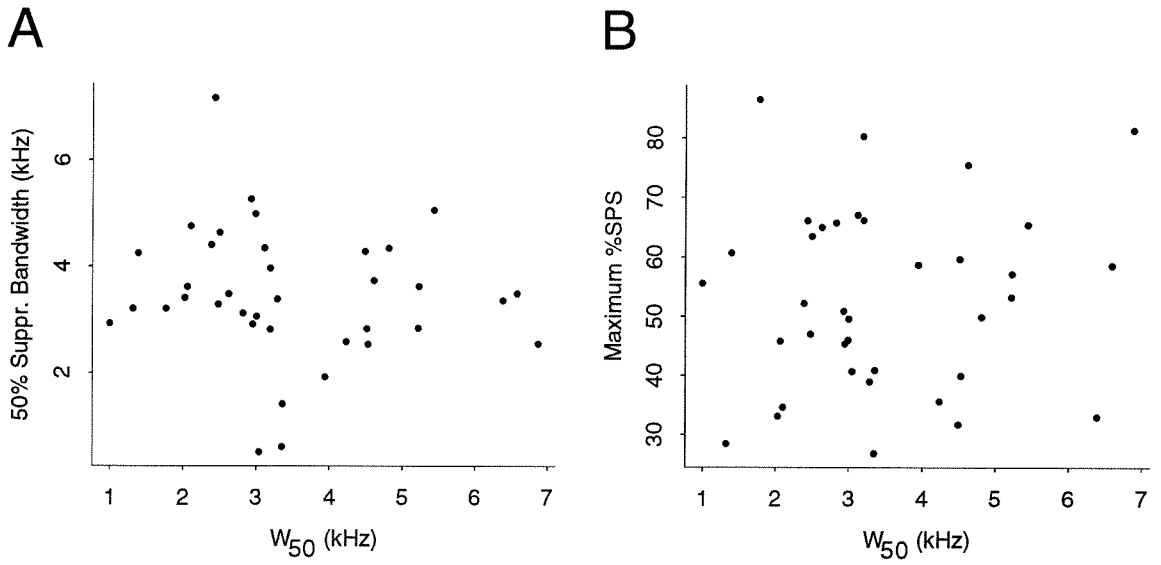

Figure 3.12: No correlation was observed between frequency tuning width (W_{50}) and (A) bandwidth at 50% suppression ($r = -0.122$, $p = 0.472$) or (B) maximum side peak suppression ($r = 0.097$, $p = 0.570$).

unweighted correlation function,

$$CCF(\delta) = \sum_{t=0}^{N} l(t-\delta)r(t),$$

where $l(t)$ and $r(t)$ represent the band limited, time-domain signals presented to the left and right ears, and δ is the lag or internal delay of the correlator. In figure 3.14, $l(t)$ and $r(t)$ are identical (*i.e.*, ITD=0 μs or autocorrelation). Finally, the resulting correlation function was divided by its maximum value to aid in comparing the CCF to normalized ITD tuning curves. In addition to generating CCFs that resemble ITD tuning curves, the correlator also exhibits a relationship between signal bandwidth and side peak suppression similar to that observed in IC neurons (compare figure 3.14 with figures 3.6 and 3.7).

Despite similarities between CCFs and ITD tuning curves, there are several important differences between the mathematical correlator and the owl's auditory system. An ideal correlator is phase ambiguous (0% SPS) in response to pure tones, but suppression occurs

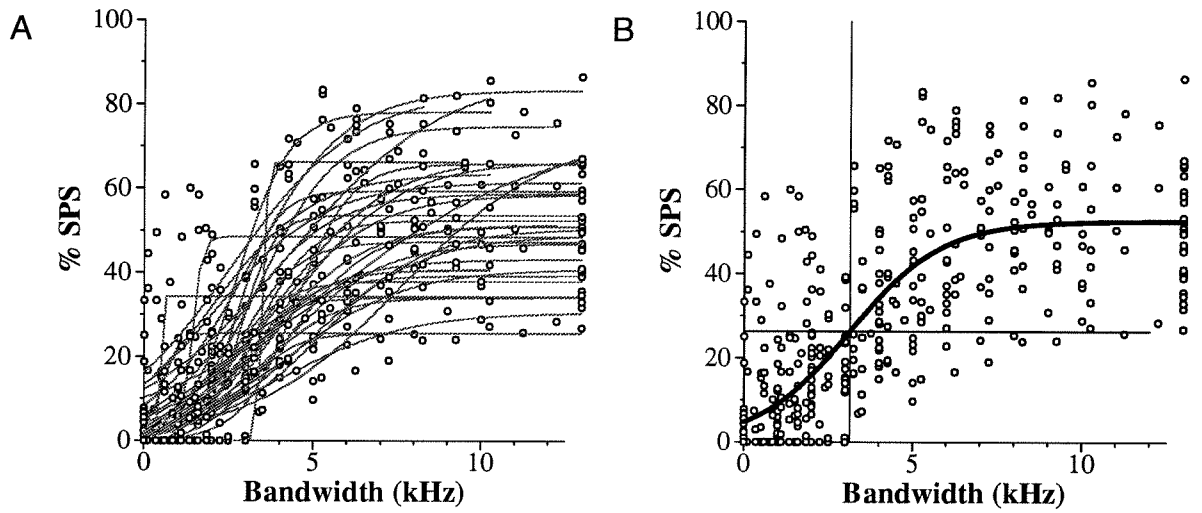

Figure 3.13: The amount of side peak suppression observed as a function of stimulus bandwidth, for the entire population of 37 cells. (A) Sigmoid fits for each of the 37 cells used in this study. In general, the fits are worse at low bandwidths, reflecting the increased variance in the response for tonal and narrow band stimuli, as described in the text and in figure 3.9. (B) A composite %SPS curve calculated by fitting the entire data set of 420 points with a single sigmoid. The solid line represents the best fitting sigmoid, and the intersection of the horizontal and vertical lines indicates the 50% maximum suppression level (27% side peak suppression) at 3.1 kHz. The amount of side peak suppression observed as a function of stimulus bandwidth, for the entire population of 37 cells.

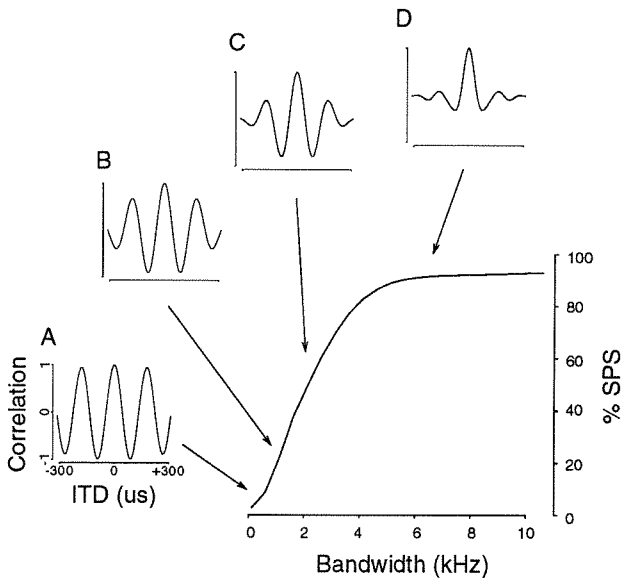

Figure 3.14: This figure shows the results of mathematically cross-correlating bandpassed noise signals similar to those used in the experiments. The main figure shows %SPS as a function in signal bandwidth, measured in the same manner used to assay %SPS *in vivo*. Inset graphs correspond to the actual cross-correlation functions calculated for representative signal bandwidths: (A) 0.6 kHz, (B) 1.6 kHz, (C) 2.6 kHz, and (D) 6.6 kHz.

for any signal bandwidth greater than that of a pure tone. Many IC neurons require a bandwidth of 2-3 kHz before any suppression is observed. For example, the cell shown in figure 3.9 requires a bandwidth of about 3 kHz before any suppression is observable. The population response of IC (figure 3.13B) indicates that, as a system, the time pathway can perform side peak suppression at relatively low bandwidths, even though some cells may not be suppressed at these low bandwidths.

Another difference between the ideal correlator and IC neurons described here occurs in the maximum amount observed side peak suppression. The correlator achieves greater than 90% suppression at bandwidths >10 kHz. Such suppression was rarely observed in individual cells (figure 3.4) and is not reflected in the population curve (figure 3.13B), which shows a maximum suppression value of only 53% (> 10 kHz). The %SPS curve for the mathematical correlator reaches a half maximal level at a bandwidth of around 2 kHz. In contrast, the LS/ICx population curve is not as steep and requires a bandwidth of about 3 kHz for half maximal suppression, at a much reduced absolute value of %SPS.

These comparisons suggest that the barn owl's ITD processing system functions as a cross-correlator, albeit a non-ideal one. The lower maximum suppression values and reduced slope of LS and ICx %SPS curves relative to the model suggest that time pathway is not as efficient at extracting ITD as an ideal correlator.

It is important to keep in mind that while IC neurons signal the cross-correlation between the unfiltered signals arriving at each ear, IC is not the site of coincidence detection. Yin and his colleagues (Yin and Chan, 1988; Yin et al., 1987) have pointed out that direct proof of coincidence detection is possible only when neurons (1) respond not only to binaural coincidence, but also to monaural stimulation and (2) exhibit phase locking.

Physiological evidence from NL recordings (Carr, 1990; Sullivan and Konishi, 1986) demonstrated that laminaris neurons satisfy these two requirements. Carr (1990) also showed that in NL the difference in the mean phase angles for period histograms obtained separately with left and right monaural tone bursts accurately predicted a neuron's best interaural time difference for dichotic stimuli, consistent with NL being the site of coincidence detection. In Core, neurons are not phase locked to auditory stimuli, though they exhibit ITD sensitivity similar to that observed in NL. Though Core cells are not themselves coincidence detec-

tors, they do encode interaural cross-correlation over a narrow frequency band as a result of a labeled line input from NL.

In the mammalian ICc, Yin et al. (1987) manipulated the amplitude and phase spectra of their stimuli to produce varying degrees of interaural correlation. Even though ICc itself is not a coincidence detector, they observed that the relationship between correlation and ITD tuning was similar to that expected for a cross-correlator, thereby providing indirect evidence that ICc neurons, in the cat, signal the interaural cross-correlation over a narrow range of frequencies (1-2.2 kHz).

A narrow band correlator, *i.e.*, a correlator receiving input over a limited spectral range, exhibits phase ambiguity. Phase ambiguity can be resolved, in the presence of a broadband input signal, either by a correlator with a broadband input or by combining the output of several narrow band correlators. Functionally, LS and ICx cells operate as broadband correlators even though the input to LS (from NL via Core) is a bank of narrow band correlators. Both the anatomical and physiological evidence argue that, in the owl, resolution of phase ambiguity depends on the combination of many narrow band correlators. Several models have been proposed to explain how this integration process takes place. The two most commonly discussed in the owl literature are: (1) linear summation across frequency channels (Yin and Chan, 1988), (2) non-linear combination across frequency channels (Takahashi and Konishi, 1986; Mori et al., 1991).

The correlator presented in figure 3.14 is mathematically equivalent to a broadband correlator or the linear summation of output of a bank of narrow band correlators. This corresponds exactly to the linear summation model. In the cat, Yin and Chan (1990) tested this model in both MSO and ICc and found that ITD tuning curves in response to noise stimuli were almost identical to those predicted by the summation of a number of pure tone ITD curves for the same cell, which is wholly consistent with linear summation. NL and Core cells, however, appear to be different. In response to broadband noise, the cells show no side peak suppression. ITD curves in NL and Core remain phase ambiguous, with a periodicity equal to the period of the cell's BF (Fujita and Konishi, 1991). This suggests that the cat and owl time processing pathways differ as early as the coincidence detection stage. At the level of ICx, Takahashi (1989) used a simple two-tone stimulus to test the linear summation

model in the owl. The stimulus was composed of two spectrum level matched tones, one at the neuron's BF (F1) and the other at the BF$\pm$1.5 kHz (F2). Their results showed that ITD tuning curves in response to F1+F2 stimuli could not be predicted by a linear combination of the responses to F1 and F2 alone, indicating some form of non-linear interaction between frequency channels.

One possible non-linear integration model is based on lateral inhibitory connections among adjacent frequency channels. Because each channel has a finite spectral bandwidth, the signal bandwidth must exceed the single channel bandwidth before it recruits the neighboring frequency channels required for suppression. This model accounts only for cells requiring stimulus bandwidths greater than the input bandwidth of a NL/Core cell for side peak suppression and does not explain why some cells have reduced side peaks at relatively narrow stimulus bandwidths. It is possible that in such cells suppression might also arise from interactions among adjacent ITD channels, either instead of or in addition to interactions across frequency channels.

Takahashi and Konishi (1986) suggested that elimination of phase ambiguity in ICx might be the result of two mechanisms: main peak facilitation and side peak suppression. In some cells they observed the main peak response for the F1+F2 stimulus was greater than the main peak response for F1 alone. In other cells, the F1+F2 stimulus resulted in the side peaks ("secondary peaks") being suppressed relative to the F1 alone condition.

The results presented here (figure 3.10) are consistent with the idea that main peak facilitation and side peak suppression are independent and that the two can occur in any possible combination. Figure 3.10 shows three cells that demonstrate different combinations of main peak facilitation and side peak suppression; A shows a cell exhibiting side peak suppression in the absence of main peak facilitation; the cell in panel B displays both suppression and facilitation, while the cell in C exhibits only main peak facilitation. It is interesting that these two mechanisms appear in different combinations in different cells, suggesting that the mechanisms underlying side peak suppression may not be the same in every cell.

The mathematical correlator does not show this combination of main peak facilitation and side peak suppression, suggesting a difference between ICx and the mathematical correlator. However, it is important to note that the formulation used here for an ideal correlator

includes a normalization term which constrains the maximum value of the cross-correlation function to be $+1$, since the signals being correlated are identical, except for a time shift. Such a correlator can not generate main peak facilitation. The observation that some LS and ICx neurons exhibit facilitation at all may be indicative of another difference between these cells and an ideal correlator. This conclusion is based on the fact that the maximum correlation for the stimuli used here is defined to be $+1$. Alternatively, it is possible that facilitation is simply due to the fact that the MP and SP data come from unnormalized ITD tuning curves. If the tuning curves are normalized, then, like the correlation functions, the maximum response is always 100% and the cells would not show main peak facilitation.

The most surprising result of this study is the lack of any systematic correlation between frequency tuning and SPS. Cells with frequency tuning widths similar to those observed in NL and Core exist in LS and can exhibit SPS. There are two possible explanations for this lack of correlation. Side peak suppression might be caused by an integration of ITD channels as well as frequency channels. Lateral inhibition between adjacent ITD channels from nearby or even the same frequency bands could be used to suppress side peaks. Alternatively, iso-intensity frequency tuning curves may not be truly representative of the entire frequency range driving a particular cell. At the level of LS and ICx, cells often have little or no spontaneous activity, so inhibitory side bands are difficult to observe using pure tone stimuli. There is some evidence of inhibitory side bands based on the responses of LS and ICx neurons to two-tone stimuli (Mazer, unpublished observations); however, it is difficult to determine the site of interaction for such stimuli, since two-tone suppression effects could arise as early as the cochlea.

The requirement of a critical bandwidth for side peak suppression may have a parallel in the barn owl's sound localization behavior. Konishi (1973b) showed that the ability of the owl to accurately strike an acoustic target in darkness was related to the spectral composition of the target. For pure tones, strike error was minimal when the frequency was 7–8 kHz. Using bandpassed noise centered at 7.5 kHz, he found that strike accuracy increased monotonically with target bandwidth. Strike accuracy asymptotically approached 70% with target bandwidths beyond 3 kHz, with a maximum accuracy observed at 4 kHz, the highest bandwidth tested. In macaques, Brown et al. (1980) reported that, as in owls, localization

accuracy increases monotonically as a function of stimulus bandwidth. Both the owl and macaque behavioral data correlate well with the observation that %SPS is monotonically related to stimulus bandwidth.

Although it is tempting to relate the shape of the %SPS curves to the behavioral data, it is not clear that the behavioral manifestation of %SPS is localization accuracy. At narrow stimulus bandwidths, phase ambiguity will lead to multiple populations of neurons active in the auditory space map (ICx). The next stage of processing, the superior colliculus, integrates sensory input from ICx and generates the motor commands required to orient the animal towards acoustic targets. If such a motor signal is generated by averaging or integrating the output of a large region of the space map, localization of targets might be biased or less accurate in the presence of phase ambiguity. While this is a plausible hypothesis to relate side peak suppression to the behaviorally observed dependence of localization acuity on target bandwidth, further experiments will be required to determine if localization accuracy is a behavioral correlate of side peak suppression.

The computation performed by time pathway in the owl's auditory system is analogous to cross-correlation. These results demonstrate that LS and ICx neurons can reconstruct the cross-correlation of the unfiltered binaural stimuli based from the output of the narrow band coincidence detectors in nucleus laminaris, as would be predicted for a cross-correlator. The differences between the physiological results and the mathematical model reported here suggest that reconstruction process is not simply the linear combination of the narrow band correlators, consistent with previous observations. Regardless of the details of the algorithm used by IC neurons to integrate the output of NL, the result is that LS and ICx encode the binaural cross-correlation of acoustic signals.

Chapter 4 Conclusions

The studies described here, as well as previous studies of the barn owl's auditory system (Sullivan and Konishi, 1984; Takahashi et al., 1984; Konishi et al., 1985; Takahashi and Konishi, 1988a, 1988b), have shown that the neural substrate of sound localization, *i.e.*, space-specific auditory neurons, is the result of the convergence of multiple parallel processing streams. The data presented here demonstrate that independent channels representing time, level and frequency cues all converge in the lateral shell of the central nucleus of the inferior colliculus. This convergence results in the elimination of phase ambiguity and the formation of elevationally restricted spatial receptive fields required by the owl for accurate sound localization in both the horizontal and vertical planes.

The distribution of neuronal tuning properties in LS suggests that the process of integration is arranged systematically across the mediolateral axis of the shell. Physiologically, the synthesis of space-specific receptive fields occurs in a graded fashion, consistent with a model in which a feed-forward network successively refining the spatial tuning properties of LS neurons. LS neurons, as a result of this feed-forward process, exhibit several emergent properties, not observed in the lower stations of the sound localization pathway: sidepeak suppression, peaked ILD tuning and broad frequency tuning.

4.1 Parallel Processing in Other Systems

A substantial amount of evidence has been collected over the years suggesting that such parallel processing schemes are not limited to the owl. Studies in several species in different sensory modalities have demonstrated that parallel processing of different stimulus features appears to be a general design of sensory processing. A brief description of a few well studied examples are presented here.

4.1.1 Vision

To date, the mammalian visual system is arguably the best understood, or at least the most aggressively studied, of all sensory modalities. Several notable examples of parallel processing have been described in the visual system. Some of these pathways originate

peripherally, at the level of the retina, and others appear to arise centrally, in telencephalic brain structures. In contrast to the auditory system of the barn owl, parallel processing in vision is not usually related to the synthesis of topographic space maps or the construction of spatially restricted receptive fields. All the visual processing streams described here contain full spatial representations of the visual field. Instead, information about different feature properties such as color, luminance, orientation and motion are processed in parallel.

In the mammalian visual system parallel processing begins at the retina with a dichotomy between ON and OFF channels. ON cells respond to light spots located in the center of the cell's receptive field, while OFF cells respond best to dark spots. The earliest neurons that can be classified as being either ON or OFF cells are the non-spiking bipolar cells in the inner plexiform layer. The segregation of visual processing into ON and OFF channels extends beyond the retina to the dorsal lateral geniculate nucleus (dLGN) of the thalamus. The dichotomy ends with the thalamocortical projection with single neurons in primary visual cortex (area V1) receiving input from both the ON and the OFF channel from the thalamus.

The studies of Schiller and his colleagues (Schiller et al., 1986; Dolan and Schiller, 1994) used the glutamate agonist 2-amino-4-phosphonobutyrate (APB) to block the ON system and used psychophysical techniques to examine the resulting visual impairments. They demonstrated that ON channel blockade led to a behavioral deficit on tasks requiring detection of small spots of light brighter than the background, consistent with the idea that the ON channel signals light increments while the OFF channel signals light decrements. Schiller (1992) speculated that one reason for the separation of ON and OFF information into separate channels could be related to the difficultly in transmitting information about the absence of stimuli using action potentials. In order to detect a decrement in the firing rate of the retinal ganglion cells, which generally have low spontaneous activity levels, activity must be integrated over a relatively long period of time. By having separate ON and OFF channels, in which both light increments and decrements are encoded as increases in firing rate, both positive and negative luminance changes can be relayed to the CNS with equally high temporal resolution.

Another second pair of parallel processing streams have also been described in the vertebrate retina. ON and OFF retinal ganglion cells can be further subdivided into two groups:

those that receive input from a single class of wavelength sensitive cone photoreceptors (color opponent, parvocellular or P cells) and those that receive input from all three cone types (broadband, magnocellular or M cells). This dichotomy is maintained by the retinogeniculate projection with color opponent cells project to the parvocellular layers of the dLGN and broadband ganglion cells projecting to the magnocellular layers. In contrast to the ON/OFF system, the separation between the color opponent and broadband channels is maintained by the thalamocortical projections to area V1. The broadband neurons of the dLGN project primarily to cortical layer 4Cα while the axons of color opponent cells terminate in layer 4Cβ.

Numerous psychophysical and physiological experiments have attempted to clarify the functional distinctions between the M and P processing streams (Merigan, 1989; Schiller et al., 1990; Nealey and Maunsell, 1994; Ferrera et al., 1994a; Schiller and Logothetis, 1990, for review). The most clearcut result of these experiments is that the P stream is responsible for color vision. Lesions of the parvocellular layers of the dLGN which receive input from the color opponent retinal ganglion cells abolish the ability of monkeys to perform psychophysical color discrimination tasks. The P system also subserves "form vision" and the perception of luminance contrast at high spatial frequencies. Lesions of the magnocellular layers of the dLGN do not interfere with color, form or contrast processing, but instead lead to deficits in motion and flicker perception. This has led to the conclusion that the M stream is primarily involved in the processing of temporal information.

Parallel processing in the visual system also occurs at the cortical level. The cortical visual circuitry can be divided into two processing streams, one primarily involved in form vision (the temporal or "what" pathway) and other thought to subserve motion processing (the parietal or "where" pathway, see figure 4.1). Neurons in the form pathway are sensitive to orientation, color and shape; in the motion pathway, neurons are primarily sensitive to the direction of motion of features present in the visual field (Felleman and Van Essen, 1991). The division between form and motion processing is in many ways similar to the M/P dichotomy originating in the retina.

In fact, until recently, the form and motion streams were thought to simply be a continuation of the P and M streams. Recent studies, however, have suggested that this is not

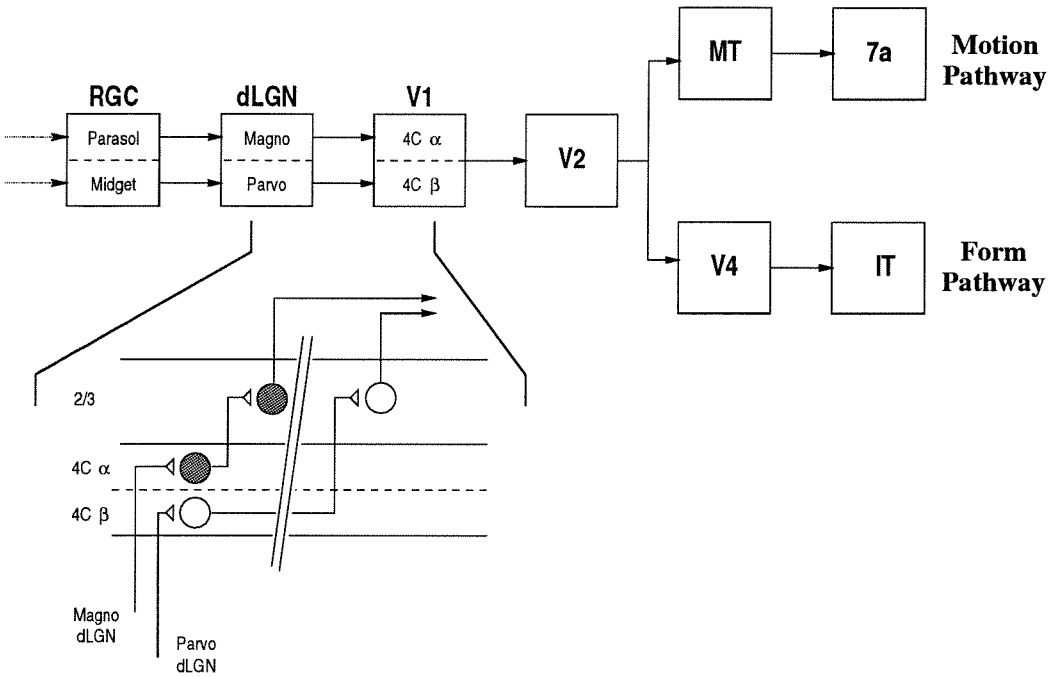

Figure 4.1: Parallel pathways in the visual system. Figure shows a schematic diagram of the connectivity of the M/P and Motion/Form pathways in the mammalian (cat and monkey) visual systems. Inset shows the structure of the laminar distribution of dLGN afferents in area V1.

completely true. Nealey and Maunsell (1994) demonstrated that as early as area V1, neurons receive both M and P channel input, consistent with an earlier report by Lachica et al. (1992) of anatomical convergence of the M and P streams in V1. Other work has demonstrated the M stream makes a functional contribution to the form processing areas beyond V1 (Ferrera et al., 1994b) and that the P stream can provide input to extrastriate motion areas (Maunsell et al., 1990; Cheng et al., 1994).

In light of these recent studies it seems that the distinction between form and motion processing in cortical structures is largely one of function which does not have a clear anatomical component. Cortical lesions of the highest levels for cortical "form" and "motion" processing, however, can lead to characteristic behavioral and psychophysical deficits. These deficits correspond closely to those expected based on the functional dichotomy defined by form and motion.

4.1.2 Weakly Electric Fish

The electrolocation system in weakly electric fish is a significantly different sensory modality in which parallel processing plays a major role. As in the auditory system, much of the information contained in the electric fields generated by these fish is not represented by the spatial activity pattern of the primary sensory neurons. Instead, spatial relationships and other important environmental features must be extracted computationally from the firing patterns of sensory afferents.

As in vision, parallel processing in the electrolocation system originates peripherally at the level of the sensory transduction organs. Gymnotiform and mormyriform fish, the best studied groups of weakly electric fish, have two classes of electroreceptors distributed over the body surface: ampullary and tuberous receptor organs. Ampullary receptors, sensitive to very low frequency electric fields, exist in virtually all non-teleost fish and are not thought to play a significant role in active electrolocation. Tuberous receptors, present in all weakly electric fish, transduce the fish's self-generated electric fields (electric organ discharge or EOD) and provide the primary source of input to the active electrolocation system.

Gymnotids and mormyrids have two distinct types of tuberous organs. Each type is sen-

sitive to a different aspect of the electric field (Zakon, 1986). Time-coders (T-units in gymnotids; knollenorgans in mormyrids) encode information about the EOD phase in the form of action potentials phase locked to the EOD, while amplitude-coders (P-units or mormyromasts) encode information about the instantaneous amplitude of the EOD. Though the names and anatomical structures are somewhat different in gymnotids and mormyrids, the dichotomy between time and amplitude processing is largely the same.

The segregation of time and amplitude processing is analogous to the separation of time and level processing in the barn owl. In the fish, however, the initial segregation occurs at the primary sensory neurons, whereas in the auditory system both time and intensity cues are transduced by the same sensory neurons and ramify one synapse later. In electric fish, the separation of time and amplitude processing is maintained by the projection from receptor to medulla (electrosensory lateral lob, ELL) and from the medulla to the midbrain electrosensory area (torus semicircularis).

To date, the South American knifefish *Eigenmannia* represents the best characterized of all weakly electric fish. The myogenic electric organ in *Eigenmannia* generates a quasi-sinusoidal electric field with a fundamental frequency between 250 and 650Hz. By detecting local perturbations in the electric field around the body, the fish is able to detect objects in its environment. Under isolated conditions (*i.e.*, in the absence of conspecifics), the electric field provides detailed information about the structure of the fish's local environment. The presence of nearby conspecifics with similar EOD frequencies interferes with the fish's own electric field. To avoid conspecific interference (jamming), *Eigenmannia* has evolved an elegant system for detecting interference and then shifting its EOD frequency to avoid contamination. This frequency shifting behavior is known as the "jamming avoidance response" or JAR (Bullock et al., 1972).

Behaviorally, when the fish detects a conspecific's EOD, it determines whether the other EOD is higher or lower in frequency than its own. If the conspecific's EOD frequency is higher, then the fish reduces its own frequency to increase signal separation in the frequency domain. Alternatively, if the conspecific's EOD is lower, the fish shifts its own EOD frequency up, towards higher frequencies. In short, the sign of the frequency difference is detected and the EOD is shifted to increase the magnitude of the difference. The neural

substrate of the JAR is a circuit which combines the independent time and amplitude information available from the T-units and P-units to determine the sign and magnitude of the EOD frequency difference.

The effects of jamming can be depicted schematically as the sum of two sine waves differing slightly in frequency and amplitude, as shown in figure 4.2A. The result of jamming is that the field measured at a contaminated point on the body surface develops an amplitude modulation and phase shift relative to the fish's own EOD (figure 4.2B, dashed curve). By comparing the phase and amplitude of the contaminated signal with that of the original EOD (figure 4.2B, solid curve), the fish can determine the jamming frequency and shift away, as described above. In *Eigenmannia*, though not all electric fish, information about the phase and amplitude of the fish's own EOD is not directly accessible to the JAR circuits, but must be extracted from electroreceptors located at relatively uncontaminated sites on the body surface.

The two separate pathways that form the basis of the JAR circuit in *Eigenmannia* originate in the periphery. The T-units encode the zero crossings of each EOD cycle at different positions on the skin and project somatotopically to phase sensitive cells in the ELL. These ELL neurons, in turn, project to a coincidence detection circuit located in the torus where the zero-crossing information from distant body positions is compared to determine the phase difference, $\Delta\Phi$. P-units, whose firing rates proportional to the instantaneous amplitude of the EOD, make a somatotopic projection to a different, nonoverlapping region of the ELL, which also projects to the torus. In the torus, the time and amplitude pathways converge onto single neurons which compute the the sign of the frequency difference necessary for the JAR.

In *Eigenmannia*, synaptic convergence appears to be an important computational mechanism and is used for more than simply the integration of the time and amplitude pathways. The accuracy of phase locking, *i.e.*, the temporal resolution of the time pathway, improves at each level in the brainstem. Improvements in phase locking were measured by Carr et al. (1986) as a reduction in temporal jitter or an increase in "vector strength" (Goldberg and Brown, 1969) at successive levels in the time pathway. Phase locking improves (*i.e.*, vector strength increases) between the primary sensory neurons and the spherical cells of the ELL

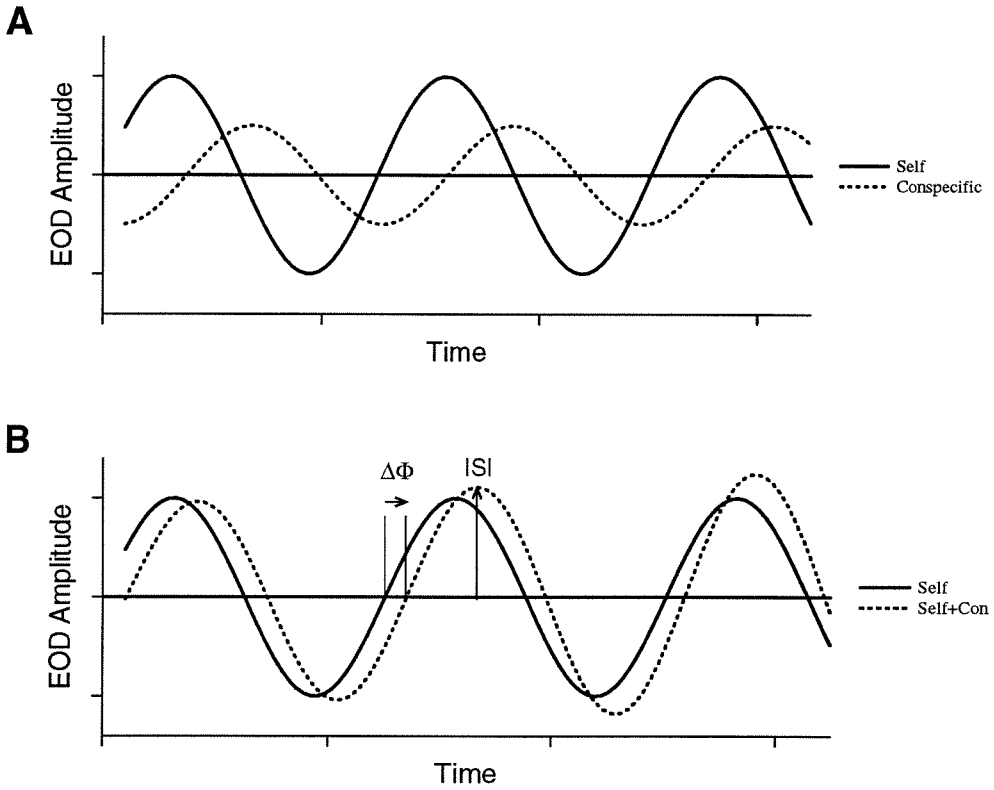

Figure 4.2: The effect of jamming in *Eigenmannia*. (A) Sinusoids representing the EODs generated by a fish (solid) and its conspecific neighbor (dashed). The neighbor's EOD has a slightly higher fundamental frequency as is attenuated by distance. (B) Fish's own EOD (solid) and the contaminated signal as measured on the body surface (dashed, sum of Self and Conspecific shown in A). The JAR relies of the phase difference between its own EOD and the contaminated EOD ($\Delta\Phi$) as well as the instantaneous amplitude of the contaminated EOD ($|S|$) to determine the direction to shift in order to eliminate jamming. After Heiligenberg (1988).

and then again between the spherical cells and the giant cells of the torus.

The increase in vector strength is consistent with the anatomically observed synaptic convergence occurring in the connections between these nuclei. Postsynaptic neurons receive afferent input from several presynaptic neurons and act as coincidence detectors as shown in figure 4.3. Synaptic convergence here has the effect of reducing the occurrence of spurious, non-phase locked signals leading to postsynaptic to action potentials. The net result of convergence is synchronization, which leads to a reduction in temporal jitter at the expense of total spike number. Interesting, recent studies of the cat auditory system have suggested that a similar circuit may exist in the anteroventral cochlear nucleus (AVCN) which improves phase locking in the auditory time pathway (Joris et al., 1994a, 1994b).

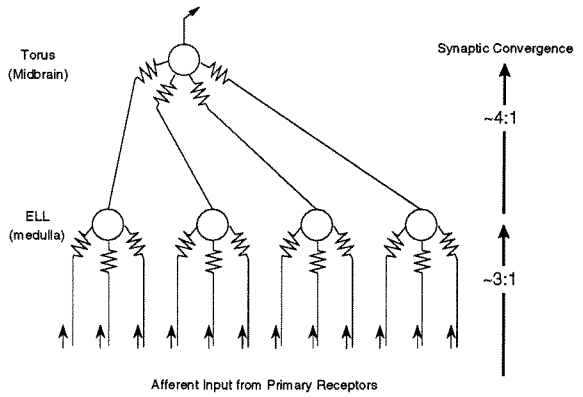

Figure 4.3: Synaptic convergence in *Eigenmannia*. Multiple (1-3) electrosensory afferents from phase-encoding electrosensory organs converge on single spherical cells in the electrosensory lateral lobe (ELL) of the medulla. Spherical cells, in turn, converge on the giant cells of the torus semicircularis in the midbrain. Resistor symbols indicate electric synapses. After Carr et al. (1986).

4.1.3 Microchiroptera (Bats)

The auditory system of echolocating bats, most notably the mustached bat, *Pteronotus parnelli rubiginosus*, provides yet another example of computational parallelism. Microchiropteran bats use both active and passive auditory cues to gather information about their environment. While both active and passive auditory cues enter the nervous system via the same set of primary sensory neurons, studies of the central nervous system in *Pteronotus*

have shown that a highly elaborate segregation into parallel processing streams occurs in the central nervous system, most notably in auditory cortex.

Pteronotus is a CF/FM bat, meaning that its echolocation call contains both constant frequency (CF) and frequency modulated (FM) components. The work of Suga (reviewed in Suga, 1988) demonstrated that the FM component is used primarily for computing target range, while the CF component provides information about target features. In particular, the CF portion of the echo contains information about target velocity and target flutter or the target's wing-beat frequency. These features are processed independently by different subdivisions of the auditory cortex (FM-FM and CF/CF areas).

The FM-FM area contains several topographic maps of target range. The CF/CF area, which is anatomically distinct from the FM-FM area, contains representation of both target velocity and flutter. 65% of the neurons in the CF/CF area are sensitive to the DC component of the CF portion of echoes. The difference between the DC component of the echolocation call (pulse) and its echo reflects the Doppler shift of the echo. The Doppler shift is directly related to target velocity.

The remaining 35% of CF/CF neurons are sensitive to the echo's AC component (Suga, 1984). Reflections from flying insects, the bat's primary food source, lead to a sinusoidal modulation of the CF component of the echo. The rate of frequency modulation is related to the wing-beat frequency of the target. The 35% of CF/CF neurons sensitive to the AC portion of the echo encode the wing-beat frequency. Information about the wing-beat frequency, encoded by these neurons, can be used by the bat to identify the type or species of the target (Kober and Schnitzler, 1990).

While there is extensive anatomical parcellation by function in the bat's auditory cortex, the representation of velocity and flutter in the CF/CF area is essentially overlapping. The heterogeneity of the CF/CF area, however, may reflect "evolutionary baggage." Heiligenberg (1988, p. 78) wrote in reference to the jamming avoidance response (JAR) in electric fish:

> Some general concepts that have emerged from studies of the JAR are the following. First, the actual neuronal solutions to problems of signal processing can be very different from those a human engineer might propose. Second,

> the perception of stimulus patterns and the control of adaptive behavioral responses are executed in a parliamentary fashion by large populations of neurons in which individual elements are of little significance ... Third, nervous systems are full of improvisations and patchwork, burdened with traces of their evolutionary history.

The co-mingled representations of target features in microchiropteran bats, therefore, could simply reflect the bat's evolutionary origins and the primitive condition of a non-echolocating ancestral species. It does, however, demonstrate that anatomical segregation is not a necessary prerequisite for parallel processing.

4.1.4 Multimodal Representations

In most parallel processing schemes, the separate streams usually converge at a higher level in the system. The most obvious examples of convergence occur in multimodal or polysensory integration areas. There parallelism is inherent in the separation of different sensory modalities. Perhaps the best documented site of multimodal integration is the superior colliculus (SC).

In virtually all vertebrates the superior colliculus or optic tectum appears to contain a multimodal representation of the environment (mammals: Drager and Hubel, 1975, Middlebrooks and Knudsen, 1984, Carlile and King, 1994; birds: Knudsen, 1982; reptiles: Hartline et al., 1978; see Stein and Meredith, 1993, chapter 9, for a review). In general, the primary representation in the superior colliculus appears to be a retinotopic visual map. In addition to the visual map, the SC also contains maps from other sensory modalities, all roughly in register with the visual map. Which other modalities actually project to the superior colliculus depends upon the species (auditory space maps: owls, cats, ferrets; somatotopic maps: rodents; infrared maps: snakes; electrosensory maps: electric fish).

The functional and gross anatomical organization of the superior colliculus is highly conserved across vertebrates. The SC is a laminar structure; about 55% of the neurons located in the deep layers receive inputs from multiple sensory modalities. The remainder of the deep layer neurons are either unimodal or non-sensory (Stein and Meredith, 1993). The

multimodal nature of the deep layer neurons reflects convergence at the level of the superior colliculus and is not thought to be the result of a projection from multimodal neurons located elsewhere (Stein, 1978; Knudsen and Mogdans, 1992). The principal projections of the multimodal collicular neurons are to the motor system.

The superior colliculus controls orientation responses in most species. Sensory input from a particular region of space drives multimodal neurons. These neurons in turn project to the brainstem motor areas and cause the animal to orient towards the sensory input. In the case of the owl, auditory and visual stimuli, or microstimulation of the deep tectal neurons, leads to head movements that orient the owl towards the stimuli (DuLac and Knudsen, 1990). In primates, tectal stimulation causes saccadic eye movements that bring stimuli onto the foveal portion of the retina (Robinson, 1972; Schiller and Stryker, 1972).

This sort of multimodal integration is analogous to an OR-gate, from a computational perspective. Activity from any one of the multiple sensory modalities projecting to a deep layer neuron can lead to activation. Activation of a sufficient number of deep layer neurons activates the brainstem motor areas and eventually leads to an orienting response. Though the organization of the superior colliculus is in no way simple, the computational role of multimodal integration seems relatively straightforward. This simplicity of function, like the high degree of conservation across species boundaries, most likely reflects the behavioral importance of generating orientation responses in nature.

4.2 General Observations

One basic principle, independent of species and sensory modality, is that time and amplitude processing are generally segregated into separate processing streams (Carr, 1993). This is evident to some extent in all the systems described above. The explanation for this dichotomy between time and amplitude processing lies in the nature of the all-or-none mechanism of neural transmission. Temporal information is encoded by the time of occurrence of action potentials, while amplitude information is encoded by neuronal firing rate. "Time-intensity" trading occurs whenever changes in the temporal properties of a stimulus can not be reliably distinguished from changes in stimulus amplitude. Simply put, time coding and

rate coding can not be combined at the level of the single neuron without leading to time-intensity trading. The use of independent processing streams for time and intensity information represents an elegant solution to this basic problem.

The downstream convergence of parallel processing streams which occurs in all sensory systems exists in a variety of forms. In the simplest case, integration can be in the form of an OR-gate, where a single neuron fires when it receives input from any channel, as occurs in the superior colliculus. The process of integration can also take the form of an AND gate, when a particular combination of inputs, from different channels, is required to for neuronal activation. Examples of AND gate integration are found in the electrosensory system, in which the AND gate serves the function of a coincidence detector to reduce the jitter associated with phase locking, and in the IPD sensitive neurons in the barn owl which act as coincidence detectors for activity from the two ears.

Parallel processing appears to exists in at least two subtly different forms. Parallel channels can encode dramatically different information about sensory stimuli, *e.g.*, time or intensity cues in the owl. Alternatively, parallel channels can encode different values of a single stimulus feature; in the owl, the parallel narrow band frequency channels originating nucleus laminaris are an example of this sort of parallelism. Each narrow band channel independently encodes interaural phase difference over a narrow range of frequencies. This is similar to the somatotopic projection from the body surface to the ELL represents in the electric fish, where different parallel channels systematically encode the phase (or amplitude) of the EOD at particular locations on the body. Just as sidepeak suppression in the owl requires integration across frequency channels, the jamming avoidance response in *Eigenmannia* requires integration over the body surface.

In recent years, neuroethologically based studies of the barn owl's auditory system have made great progress towards elaborating the neural substrates of sound localization, both in owls and other species. The data presented here provide evidence for a hierarchically organized network in the lateral shell that combines the parallel processing streams for time, intensity and frequency. Both anatomically and physiologically, this model of convergence bears striking resemblances to those described in other systems and in other species. Most notably, the convergence that takes place in the lateral shell of the owl shares remarkable

similarities to the convergence of phase and amplitude channels in the ELL and torus semicircularis of *Eigenmannia*. The studies of the organization of the lateral shell described here provide further evidence that the study of sound localization in the barn owl can provide valuable insights into the organization of other sensory systems, such as electroreception and vision. More generally, ethologically based studies of sensory processing, which serve to clarify the relationship between natural behavior and neural structure, can yield information about nervous system function that transcends both species and modality boundaries.

Bibliography

Adolphs, R. (1993a). Acetylcholinesterase staining differentiates functionally distinct auditory pathways in the barn owl. *J. Comp. Neurology*, 329(3):365–377.

Adolphs, R. (1993b). Bilateral inhibition generates neuronal responses tuned to interaural level differences in the auditory brain-stem of the barn owl. *J. Neurosci.*, 13(9):3647–3668.

Barlow, H. B. (1953). Summation and inhibition in the frog's retina. *J. Phsyiol.*, 119:69–88.

Batteau, D. W. (1967). The role of the pinnae in human localization. *Proc. Roy. Soc. London B*, 168:158–180.

Beitel, R. E. (1991). Localization of azimuthal sound direction by the great horned owl. *J. Acoust. Soc. Am.*, 90(5):2843–2846.

Blauert, J. (1969/70). Sound localization in the median plane. *Acustica*, 22:205–13.

Blauert, J. (1983). *Spatial Hearing: The Psychophysics of Human Sound Localization*. MIT Press, Cambridge.

Brown, C. H., Beecher, M. D., Moody, D. B., and Stebbins, W. C. (1980). Localization of noise bands by old world monkeys. *J. Acoust. Soc. Am.*, 68(1):127–132.

Bullock, T. H., Hamstra, R. H., and Scheich, H. (1972). The jamming avoidance response of high-frequency electric fish. *J. Comp. Physiol*, 103:1–48.

Carlile, S. and King, A. J. (1994). Monaural and binaural spectrum level cues in the ferret - acoustics and the neural representation of auditory space. *J. Neurophysiol.*, 71(2):785–801.

Carr, C. E. (1990). Evolution of the central auditory-system in reptiles and birds. *Am. Zoologist*, 30(4):48–48.

Carr, C. E. (1993). Processing of temporal information in the brain. *Ann. Rev. Neuro.*, 16:223–243.

Carr, C. E., Heiligenberg, W., and Rose, G. J. (1986). A time-comparison circuit in the electric fish midbrain .1. behavior and physiology. *J. Neurosci.*, 6(1):107–119.

Carr, C. E. and Konishi, M. (1988). Axonal delay-lines for time measurement in the owls brain-stem. *Proc. Natl. Acad. Sci. USA*, 85(21):8311–8315.

Carr, C. E. and Konishi, M. (1990). A circuit for detection of interaural time differences in the brain-stem of the barn owl. *J. Neurosci.*, 10(10):3227–3246.

Chan, J. C. K., Yin, T. C. T., and Musicant, A. D. (1987). Effects of interaural time delays of noise stimuli on low-frequency cells in the cats inferior colliculus .2. responses to band-pass filtered noises. *J. Neurophysiol.*, 58(3):543–561.

Cheng, K., Hasegawa, T., Saleem, K. S., and Tanaka, K. (1994). Comparison of neuronal selectivity for stimulus speed, length, and contrast in the prestriate visual cortical areas V4 and MT of the Macaque monkey. *J. of Neurophysiol.*, 71(6):2269–2280.

Colburn, H. S., Han, Y. A., and Culotta, C. P. (1990). Coincidence model of mso responses. *Hearing Research*, 49(1-3):335–346.

Desimone, R., Albright, T. D., Gross, C. G., and Bruce, C. J. (1984). Stimulus-selective properties of inferior temporal neurons in the macaque. *J. Neurosci.*, 4:2051–2062.

Dolan, R. P. and Schiller, P. H. (1994). Effects of on channel blockade with 2-amino-4-phosphonobutyrate (apb) on brightness and contrast perception in monkeys. *Vis. Neurosci.*, 11(1):23–32.

Drager, U. C. and Hubel, D. H. (1975). Topography of visual and somatosensory projections in the mouse superior colliculus. *J. Neurophysiol*, 39:690–713.

DuLac, S. and Knudsen, E. I. (1990). Neural maps of head movement vector and speed in the optic tectum of the barn owl. *J. Neurophysiol.*, 63(1):131–146.

Felleman, D. and Van Essen, D. (1991). Distributed hierarchical processing in the primate cerebral cortex. *Cereb. Cortex*, 1(1):1–47.

Ferrera, V. P., Nealey, T. A., and Maunsell, J. H. R. (1994a). Responses in Macaque visual area V4 following inactivation of the parvocellular and magnocellular LGN pathways. *J. Neurosci.*, 14(4):2080–2088.

Ferrera, V. P., Rudolph, K. K., and Maunsell, J. H. R. (1994b). Responses of neurons in the parietal and temporal visual pathways during a motion task. *J. Neurosci.*, 14(10):6171–6186.

Fisher, H. G. and Freedman, S. J. (1968). The role of the pinna in auditory localization. *J. Audit. Res.*, 8:15–26.

Fujita, I. and Konishi, M. (1991). The role of GABAergic inhibition in processing of interaural time difference in the owl's auditory-system. *J. Neurosci.*, 11(3):722–739.

Fuzessery, Z. M. (1986). Speculations on the role of frequency in sound localization. *Brain Behavior and Evolution*, 28(1-3):95–108.

Goldberg, J. M. and Brown, P. B. (1969). Response of binaural neurons of dog superior olivary complex to dichotic tonal stimuli: Some physiological mechanisms for sound localization. *J. Neurophysiol.*, 32:613–636.

Greenwood, D. D. (1961). Critical bandwidth and the frequency coordinates of the basilar membrane. *J. Acoust. Soc. Am.*, 44:1344–1356.

Hartline, P. H., Kass, L., and Loop, M. S. (1978). Merging of modalities in the optic tectum; infrared and visual integration in rattlesnakes. *Science*, 199:1225–1229.

Heffner, R. S. and Heffner, E. H. (1992). Evolution of sound localization in mammals. In Webster, D. B., Fay, R. R., and Popper, A. N., editors, *The Evolutionary Biology of Hearing*, pages 691–715. Springer-Verlag, New York.

Heiligenberg, W. (1988). Neural mechanisms of perception and motor control in a weakly electric fish. *Advances in the Study of Behavior*, 18:73–98.

Heiligenberg, W. (1991). The neural basis of behavior - a neuroethological view. *Ann. Rev. Neuro.*, 14:247–267.

Hubel, D. H., Wiesel, T. N., and Stryker, M. P. (1978). Anatomical demonstrations of orientation columns in macaque monkey. *J. Comp. Neurol.*, 177:361–380.

Jeffress, L. A. (1948). A place theory of sound localization. *J. Comp. Physiol. Psychol.*, 41:35–39.

Joris, P. X., Carney, L. H., Smith, P. H., and Yin, T. C. T. (1994a). Enhancement of neural synchronization in the anteroventral cochlear nucleus .1. responses to tones at the characteristic frequency. *J. Neurophysiol.*, 71(3):1022–1036.

Joris, P. X., Smith, P. H., and Yin, T. C. T. (1994b). Enhancement of neural synchronization in the anteroventral cochlear nucleus .2. responses in the tuning curve tail. *J. Neurophysiol.*, 71(3):1037–1051.

Karnovsky, M. J. and Roots, L. (1964). A "direct-coloring" thiocholine method for cholinesterases. *J. Histochem. Cytochem.*, 12:219–221.

Knudsen, E. I. (1982). Auditory and visual maps of space in the optic tectum of the owl. *J. Neurosci.*, 2(9):1177–1194.

Knudsen, E. I., Esterly, S. D., and DuLac, S. (1991). Stretched and upside-down maps of auditory space in the optic tectum of blind-reared owls - acoustic basis and behavioral-correlates. *J. Neurosci.*, 11(6):1727–1747.

Knudsen, E. I. and Konishi, M. (1978a). Center-surround organization of auditory receptive fields in the owl. *Science*, 202:778–780.

Knudsen, E. I. and Konishi, M. (1978b). A neural map of auditory space in the owl. *Science*, 200:795–797.

Knudsen, E. I. and Konishi, M. (1979). Mechanisms of sound localization in the barn owl (*Tyto alba*). *J. Comp. Physiol. A*, 133:13–21.

Knudsen, E. I. and Mogdans, J. (1992). Vision-independent adjustment of unit tuning to sound localization cues in response to monaural occlusion in developing owl optic tectum. *J. Neurosci.*, 12(9):3485–3493.

Kober, R. and Schnitzler, H. U. (1990). Information in sonar echoes of fluttering insects available for echolocating bats. *J. Acoust. Soc. Am.*, 87(2):882–896.

Konishi, M. (1973a). How the owl tracks its prey. *Am. Scientist*, 61:414–424.

Konishi, M. (1973b). Locatable and nonlocatable acoustic signals for barn owls. *Am. Naturalist*, 107:775–785.

Konishi, M. (1985). Birdsong - from behavior to neuron. *Ann. Rev. Neuro.*, 8:125–170.

Konishi, M. (1986). Centrally synthesized maps of sensory space. *TINS*, 9(4):163–168.

Konishi, M. (1989). Birdsong for neurobiologists. *Neuron*, 3(5):541–549.

Konishi, M., Sullivan, W. E., and Takahashi, T. (1985). The owl's cochlear nuclei process different sound localization cues. *J. Acoust. Soc. Am.*, 78(1):360–364.

Konishi, M., Takahashi, T. T., Wagner, H., Sullivan, W. E., and Carr, C. E. (1988). Neurophysiological and anatomical substrates of sound localization in the owl. In Edelman, G. M., Gall, W. E., and Cowan, W. M., editors, *Auditory Function: Neurobiological bases of hearing*, pages 721–745. John Wiley & Sons, New York.

Kuffler, S. W. (1953). Discharge patterns and functional organization of the mammalian retina. *J. Neurophysiol.*, 16:37–68.

Kuhn, G. F. (1977). Model for the interaural time differences in the azimuthal plane. *J. Acoust. Soc. Am.*, 62:157–167.

Lachica, E. A., Beck, P. D., and Casagrande, V. A. (1992). Parallel pathways in Macaque monkey striate cortex - anatomically defined columns in layer-III. *Proc. Natl. Acad. Sci. USA*, 89:3566–3570.

Lewicki, M. S. (1994). Bayesian modeling and classification of neural signals. *Neural Computation*, 6:1005–1030.

Licklider, J. C. R. (1959). Three auditory theories. In Koch, S., editor, *Psychology: A Study of a Science, Vol 1*. McGraw-Hill, New York.

Makous, J. C. and Middlebrooks, J. C. (1990). 2-dimensional sound localization by human listeners. *J. Acoust. Soc. Am.*, 87(5):2188–2200.

Manley, G. A., Köppl, C., and Konishi, M. (1988). A neural map of interaural intensity differences in the brain-stem of the barn owl. *J. Neurosci.*, 8(8):2665–2676.

Maunsell, J. H. R. and Gibson, J. R. (1992). Visual response latencies in striate cortex of the Macaque monkey. *J. of Neurophysiol.*, 68(4):1332–1344.

Maunsell, J. H. R., Nealey, T. A., and DePriest, D. D. (1990). Magnocellular and parvocellular contributions to responses in the middle temporal visual area (MT) of the Macaque monkey. *J. Neurosci.*, 10:3323–3334.

Merigan, W. H. (1989). Chromatic and achromatic vision of Macaques: Role of the P pathway. *J. Neurosci.*, 9(3):776–783.

Middlebrooks, J. C. and Green, D. M. (1991). Sound localization by human listeners. *Ann. Rev. Psych.*, 42:135–159.

Middlebrooks, J. C. and Knudsen, E. I. (1984). A neural code for auditory space in the cats superior colliculus. *J. Neurosci.*, 4(10):2621–2634.

Middlebrooks, J. C., Makous, J. C., and Green, D. M. (1989). Directional sensitivity of sound-pressure levels in the human ear canal. *J. Acoust. Soc. Am.*, 86(1):89–108.

Mogdans, J. and Knudsen, E. I. (1994). Representation of interaural level difference in the vlvp, the first site of binaural comparison in the barn owls auditory-system. *Hearing Research*, 74(1-2):148–164.

Moiseff, A. (1989). Bi-coordinate sound localization by the barn owl. *J. Comp. Physiol. A*, 164(5):637–644.

Moiseff, A. and Haresign, T. (1992). Response of auditory units in the barn owl's inferior colliculus to continuously varying interaural phase differences. *J. Neurophysiol.*, 67(6):1428–1436.

Moiseff, A. and Konishi, M. (1981). Neuronal and behavioral sensitivity to binaural time differences in the owl. *J. Neurosci.*, 3:2553–2562.

Mori, K., Fujita, I., and Konishi, M. (1991). GABAergic inhibition contributes to non-linear summation amoung multiple frequency channels in the barn owl's inferior colliculus. In *Soc. Neurosci. Abstr.*, volume 22.

Nealey, T. A. and Maunsell, J. H. R. (1994). Magnocellular and parvocellular contributions to the responses of neurons in Macaque striate cortex. *J. Neurosci.*, 14(4):2069–2079.

Olsen, J. F., Knudsen, E. I., and Esterly, S. D. (1989). Neural maps of interaural time and intensity differences in the optic tectum of the barn owl. *J. Neurosci.*, 9(7):2591–2605.

Overholt, E. M., Rubel, E. W., and Hyson, R. L. (1992). A circuit for coding interaural time differences in the chick brain-stem. *J. Neurosci.*, 12(5):1698–1708.

Payne, R. S. (1971). Acoustic location of prey by barn owls (*Tyto alba*). *J. Exp. Biol.*, 54:535–573.

Pettigrew, J. D. and Konishi, M. (1976). Neurons selective for orientation and binocular disparity in the visual wulst of the barn owl (*tyto alba*). *Science*, 193:675–678.

Proctor, L. (1993). *Characterization of the Auditory Thalamic Nucleus of the Barn Owl.* Ph.D. thesis, California Institute of Technology.

Raman, I. M., Zhang, S., and Trussell, L. O. (1994). Pathway-specific variants am.a receptors and their contribution to neuronal signaling. *J. Neurosci.*, 14(8):4998–5010.

Rayleigh, L. (1907). On our perception of sound direction. *Phios. Mag.*, 13:214–32.

Robinson, D. A. (1972). Eye movements evoked by collicular stimulation in the alert monkey. *Vis. Res.*, 12:1796–1808.

Rose, J. E., Gross, N. B., Geisler, C. D., and Hind, J. E. (1966). Some neural mechanisms in the inferior colliculus of the cat which may be relevent to localization of a sound source. *J. Neurophysiol.*, 29:288–314.

Sanes, D. H. (1990). An *in vitro* analysis of sound localization mechanisms in the gerbil lateral superior olive. *J. Neurosci.*, 10(11):3494–3506.

Schiller, P. H. (1992). The ON and OFF channels of the visual-system. *TINS*, 15(3):86–92.

Schiller, P. H. and Logothetis, N. K. (1990). The color-opponent and broad-band channels of the primate visual-system. *TINS*, 13(10):392–398.

Schiller, P. H., Logothetis, N. K., and Charles, E. R. (1990). Role of the color-opponent and broad-band channels in vision. *Vis. Neurosci.*, 5(4):321–346.

Schiller, P. H., Sandell, J. H., and Maunsell, J. H. R. (1986). Functions of the ON and OFF channels of the visual-system. *Nature*, 322(6082):824–825.

Schiller, P. H. and Stryker, M. (1972). Single unit recording and stimulations in superior colliculus of the alert rhesus monkey. *J. Neurophysiol*, 35:915–924.

Schneider, D. (1974). The sex-attractant receptor of moths. *Sci. Am.*, JUL:55–62.

Shackleton, T. M., Meddis, R., and Hewitt, M. J. (1992). Across frequency integration in a model of lateralization. *J. Acoust. Soc. Am.*, 91(4):2276–2279.

Stein, B. E. (1978). Nonequivalent visual, auditory and somatic corticotectal influences in cat. *J. Neurophysiol*, 41:55–64.

Stein, B. E. and Meredith, M. A. (1993). *The Merging of the Senses*. MIT Press, Cambridge.

Stern, R. M. and Trahiotis, C. (1992). The role of consistency of interaural timing over frequency in binaural lateralization. *Advances in the Biosciences*.

Stern, R. M., Zeiberg, A. S., and Trahiotis, C. (1988). Lateralization of complex binaural stimuli - a weighted-image model. *J. Acoust. Soc. Am.*, 84(1):156–165.

Stevens, S. S. and Newman, E. B. (1936). The localization of actual sources of sound. *Am. J. Psychol.*, 48:297–306.

Suga, N. (1984). Neural mechanisms of complex-sound processing for echolocation. *TINS*, 7(1):20–27.

Suga, N. (1988). The extent to which biosonar information is represented in the bat auditory cortex. In Edelman, G. M., Gall, W. E., and Cowan, W. M., editors, *Auditory Function: Neurobiological bases of hearing*, pages 315–38. John Wiley & Sons, New York.

Sullivan, W. E. and Konishi, M. (1984). Segregation of stimulus phase and intensity coding in the cochlear nucleus of the barn owl. *J. Neurosci.*, 4(7):1787–1799.

Sullivan, W. E. and Konishi, M. (1986). Neural map of interaural phase difference in the owl's brain-stem. *Proc. Natl. Acad. Sci. USA*, 83(21):8400–8404.

Takahashi, T. and Konishi, M. (1986). Selectivity for interaural time difference in the owls midbrain. *J. Neurosci.*, 6(12):3413–3422.

Takahashi, T., Moiseff, A., and Konishi, M. (1984). Time and intensity cues are processed independently in the auditory-system of the owl. *J. Neurosci.*, 4(7):1781–1786.

Takahashi, T. T. (1989). Construction of an auditory space map. *Ann. New York Acad. Sci.*, 563:101–113.

Takahashi, T. T. and Keller, C. H. (1992). Commissural connections mediate inhibition for the computation of interaural level difference in the barn owl. *J. Comp. Physiol. A*, 170(2):161–169.

Takahashi, T. T. and Keller, C. H. (1994). Representation of multiple sound sources in the owl's auditory space map. *J. Neurosci.*, 14(8):4780–4793.

Takahashi, T. T. and Konishi, M. (1988a). Projections of nucleus angularis and nucleus laminaris to the lateral lemniscal nuclear-complex of the barn owl. *J. Comp. Neurology*, 274(2):212–238.

Takahashi, T. T. and Konishi, M. (1988b). Projections of the cochlear nuclei and nucleus laminaris to the inferior colliculus of the barn owl. *J. Comp. Neurology*, 274(2):190–211.

Takahashi, T. T., Wagner, H., and Konishi, M. (1989). Role of commissural projections in the representation of bilateral auditory space in the barn owl's inferior colliculus. *J. Comp. Neurology*, 281(4):545–554.

Tinbergen, N. (1989). *The Study of Instinct.* Oxford University Press, Oxford.

Trahiotis, C. and Stern, R. M. (1989). Lateralization of bands of noise - effects of bandwidth and differences of interaural time and phase. *J. Acoust. Soc. Am.*, 86(4):1285–1293.

Trahiotis, C. and Stern, R. M. (1994). Across-frequency interaction in lateralization of complex binaural stimuli. *J. Acoust. Soc. Am.*, 96(6):3804–3806.

Volman, S. F. and Konishi, M. (1989). Spatial selectivity and binaural responses in the inferior colliculus of the great horned owl. *J. Neurosci.*, 9(9):3083–3096.

Volman, S. F. and Konishi, M. (1990). Sound localization in four species of owls. *Brain Behavior and Evolution*, 36(4):196–215.

Wagner, H. (1993). Sound-localization deficits induced by lesions in the barn owls auditory space map. *J. Neurosci.*, 13(1):371–386.

Wagner, H., Takahashi, T., and Konishi, M. (1987). Representation of interaural time difference in the central nucleus of the barn owl's inferior colliculus. *J. Neurosci.*, 7(10):3105–3116.

Wehner, R. (1989). Neurobiology of polarization vision. *TINS*, 12(9):353–359.

Werblin, F. S. and Dowling, J. E. (1969). Organization of the retina of the mudpuppy, *necturus maculosus*. ii. intracellular recording. *J. Neurophysiol*, 32:339–355.

Yin, T. C. T. and Chan, J. C. K. (1988). Neural sensititivity to interaural time differences. In Edelman, G. M., Gall, W. E., and Cowan, W. M., editors, *Auditory Function: Neurobiological bases of hearing*, pages 385–430. John Wiley & Sons, New York.

Yin, T. C. T. and Chan, J. C. K. (1990). Interaural time sensitivity in medial superior olive of cat. *J. Neurophysiol.*, 64(2):465–488.

Yin, T. C. T., Chan, J. C. K., and Carney, L. H. (1987). Effects of interaural time delays of noise stimuli on low-frequency cells in the cats inferior colliculus .3. evidence for cross-correlation. *J. Neurophysiol.*, 58(3):562–583.

Yin, T. C. T., Chan, J. C. K., and Irvine, D. R. F. (1986). Effects of interaural time delays of noise stimuli on low-frequency cells in the cats inferior colliculus .1. responses to wide-band noise. *J. Neurophysiol.*, 55(2):280–300.

Zakarauskas, P. and Cynader, M. S. (1993). A computational theory of spectral cue localization. *J. Acoust. Soc. Am.*, 94(3):1323–1331.

Zakon, H. H. (1986). The electroreceptive periphery. In Bullock, T. H. and Heiligenberg, W., editors, *Electroreception*, chapter 4, pages 103–156. Wiley & Sons, New York.